Synthesis, Characterization and Catalytic Applications of Doped Metal Oxides

A thesis submitted to the

Vijayanagara Sri Krishnadevaraya University, Ballari

For the degree of

Doctor of Philosophy

In

Chemistry

Mr. OBAIAH G O M.Sc.
Reg. No: 14CHP017

Under the Supervision of

Dr. K. H. SHIVAPRASAD, M.Sc., Ph.D.
Professor, Dept. of Chemistry,
Vijayanagara Sri Krishnadevaraya University,
Ballari-583105

MARCH – 2020

Dedicated to............

My Beloved

Parents & Wife

Obaiah G O, M.Sc.,

Research Scholar (**14CHP017**)

Department of Chemistry/Industrial Chemistry,

Vijayanagara Sri Krishnadevaraya *University*,

Ballari, Karnataka, India, Mobile: +91 9741913492, e-mail: obavasu@gmail.com

Declaration

I hereby declare that thesis entitled *"Synthesis, Characterization and Catalytic Applications of Doped Metal Oxides"* is carried out by me under the supervision of **Dr. K. H. SHIVAPRASAD**, Professor, Department of Studies in Chemistry/Industrial Chemistry, Vijayanagara Sri Krishnadevaraya University, *Ballari.* I am submitting this thesis for the award of the degree of Doctor of Philosophy in Chemistry, of Vijayanagara Sri Krishnadevaraya *University*, Ballari.

I further declare that this thesis or any part of it has not been submitted elsewhere for any other department or diploma, Degree, Associateship or any other similar title to any other University/Institution.

Research Scholar

Place: Ballari   **(Obaiah G O)**

Date:

Dr. K. H. Shivaprasad, M.Sc., Ph.D.
Professor, Dept. of Chemistry
Vijayanagara Sri Krishnadevaraya University,   **Mobile:** +91 9886433203
Ballari - 583105, Karnataka, India.   **Email:** khsprasad60@gmail.com

Certificate

This is to certify that the work reported in this thesis entitled

"*Synthesis, Characterization and Catalytic Applications of Doped Metal*

Oxides" is the result of research work carried out by **Mr. Obaiah G O,** in

the Department of Studies in Chemistry/Industrial Chemistry,

Vijayanagara Sri Krishnadevaraya University, Ballari, under my guidance

and supervision. He is hereby permitted to submit the same to the

Vijayanagara Sri Krishnadevaraya University, for the award of **DOCTOR**

OF PHILOSOPHY IN CHEMISTRY.

The material presented in this thesis has not been previously formed

the basis for the award of any Degree, Diploma or such other similar title.

Place: Ballari   (**Dr. K. H. Shivaprasad**)

Date: **Research Guide**

ACKNOWLEDGEMENTS

encouraging me in all of my pursuits and inspiring me to follow my dreams.

CONTENTS

LIST OF TABLES

LIST OF FIGURES

Introduction, Materials & Methods

<div align="right">**CHAPTER-1**</div>

1.1 INTRODUCTION

The catalysts are useful in catalysis, environmental science, biochemistry, electronics, and biomedical science. For example, TiO_2 anatase exhibits highly demanding photocatalytic activity. A large bandgap (3.2 eV) restricts its application as quickly as a control addict. TiO_2 is a suitable photocatalyst for its cost-effective performance, its high stability, and its high potential for degradation in a wide variety of materials. TiO_2 is a great significance, and the photoactivity of TiO_2 is the ability to separate water from sunlight. Responses to the improvement of Photo TiO_2 properties have been investigated using different ion and non-metallic ions and utilize in other experiments. CeO_2 is known to be inactive and reactive under high temperatures. TiO_2 and CeO_2 are the most important derivatives. There are numerous reports on the preparation, processing, and properties of mixed CeO_2-TiO_2 oxides. CuO, TiO_2, CeO_2, and ZnO, nanoparticles (NPs) are the first nanoscale products utilized in pharmacies. The TiO_2 and ZnO are now used on cosmetics and sunscreen [1, 2] and are being used to improve TiO_2 heat exposure as a fuel-based impudence [2, 3]. These blends showed a great deal of potential for solar-powered projects, such as those seeking different services, as well as those using water and property. Nano metal oxides make up the essential properties of inorganic nonmaterials. Metal oxides exhibit optical, electrical, magnetic, and mechanical properties [2]. Nano metals such as TiO_2, ZnO, CeO_2, ZrO_2, etc. have been studied. For example, a useful metal band of catalysts, environmental science, electronics, electronics, and biomedical science [4, 5], TiO_2 anatase exhibits good photocatalytic activity [6]. Still, its large bandgap (3.2 eV) limits its application as a dielectric photodetector. CeO_2 is known to be

inactive and reactive under extreme temperatures [7 8]. These semiconductors can produce differential photocatalysis processes and even more photosensitive lead. The dopants include anion, cations, and ions. The content of dopant changes the interfacial transfer rate; this affects the e- / h+ link rate or reduces the open area of the photocatalyst doped. Besides, it is essential to maintain a level of concentration to prevent the creation of new drugs. The dopants commonly utilized to impregnation, co-precipitate, and sol-gel method. To activate TiO_2 in the visible light, anionic anions and cations are used to replace oxygen and TiO_2 to close the bandgap. However, high-valence valence (VB) stimulation results not only in the narrowing of the bandgap but also in the reduction of "oxidizing" holes. In the meantime, the electromagnetic-field potential is too high.
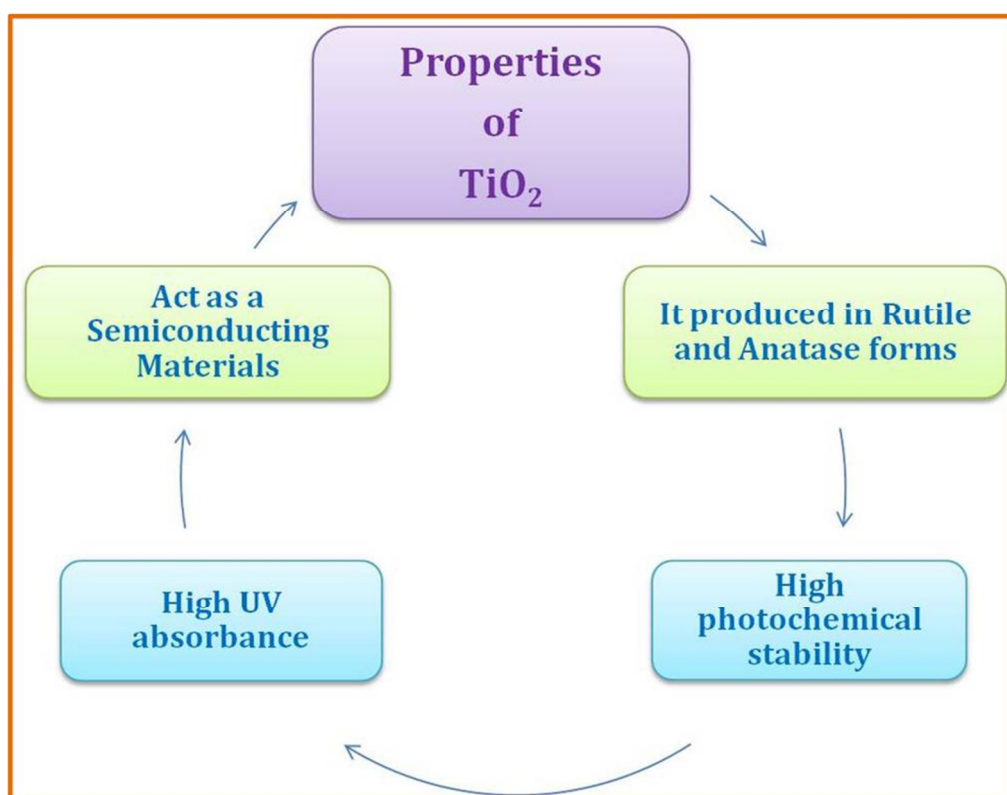
Fig.1.1: The properties of TiO_2

The change from photocatalytic activity by the addition of p-type metal ion dopants is due to the difference in the energy-adsorption, the adsorption capacity of the substrate, as well as free TiO_2 photocatalyst transfer. As the ion is added to the TiO_2 lattice, the pure energy level is added to the TiO_2 bandgap, and the magnetic field is reduced. Loadings nanoparticles include sol-gel method [9, 10], mechanical mixtures [11 12], chemical adsorption [13], water precipitation reduction [14], and photoelectronic deposition [15-16]. There have been reports of metals such as Pt, Pd, Ag, Au, Rh, Cu, and Ni for metallic coating. The ceramic cordierite monolith $(2MgO_2Al_2O_{35}SiO_2)$ is a substrate utilized in many applications and several wonderful properties, including low humidity, high lightness, and heat shock resistance, excellent numerical retention, good porosity, complete rotation, and small absorption properties [17-18], therefore, a unique method to apply materials that display energy and water. Monolithic buildings manufactured in the 1960s and 1970s because they have excellent features such as allowing high gases from low continents, low viscosity, upper surface area, short wavelength, low energy.
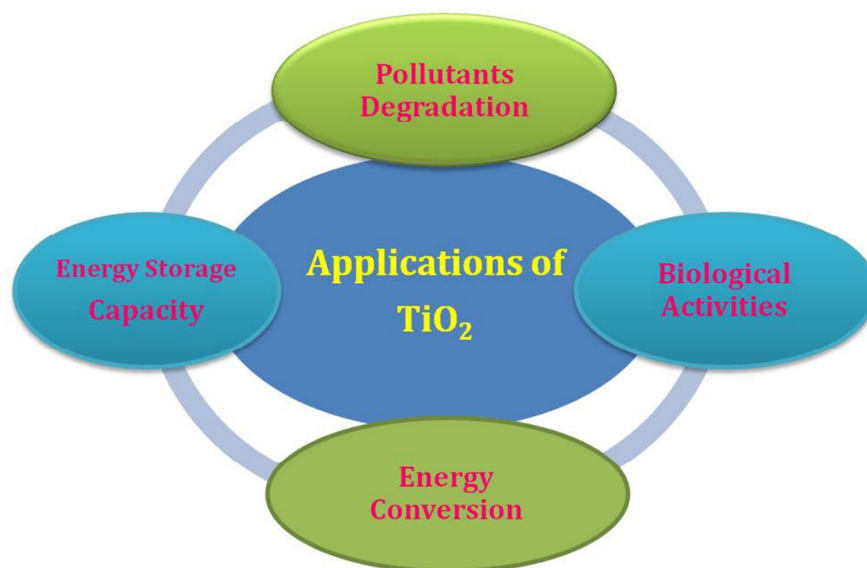
Fig.1.2 : The application of TiO_2

At higher altitudes, higher storage capacity, greenhouse gas emissions, as well as warming various approaches for the synthesis of ceramic monolithic [19-20]. Luca et al. [21] and Lachmann et al. [22–25] Nijhuis et al. [26], the mental transformation is a good explorer catalytic test. In general, ceramic composites are being used ($Mg_2Al_4Si_5O_{18}$), which is stable at least $1000°C$, and contributes to low space quality [27]. There are several techniques for applying to the coating on ceramic monolith coatings, i.e., colloidal coating [28], Sol-gel coating [29], and slurry coating [30]. TiO_2 has been the 'standard model' in mind for this application in terms of light. In 2009, the photosynthetic degradation of methylene was demonstrated under sunlight using TiO_2-based CeO_2 are shown in a 'semiconductor' system [31]. Here, the CeO_2 support layer provides visible photons (due to the increase of Ce^{3+} at the grain surface) and transmits the electronic effects on TiO_2 due to its dominant barrier mechanism. New evidence has shown that Ce^{3+} and CeO_2-TiO_2 compounds show increased molecular weight (MMO) complexes and Ce-4f complexes that contribute to TiO_2 release, reducing bandgap strength [32]. All the photocatalysts, TiO_2 was found to be the leading photocatalyst for environmental degradation due to the potential of oxidizing under ultraviolet irradiation, chemical soil, and other materials.

On the other hand, for pure TiO_2 interface with the application for broadband (e. g. 3.2 eV for TiO_2). Only the UV part of sunlight can activate wind power and this will cause electronics to fall off the influence of bandwidth and primitive of TiO_2. Also, UV radiation supplies 5% of the total solar power available worldwide. So the most solar power is lost [34-36]. To promote TiO_2 applications in photocatalysis, you need to increase the receptor surface in the optical region and reduce the concept of two electronics. Various technologies such as doping with metal/non-metallic

substances have been tested [37], the use of various substrates/support or TiO_2 components [33], oxygen reduction [38], and TiO_2 structures, etc. radiation prediction tested for TiO_2 form by the selection of significant photocatalytic activity for sunlight.

In recent years, the application of TiO_2 to environmental cleaning using solar energy has been another area of concern for TiO_2 research [39, 40]. The benefits of using TiO_2 as a photocatalyst are highly sought after and include low cost, environmental compatibility, and photography. However, the spectrum (3.0– 3.2 eV) prevents TiO_2 from performing the necessary functions, Adsorption of Pd, Cu, Pt, and Rh to CeO_2 published a significantly higher activity than the other [41-46]. The interaction of positive ion with CeO_2 support has played an essential role in catalytic reactions in descending energy conditions. OSC-mediated energy, known as the signaling factor of CeO_2, acts as an oxygen molecule in redox reactions. Replacing Noble metals with CeO_2 promotes a reduction in support at low temperatures. However, the amount of reactive oxygen species involved in the redox reaction is insufficient in CeO_2 in our recent study [47].

The substitution of Pd^{2+} ions for Ce^{4+} in nano CeO^2 particles can lead to the highest possible dispersion for a given loading of Pd and higher chemical and structural stability of Pd^{2+} ions because of the oxygen bonded to Ce^{4+} ions in the CeO_2 matrix. In the past few years, extended X-ray absorption fine structure (EXAFS) analysis has been used extensively for probing the local structure and identification of the active species of Pd supported on Al_2O_3, niobium, $LaAl_2O_3$, zeolite, and carbon materials. [48-54]. this is a potentially important source of NPs contamination due to wash-off from individuals into the environment, which can contaminate water and

soil. TiO_2 Nps is also useful for the treatment of wastewater [55]. Cerium oxide (CeO_2) Nps can act as oxygen sensors and fuel additives to improve the efficiency of combustion [56], and they can also reduce oxidative stress in biological systems as a free radical scavenger [57]. Other metal oxide Nps includes aluminum oxide (Al_2O_3), Cerium oxide (CeO_2) and its related materials have been extensively studied and applied in energy conversion and pollution control [1–9], owing to their good chemical and physical stability, high oxygen mobility, and special optical properties. CeO_2 is a cheap and environmentally friendly photocatalyst for the degradation of some organic pollutants [58–62]. However, its photo catalytic efficiency is still not desirable due to low light absorption efficiency and a high recombination rate of photogenerated electron-hole pairs [63, 64, and 65]. It is, therefore, crucial to explore the novel CeO_2 photocatalytic system with high efficiency and stability. CeO_2 has are a particularly effective catalyst, in part due to the redox potential of the Ce^{4+}/Ce^{3+} couple, as well as its resistance to chemical and photo corrosion, and strong light absorption in the UV region (absorption edge,385–400 nm). Unfortunately, the large bandgap (3.2 eV) limits the further application of CeO_2 [66–67]. Among heterogeneous photocatalysts, cerium dioxide (CeO_2) is one of the most efficient due to its effectiveness in degrading the organic pollutant compounds in water. However, the narrow bandgap of CeO_2 (3.0–3.4 eV) has limited its photocatalytic efficiency by the recombination of photoexcited electron/hole pairs during light irradiation [68–70]. Therefore, it is necessary to inhibit this process by doping with metal ions, which can create impurity levels in the band structure of CeO_2 for a charge–carrier trapping and significantly reduces the electron-hole recombination rate as well as subsequently supporting the redox reactions on the surface of photocatalysts [72–74]. Doping with

metal ions such as palladium ions has been considered a potential applicant is owing to the energy level of Pd^{2+}/Pd^{3+} and Pd^+/Pd^{2+}, which may act as shallow trapping for electron or hole depending on the position of the Fermi level and their occupancy [71].

This work aimed to modify undoped TiO_2 and CeO_2 by doping with Pd ions using different weight percentages (0.5, 1.0, 1.5, and 2.0 wt %) with homogeneous precipitation, impregnation, and calcinations methods. The structural, optical, and morphological properties of CeO_2 due to the Pd dopant were investigated by XPS, XRD, FESEM/EDS, and PL methods. The photocatalytic activity of bare CeO_2 was compared with Pd–doped CeO_2 over the degradation of methyl orange (MO) as the model organic pollutant under visible light. One approach to producing strongly luminescent nanoparticles is to inject small quantities of dopants like transition metal elements. Accordingly, some transition metal ion dopants such as Fe, Mn, Ti, Pd, and Co have been identified for the magnetic, optical, and photocatalytic properties of the CeO_2 nanoparticles [75]. Photocatalytic degradation is one of the unique green chemistry technologies to treat the dyes due to its nontoxicity, inexpensive, and harm-less by-products. However, to the best of our knowledge, the use of CeO_2/alumina nanocomposite as a photocatalyst to degrade dye has not been reported yet. Photocatalysis has produced great concerns a promising technique in treating environmental deterioration and utilizing light energy [76–79]. CeO_2 is one of the most important semiconductors with a bandgap of 3.1 eV [80–82] and exhibit excellent activity to degrade dyes. In this paper, a wet chemical synthesis method has been adopted to prepare CeO_2 nanocubes, and it was characterized in detail, moreover synthesized CeO_2 nanocubes show

excellent photocatalytic activity to degrade dyes. We have been pursuing the plan of noble metal ions as the active sites for catalytic oxidation-reduction reactions [83].

Noble metal ions are stabilized by the substitution of noble metals in reducible oxides such as CeO_2 forming single-phase $Ce_{1-x}MxO_{2-\delta}$ (M=Ru, Rh, Pd, Pt). [83] Pd-substituted CeO_2 has been studied for the activation of C−H bonds in CH_4 [84]. TiO_2 is nontoxic reducible oxide support, and noble metal ions can be substituted in TiO_2. Indeed, $Ti_{1-x}Pd_xO_{2-x}$(x=0.01) where Pd is in the +2 oxidation state showed high rates of NOx reduction by CO, [85] High rates of hydrogen−oxygen recombination at 40−50 °C, [86] and good photocatalytic activity for CO oxidation. [87].
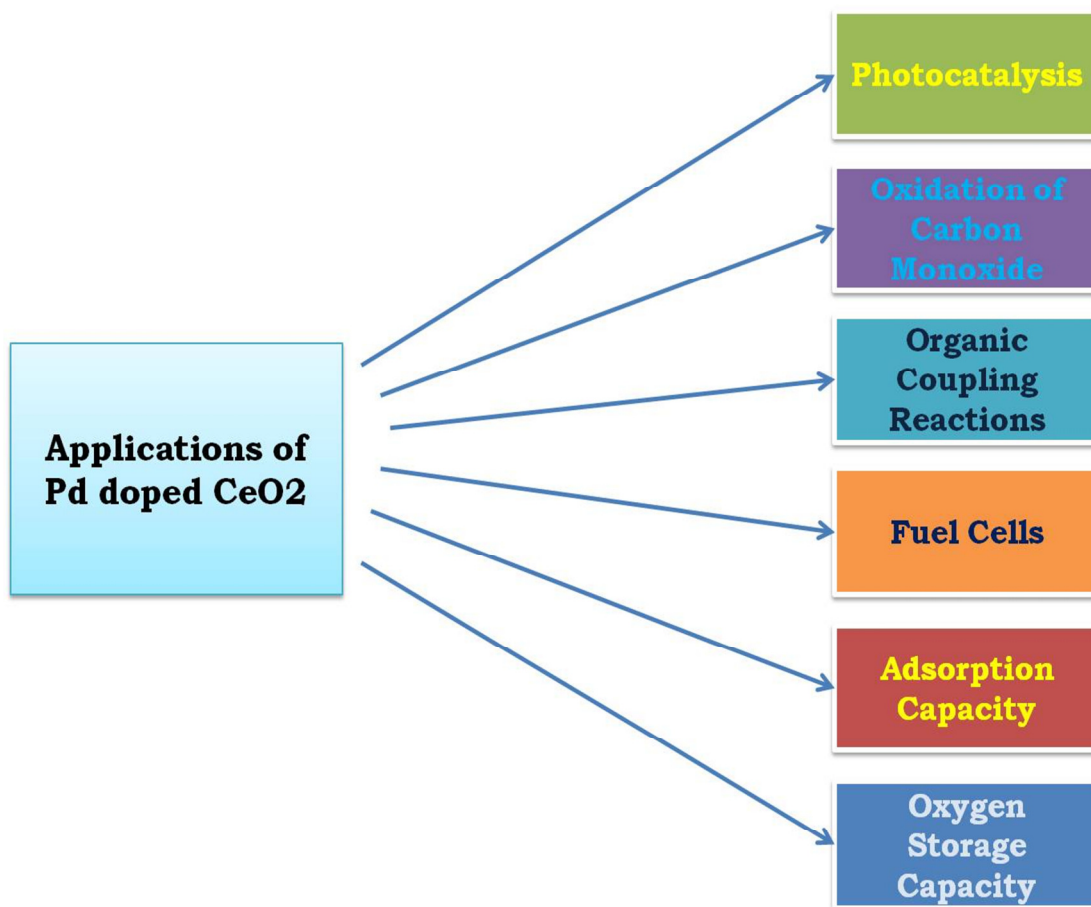
Fig.1.3 : The application of Pd doped CeO_2

Among organic pollutant compounds, the organic AZO dye, such as Congo red (CR), is one of the most widely used in almost all these industries? Dyes photocatalytic degradation is an effective and distinguishable process for dye removal from waste and freshwater. Along with the last few decayed, the photocatalysis process using semiconductors has attracted much great attention since it offers eco-friendly and economic features [88-90]. Catalysts play a vital role in the further application of catalytic combustion technology. In particular, noble metal catalysts, such as Pt and Pd, show high activities for the oxidation of VOCs [91]. However, an extremely high cost and susceptibility to deactivation limit their application in industry. In recent years, many efforts have been devoted to the development of more efficient, stable, and cheaper non-noble metal oxides [92-93]. Metal oxides have attracted increasing attention as potential oxidation catalysts owing to their unique redox properties and high oxygen storage capacity [94]. It is well known that CeO_2 can form oxygen vacancies in the surface or bulk, thus providing lattice oxygen for catalytic combustion reactions. It is well known that CeO_2 can form oxygen vacancies in the surface or bulk, thus providing lattice oxygen for catalytic combustion reactions. Moreover, CeO_2 can store or release oxygen through the cycle of oxidation-reduction between Ce^{4+} and Ce^{3+} [95-97], Showed that Pd^{2+} and CeO_2 are dissociated with a high activity of dissolved dispersions in CeO_2. Pd^{2+} ion is higher dispersed than Al_2O_3.

In general, the effects of metal oxides on the therapeutic impact of microorganism species are at work as well as experimental conditions. However, there is important information that the potential of MONPs is in the process of anaerobic oxidation of ammonium (anammox) (Amiri et al., 2017; Ansari et al., 2018;

Nazari et al., 2017; Peternel et al., 2007; Zhang et al., 2015). Therefore, this study required investigating the molecular dynamics of the four MONPs (TiO_2, Al_2O_3, CO_2, and CO_2) and the Amemix system, and this involves transparency. First, analysis of the deletion of Marmoset rats revealed MONPs at different levels. Using photocatalytic techniques to remove impurities and these substances can lead to destruction not only of cosmetics. In different photocatalysts, titanium dioxide (TiO_2) is widely utilized for low cost, high chemical stability, non-toxicity as well as environmental control. In photocatalysis, TiO_2 has Ultraviolet (UV) light to remove electron-holes from a track (Subramanian et al., 2017). One limitation is that the TiO_2 band gap is substantial (~3.2), which means TiO_2 is only driven within UV light limits. Also, higher conversion rates in men result in lower results in addition to photoelectric performance, even leading to TO_2 photo-response in UV regions. TiO_2 inhibitors and fine metals such as Pt, Pd, and non-contrast properties and high stability (Banerjee et al., 2016) are utilized to improve phenolic power at a faster pace. Another useful idea is published in this article, which is unacceptable. Additionally, this metal can act as an electron transport site, thus increasing photo-based $TO2$ activity. Palladium (Pd) is a popular metal with a new character; For example, it's the best tool for having a bull as support. Previous research has shown that photo-component activity in Pd doped TiO_2 affects the crystal formation and appearance of Pd. Pd doped TiO_2 is considered to be very efficient (Li et al., 2008). On the other hand, the chosen nano-postulate can avoid damage to the problem, while the brakes and nanotubes can be recovered. Agglomeration can be controlled by modification of TiO_2 nanoparticles while chitosan is present (Abdelaal and Mohamed, 2013). However, the bandwidth of the TiO_2 is 3.2 eV, requiring waves <387.5 nm,

and their solar power is not limited so that 4% of the total solar energy is utilized. Thus, high development, non-toxic, and chemical applications are required under radiation. Semiconductor (Sangami and Dharmaraj, 2012), provides support such as CO_2 (Yongchuan et al., 2014), those metal chalcogenides have investigated for environmental applications. However, their use is mainly due to their low chemical activity in sunlight, photo- and chemical death, as well as resistance to toxic substances. The photocatalytic activity of CO_2 has been investigated; Broadband gap energy and electric energy and the presence and vibration of this film prohibit photographers from using solar power.

Various techniques have been adopted in water systems for handling various materials, including sample filters as well as colloidal or semiconductor colloidal polymers (Bian et al., 2008). Therefore, image enhancement by population size has always been a problem among researchers. Different ways of metals and copper are contaminated with toxic metals, toxic metals, among them, and to be found on gold levels, specific activity, which reflects a high risk for such reactions. Moreover, the adsorption and catalytic activity of metals are present in potential solutions. Various transformations have been reported for catalytic oxidation of alcohols as metallic and metallic oxide-based catalysts, of which mixed metallic oxide nanocatalysts are very effective, which has shown great catalytic activity for this national reaction. Accordingly, it has been widely reported that the catalytic activity of doping with other elements of the mixed metal oxide nanocatalyst (Fu et al., 2003; Siddiqui et al., 2012; Adil et al., 2015; Alabbad et al., 2013). Metal oxide nanoparticles (MONPs) such as titanium dioxide (TO_2), cerium dioxide (CO_2), aluminum oxide (Al_2O_3) and silicon dioxide (SiO_2) are widely used in commercial and industrial products due to

their optical, catalytic, and antibacterial properties (Li et al., 2017a; Mu et al., 2011). TO_2NPs have been widely used in catalysts, cosmetics, paints, sunscreens, and plastics (Mu et al., 2011). Al_2O_3 NPs catalysts are widely applied to sunscreens and additives in paints, rubber, and plastics. CeO_2NPs have has been widely used as a corrosive, ultraviolet absorber, and fuel additive (Ma et al., 2013; You et al., 2017).

1.2 MATERIALS AND METHODS

All the chemicals and reagents used for the research work were of different standard grades and purchased from different suppliers. Aromatic nitro compounds, different solvents such as ethanol, methanol and n-butanol, Aryl halides (Iodobenzene and Bromobenzene), and amines (aniline) were used as purchased without further purification, TLC plates and cordierite monolith honeycomb were procured from Merck. The important chemicals used for the preparation of oxides, metal oxides, and doped metal oxides by using solution combustion method given in the below Table.1.1

Table 1.1

Name/ Molecular formula	Specification	Suppliers
Titanium tetra (IV) isopropoxide (Ti $(OC_3H_7)_4$)	Molar mass: 284.22 g/mol Density: 0.96 g/cm3	Sigma-Aldrich
Cerric ammonium nitrate $(NH_4)_2Ce(NO_3)_6$	Molar mass: 548.26 g/mol Density: 1.14 g/cm3	Sigma-Aldrich
Palladium chloride $(PdCl_2)$	Molar mass: 177.33 g/mol Density: 4 g/cm3	Sigma-Aldrich
Glycine (NH_2CH_2COOH)	Molar mass: 75.07 g/mol Density: 1.61 g/cm3	Merck

The different glass wares used for the synthesis and experimental purpose were cleaned by using chronic acid followed by soap water and finally distilled water. The glassware was dried in a hot oven before and after the use. Double distilled water was used for the preparation of dye solution and washed for several reaction yields.

1.3 SYNTHESIS OF METAL OXIDES AND DOPED METAL BY USING SCS

The single-phase compounds have been synthesizing. The combustion way [98] was carried out exothermic redox reaction of an aqueous solution containing the stoichiometric amount of an oxidizer such as metal nitrates in fuel, which are the so-called nitrogen atoms. The stoichiometric mixture of the oxidizer and fuel is slower at 350 ^{O}C to 450 ^{O}C. After a complete wet cleaning of the reaction mixture, the residue is heated, brightening. The flame lasted for 10-20 min. The first approach is to:

a)   The benefits of a liquid phase such as the stoichiometry of substituting the electrons of the dopant atom.

b)   The use of a particle and c) the potential of a single-phase.

d)   It initiated a low-level process.

e)   The redox reaction was highly variable.

f)   It propagated itself.

g)   Changes in air mass, surface area. Local, acquired, and collaborative products,

h)   Metastable systems.

i)   This process is simple, fast, and economical [99-102].

K.C provided a dissemination program. Patil and co-workers to use dye socks to thicken heavy clay socks and make good oil from. The stoichiometric composition of

the oxidizer and the oil for Wood is calculated based on oxidation and reduces the velour of the 'fuel' (F) of the oxidation. The condition of the oxidation of the that produces the oil is unity, and the reaction to the heat is the highest [103].

Based on the basic assumptions of synthetic chemistry, ion, carbons and hydrogen's are considered to be minimizing valencies + M (valency of metal ion compound), +4, and +1 respectively united. The valency of nitrogen (N) is found to be negligible Due to the transformation of molecular nitrogen (N_2) during oxidation reactions, and oxygen valency (O) is -2. Based on the total oxidizing valency of metal nitrates, M (NO_3)$_2$ and reduced the valency of Glycine ($C_2H_5NO_2$). In this chapter, we will use Titanyl nitrate to synthesize (O) and Glycine as a fuel (F). The ratio of O / F. can calculate the synthesis of nitrate metal in the fuel. The nitrates are similar to -10 oxidizing, +9 reducing the value in the reaction mixture. The solvent was transferred into a muffle towel at 350-350 ^{o}C initially, the resulting liquid is sulfur and foam followed by a fire, and the combustion produces a solid product that works in two minutes. Due to the extremely high temperature and the resulting combustion, heavy metal oxides are formed. The mechanical properties of the complex material are minimized because of changes in the range of motion and humidity.
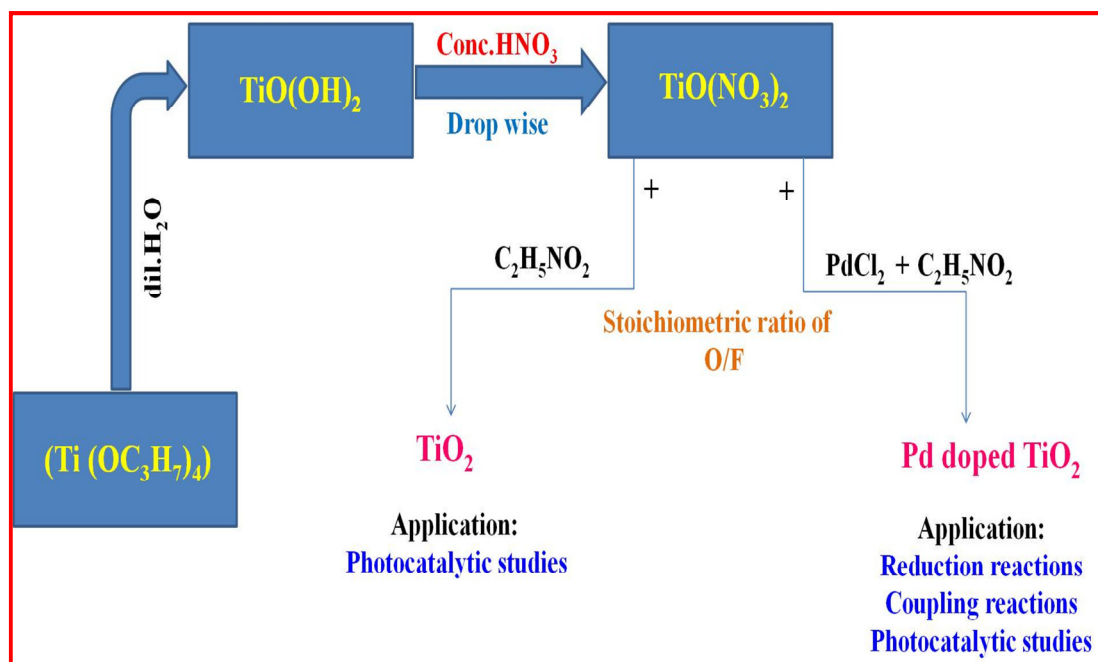
Fig.1.4 : Flowchart for the synthesis of TiO_2 and Pd doped TiO_2 by using solution combustion method
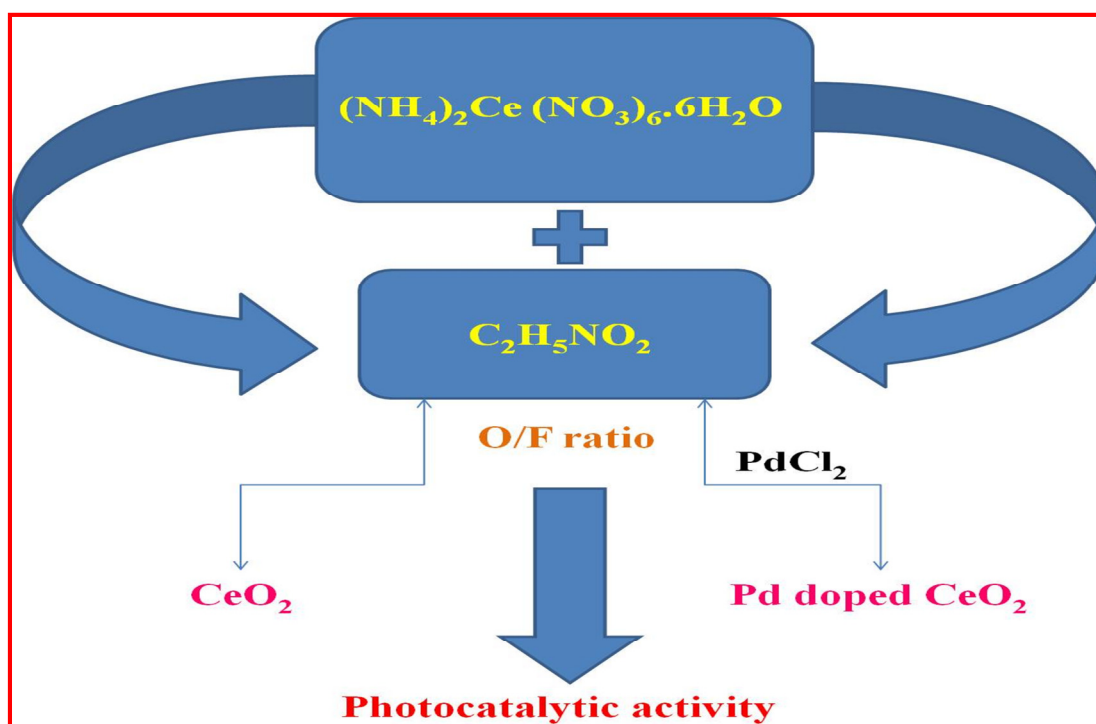
Fig.1.5 : Flowchart for the synthesis of TiO_2 and Pd doped TiO_2 by using solution combustion method

1.4 INSTRUMENTS USED FOR THE CHARACTERIZATION OF METAL OXIDES AND DOPED METAL OXIDES

Synthesized metal oxides and doped metal oxides were characterized by PXRD, FT-IR, XPS, FE-SEM, NMR studies.

1.4.1 Powder X-Ray Diffraction Analysis (PXRD)

Bruker D_2 Advance X-ray diffraction machine Principle: X-ray diffraction (XRD) experiment involves the scattering of a monochromatic X-ray beam from the surface of a sample and measurement of surface reflectivity or determination of the diffraction pattern.

Fig.1.6 Diffraction of X-rays in a Diffractometer.

1.4.2 FT-IR Spectroscopy

FTIR- Perkin Elmer Spectrum-Two spectrophotometer, Range: (I.R.) 4000—400 cm^{-1}, the operating conditions are: 4000 - 400 cm^{-1} spectral width, 32 accumulations, 1 gain and 4 cm^{-1} resolution.

Pellet Press Method: Techno search Instrument **Model:** KBr press model -16

Fig.1.7 : Image of FT-IR Instrument and pellet press accessories.

1.4.3 SEM and Energy Dispersive X-Ray Spectroscopy

S.E.M. micrographs of the fractured surface of the tested specimens are obtained using the "Hitachi SU1500" S.E.M. instrument (Fig. 1.8).

Fig.1.8 : Oxford instruments E.D.S. Spectroscopy.

1.4.4. Thermogravimetry Analysis (TGA)

STA 6000 machine from ambient to 700 ^{o}C at a heating rate of 10 ^{o}C min^{-1} and with a flow rate of air at 30 mL min^{-1}. Differential scanning calorimetry (D.S.C.) (Model- Mettler DSC-823, Temp range: 25°C to 500°C).

Fig.1.9 : TGA instrument.

1.4.5. N.M.R. Studies

a)   N.M.R. spectroscopy Make & Model: ^{1}H N.M.R. spectra were recorded on Bruker AMX-400 for the synthesized metal oxides and doped metal oxides. The ^{1}H NMR and ^{13}C NMR spectra were recorded on an AMX-400 MHz spectrometer using $CDCl_3$ as the solvent and TMS as an internal standard.

Fig.1.10 : Schematic representation of N.M.R. spectrometer.

1.4.6. UV-Visible Spectroscopy

Model: Shimadzu Solid UV-1800 spectrophotometer instrument.
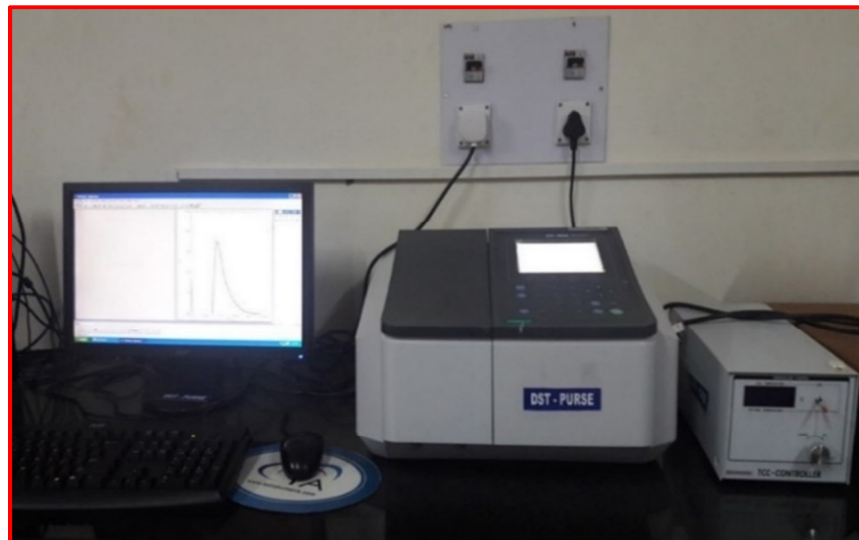
Fig.1.11 : Shimadzu Liquid UV-1800 spectrophotometer instrument.

1.4.7. XPS Instrument

Fig.1.12 : Shimadzu Solid UV-1800 spectrophotometer instrument.

1.4.8. Gas Chromatography
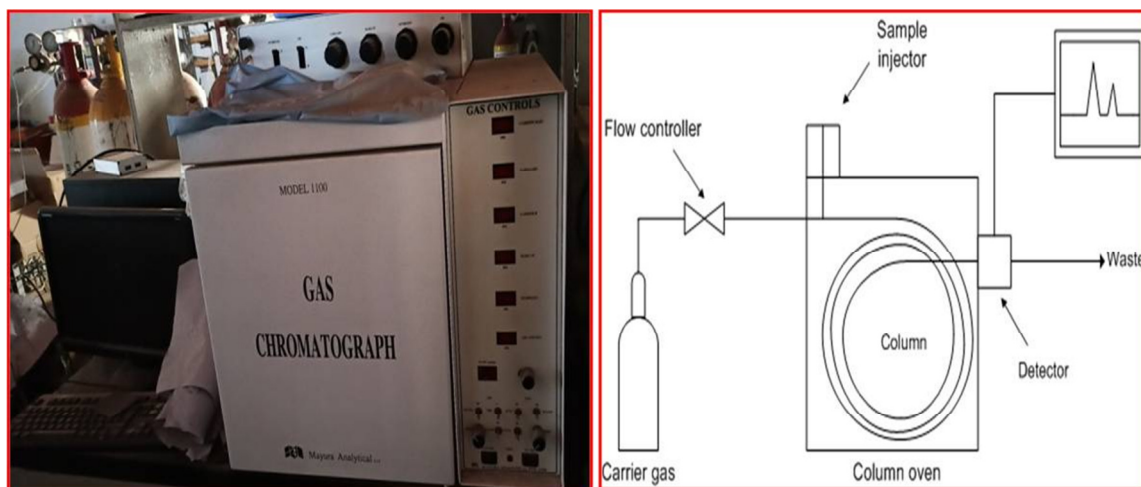
Fig.1.13 : Gas chromatography instrument with a schematic diagram

1.4.9. UV-Cabinet
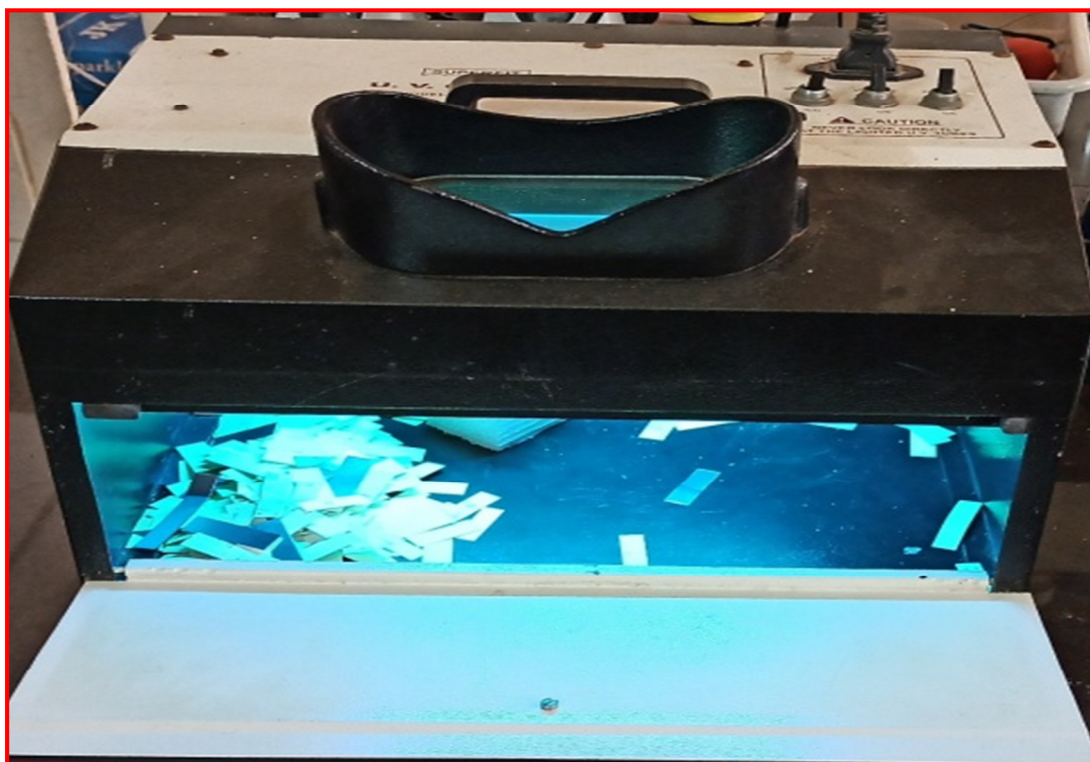
Fig. 1.14 : UV cabinet

1.4.10 Rotary Evaporator

Fig.1.15 : Rotary evaporator

References

[1]   Anselmann, R Nanoparticles, and nanolayers in commercial applications J Nanopart Res (2001), 3, 329–336.

[2]   Klaine, S J; Alvarez, P J J; Batley, G E; Fernandes, T F; Handy, R D; Lyon, D Y; Mahendra, S; McLaughlin, M J; Lead, J R Nanomaterials in the environment: behavior, fate, bioavailability and effects Environ Toxicol Chem (2008), 27 (9), 1825–1851

[3]   Jung, H; Kittelson, D B; Zachariah, M R The influence of a cerium additive on ultrafine diesel particle emissions and kinetics of oxidation Combust Flame (2005), 142, 276–288

[4]   J Ameta, A Kumar, R Ameta, V K Sharma, S C Ameta, Synthesis and characterization of $CeFeO_3$ photocatalyst utilize in photocatalytic bleaching of gentian violet, J Iran Chem Soc, 6 (2) (2009) 293-299.

[5]   K Nagaveni, M S Hegde, N Ravishankar, G N Subbanna, G Madras, Synthesis and structure of nanocrystalline TiO_2 with lower bandgap showing high photocatalytic activity, Langmuir, 20 (2004) 2900-2907

[6]   Carp, O; Huisman, C L; Reller, A Prog Solid State Chem (2004), 32, 33

[7]   Kaspar, J, Fornasiero, P Eds Catalysis by Ceria and Related Materials; Imperial College Press: London, (2002)

[8]   Trovarelli, A Catal ReV. Sci Eng (1996), 38, 439

[9]   Moon, S C, Mametsuka, H, Suzuki, E, & Nakahara, Y (1998) Characterization of titanium-boron binary oxides and their photocatalytic activity for stoichiometric decomposition of water Catalysis today, 45(1), 79-84

[10] Antonelli, D M, & Ying, J Y (1995) Synthesis of hexagonally packed mesoporous TiO_2 by a modified sol-gel way Angewandte Chemie International Edition in English, 34(18), 2014-2017

[11] Vorontsov, A V, Savinov, E N, & Zhensheng, J (1999) Influence of the form of photo deposited platinum on Titania upon its photocatalytic activity in CO and acetone oxidation Journal of Photochemistry and Photobiology A: Chemistry, 125(1), 113117

[12] Ohtani, B, Kakimoto, M, Nishimoto, S I, & Kagiya, T (1993) Photocatalytic reaction of neat alcohols by metal-loaded titanium (IV) oxide particles Journal of Photochemistry and Photobiology A: Chemistry, 70(3), 265-272

[13] Chen, J, Ollis, D F, Rulkens, W H, & Bruning, H (1999) Photocatalyzed oxidation of alcohols and organ chlorides in the presence of native TiO_2 and metalized TiO_2 suspensions Part (I): photocatalytic activity and pH influence Water Research, 33(3), 661-668

[14] Chan, S C, & Barteau, M A (2005) Preparation of highly uniform Ag/TiO_2 and Au/TiO_2 supported nanoparticle catalysts by photodeposition Langmuir, 21(12), 5588-5595

[15] Behnajady, M A, Modirshahla, N, Shokri, M, & Rad, B (2008) Enhancement of photocatalytic activity of TiO_2 nanoparticles by silver doping: photo deposition versus liquid impregnation ways Global NEST Journal, 10(1), 1-7

[16] Jacobs, J W M, Kampers, F W H, Rikken, J M G, Bulle☐Lieuwma, C W T, & Koningsberger, D C (1989) Copper photodeposition on TiO_2 studied with HREM and EXAFS Journal of the Electrochemical Society, 136(10), 2914-2923

[17]   A Bueno-López, D Lozano-Castelló, I Such-Basáñez, J García-Cortés, M Illán-Gómez and C S -M De Lecea, Appl Catal, B, (2005), 58, 1-7

[18]   J L Williams, Catal Today, (2001), 69, 3-9

[19]   Gulati S T (1998) In Ceramic catalyst supports for gasoline fuel A Cybulski and J A Moulijn (Ed) (New York: Marcel Dekker) p 15

[20]   Elmer T H (1976) Ultra-low expansion ceramic articles U S Patent 3958058 A

[21]   Luca J P D and Lampbell L E (1977) In Advanced materials in catalysis (New York: Academic Press)

[22]   Lachmann I M (1986) Ceramic honeycombs for catalysis and industrial applications Sprechsaal 119, 1116

[23]   LachmannIMandMcNallyRN1981Hightemperature monolithic supports for automobile exhaust catalysis Ceram Eng Sci Proc 2 337

[24]   Lachmann I M and McNally R N (1985) Monolithic honeycomb supports for catalysis Chem Eng Progr 18, 29

[25]   Lachmann I M and Willians J L 1992 Extruded monolithic catalyst supports Catal Today 14 317

[26]   Nijhuis T A, Beers A E W, Vergunst T, Hoek I, Kapteijn F, and Moulijn J A (2001) Preparation of monolithic catalysts Catal Rev Sci Eng 43 345

[27]   Boger T, Heibel A K and Sorensen C M (2004) Monolith IC catalysts for the chemical industry Ind Eng Chem Res 43, 4602

[28]   Beauseigneur P A, Lachmann I M, Patil M D, Swaroop S H and Wusirika R R (1994) Pore impregnated catalyst device U S Patent 5334570

[29] Zwinkels M F M, Jaras S G and Menon P G (1995) Preparation of combustion catalysts by wash coating alumina whiskers-covered metal monoliths using a sol-gel way Stud Surf Sci Catal 91, 85

[30] Blachou V, Goula D and Phillippopoulos C (1992) wet milling of alumina and preparation of slurries for monolithic structures impregnation Ind Eng Chem Res 31,364

[31] G Magesh et al Indian J Chem (2009), 48A, 480-88

[32] S Kundu et al J Phys Chem (2012), 116, 14062-70

[33] B Shrikanth, R Goutham, R Badri Narayan, A Ramprasath, K P Gopinath, A R Sankaranarayanan, Recent advancements in supporting materials for immobilized photocatalytic applications in wastewater treatment, J Environ Manage 200 (2017), 60–78, https://doi org/10 1016/j jenvman 2017 05 063

[34] V Likodimos, Photonic crystal-assisted visible light-activated TiO_2 photocatalysis, Appl Catal B Environ 230 (2018) 269–303, https://doi org/10 1016/j apcatb 2018 02 039

[35] H Abdullah, M R Khan, H R Ong, Z Yaakob, Modified TiO_2 photocatalyst for CO_2 photocatalytic reduction: an overview, J CO_2 Util 22 (2017) 15–32, https:// doi org/10 1016/j jcou 2017 08 004

[36] S Varnagiris, M Urbonavicius, S Tuckute, M Lelis, D Milcius, Development of photocatalytically active TiO2 thin films on expanded polystyrene foam using magnetron sputtering, Vacuum 143 (2017) 28–35, https://doi org/10 1016/j vacuum 2017 05 031

[37] M Pelaez, N T Nolan, S C Pillai, M K Seery, P Falaras, A G Kontos, P S M Dunlop, J W J Hamilton, J A Byrne, K O'Shea, M H Entezari, D D Dionysiou, A review on the visible light active titanium dioxide photocatalysts for environmental applications, Appl Catal B Environ 125 (2012) 331–349, https://doi org/10 1016/j apcatb 2012 05 036

[38] W Fang, M Xing, J Zhang, Modifications on reduced titanium dioxide photocatalysts: A review, J Photo chem Photo biol C Photochem Rev 32 (2017) 21–39, https://doi org/10 1016/j jp hotochemrev 2017 05 003

[39] A L Linsebigler, G Lu, John T Yates, J Chem Rev 95 (1995) 735

[40] M R Hoffmann, S T Martin, W Choi, D W Bahnemannt, Chem Rev 95 (1995) 69

[41] P Bera, KC Patil, V Jayaram, G N Subbanna, and MS Hegde, J Catal 196, 293 (2000)

[42] K R Priolkar, P Bera, P R Sarode, M S Hegde, S Emura, R Kumashiro, and NP Lalla, Chem Mater 14, 2120 (2002)

[43] P Bera, K R Priolkar, P R Sarode, M S Hegde, S Emura, R Kumashiro, V Jayaram, and NP Lalla, Chem Mater 14, 3591 (2002)

[44] P Bera, K R Priolkar, A Gayen, P R Sarode, M S Hegde, S Emura, R Kumashiro, V Jayaram, and G N Subbanna, Chem Mater 15, 2049 2003

[45] A Gayen, K R Priolkar, P R Sarode, V Jayaram, M S Hedge, G N Subbanna, and S Emura, Chem Mater 16, 2317 (2004)

[46] P Bera, A Gayen, M S Hegde, N Lalla, L Spadaro, F Frusteri, and F Arena, J Phys Chem B 107, 61222003

[47] Bera, P; Patil, KC; Jayaram, V; Subbanna, G N; Hegde, M S J Catal (2000), 196, 293

[48] Lesage-Rosenberg, E; Vlaic, G; Dexpert, H; Lagarde, P; Freund, E Appl Catal (1986), 22, 211

[49] Renouprez, A J; Trillot, J F; Moraweck, B; Massardier, J; Bergeret, G J Catal (1998), 179, 390

[50] Noronha, F B; Schmal, M; Moraweck, B; Deliche`re, P; Brun, M; Villain, F; Fre´ty, R J Phys Chem B (2000), 104, 5478

[51] Cho, S J; Kang, S K J Phys Chem B (2000), 104, 8124

[52] Holles, J H; Davis, R J J Phys Chem B (2000), 104, 9653

[53] Okamura, K; Niwa, M J Phys Chem B (2000), 104, 9670

[54] Park, E D; Choi, SH; Lee, J S J Catal (2000), 194, 33

[55] Ju-Nam, Y; Lead, J R Manufactured nanoparticles: An overview of their chemistry, interactions and potential environmental implications Sci Total Environ (2008), 400, 396–414 [CrossRef] [PubMed]

[56] Gaiser, B K; Fernandes, T F; Jepson, M A; Lead, J R; Tyler, C R; Baalousha, M; Biswas, A; Britton, G J; Cole, P A; Johnston, BD; et al Interspecies comparisons on the uptake and toxicity of silver and cerium dioxide nanoparticles Environ Toxicol Chem (2012), 31, 144–154 [CrossRef] [PubMed]

[57] Schubert, D; Dargusch, R; Raitano, J; Chan, S -W Cerium and yttrium oxide nanoparticles are neuroprotective Biochem Biophys Res Commun (2006), 342, 86–91 [CrossRef] [PubMed]

[58] D Channei, A Nakaruk, S Phanichphant, S Phanicchphant, Influence of graphene oxide on the photocatalytic enhancement of cerium dioxide, Mater Lett 209 (2017) 43–47

[59] A Trovarelli, Catalytic properties of ceria and CeO_2-containing materials, Catal Rev 38 (1996) 439–520

[60] Z L Wang, G R Li, Y N Ou, Z P Feng, D L Qu, Y X Tong, Electrochemical deposition of Eu^{3+}-doped CeO_2 nanobelts with enhanced optical properties, J Phys Chem C 115 (2010) 351–356

[61] G A Deluga, J R Salge, L D Schmidt, X E Verykios, Renewable hydrogen from ethanol by auto thermal reforming, Science 303 (2004) 993–997

[62] A Corma, P Atienzar, H García, J Y Chaneching, Hierarchically mesostructured doped CeO2 with potential for solar-cell use, Nat Mater 3 (2004) 394–397

[63] D G Yin, F F Zhao, L Zhang, X Y Zhang, Y M Liu, T T Zhang, C L Wu, D W Chen, Z W Chen, Greatly enhanced photocatalytic activity of semiconductor CeO2 by integrating with up conversion nanocrystals and graphene, RSC Adv 6 (2016) 103795–103802

[64] Y T Hao, L Li, J J Zhang, H X Luo, X Y Zhang, E Chen, Multilayer and open structure of dendritic cross-linked CeO_2-ZrO_2 composite: enhanced photocatalytic degradation and water splitting performance, Int J Hydrogen Energy 42 (2017) 5916–5929

[65] D T You, B Pan, F Jiang, Y G Zhou, W Y Su, CdS nanoparticles/CeO_2 nanorods composite with high-eciency visible-light-driven photocatalytic activity, Appl Surf Sci 363 (2016) 154–160

[66] Magesh, G, Viswanathan, B, Viswanath, R P & Varadarajan, T K Photocatalytic behavior of CeO_2-TiO_2 system for the degradation of methylene blue Indian J Chem B Org 3, 480–488 (2009)

[67] Truffault, L et al Application of Nanostructured Ca doped CeO2 for ultraviolet filtration Mater Res Bull 45, 527–535 (2010)

[68] D Channei, B Inceesungvorn, N Wetchakun, S Ukritnukun, A Nattestad, J Chen, S Phanichphant, Photocatalytic degradation of methyl orange by CeO2 and Fe–doped CeO2 films under visible light irradiation, Sci Rep 4 (2014) 1–7

[69] A Akbari–Fakhrabadi, R Saravanan, M Jamshidijam, R V Mangalaraja, M A Gracia, Preparation of nanosized yttrium doped CeO_2 catalyst utilizes for photocatalytic application, J Saudi Chem Soc 19 (2015) 505–510

[70] N Sabari Arul, D Mangalaraj, T Whan Kim, P Chi Chen, N Ponpandian, P Meena, Y Masuda, Synthesis of CeO2 nanorods with improved photocatalytic activity: Comparison between precipitation and hydrothermal process, J Mater Sci-Matter El 24 (2013) 1844–1650

[71] S Ye, K Ullah, L Zhu, Z D Meng, Q Sun, W C Oh, Easy and Fast Synthesis of Pd–MWCNT/TiO2 by the Sol-Gel Way and its recycling photodegradation of Rhodamine BJ Korean Ceram Soc 50 (2013) 251–256

[72] S Jayapalan, KS Ranjith, S Padmanapan, D Mangalaraj, R T Rajendrakumar, Cobalt–doped cerium oxide nanoparticles: Enhanced photocatalytic activity under UV and visible light irradiation, Mat Sci Semicon Proc 26 (2014) 218–224

[73] L Truffault, Application of Nanostructured Ca doped CeO_2 for ultraviolet filtration, Mater Res Bull 45 (2010) 527–535

[74] J M A Almeida, P E C Santos, L P Cardoso, C T Meneses, A simple way to obtain Fe–doped CeO_2 nanocrystals at room temperature, J Magn Magn Mater 327 (2013) 185–188

[75] L Yue, X M Zhang, Structural characterization and photocatalytic behaviors of doped CeO_2 nanoparticles, J Alloys Compd 475 (2009) 702-705

[76] D Ma, Y Zhao, J Zhao, Y Li, Y Lu, D Zhao, Aqueous synthesis of hierarchical bismuth nanobundles with high catalytic activity to organic dyes, Super lattice Microst 83 (2015) 411–421

[77] K H Kim, S K Ihm, Heterogeneous catalytic wet air oxidation of refractory organic pollutants in industrial wastewaters: a review, J Hazard Mater 186 (2011) 16–34

[78] P Ji, J Zhang, F Chen, M Anpo, Study of adsorption and degradation of acid orange 7 on the surface of CeO_2 under visible light irradiation, Appl Catal B: 484 Environ 85 (2009) 148–154

[79] B Subash, B Krishnakumar, R Velmurugan, M Swaminathan, M Shanthi, Synthesis of Ce co-doped Ag–ZnO photocatalyst with excellent performance for NBB dye degradation under natural sunlight illumination, Catal Sci 488 Technol 2 (2012)2319-2326

[80] Y Li, Q Sun, M Kong, W Shi, J Huang, J Tang, X Zhao, J Phys Chem C 115 (2011) 14050–14057

[81] A D Liyanage, S D Perera, K Tan, Y Chabal, K J Balkus Jr, ACS Catal 4 (2) (2014) 577–584

[82] S A Ansari, M M Khan, M O Ansari, S Kalathil, J Lee, M H Cho, RSC Adv 4 (2014) 16782–16791

[83] Hegde, M S; Madras, G; Patil, KC Acc Chem Res 2009, 42, 704

[84] Misch, L M; Kurzman, J A; Derk, A R; Kim, Y; Seshadri, R; Metiu; McFarland W; Stucky D Chem Mater 2011,23,5432

[85] Roy, S; Aarthi, T; Hegde, M S; Madras, G Ind Eng Chem Res 2007, 46, 5798

[86] Sharma, S; Hegde, M S ChemPhysChem 2009, 10, 637

[87] Roy, S; Hegde, M S; Ravishankar, N; Madras, G J Phys Chem C 2007, 111, 8153

[88] K Maeda, K Domen, Photocatalytic properties of RuO_2-loaded b-Ge_3N_4 for overall water splitting, J Phys Chem C 111 (12) (2007) 4749–4755

[89] Y Inoue, Photocatalytic water splitting by RuO_2-loaded metal oxides and nitrides with d^0- and d^{10}-related electronic configurations, Energy Environ Sci 2 (4) (2009) 364–386

[90] A Kudo, Y Miseki, Heterogeneous photocatalyst materials for water splitting, Chem Soc Revis 38 (1) (2009) 253–278

[91] Huang B, Isse A A, Durante C, Electrocatalytic properties of transition metals toward reductive decolorization of polychloroethanes, Electrochim Acta, 2012, 70, 50-61

[92] Li WB, Wang J X, Gong H, Catalytic combustion of VOCs on non-noble metal catalysts, Catal Today, 2009, 148, 81-87

[93] Hepel M, Hazelton S, Photoelectrocatalytic degradation of diazo dyes on Nanostructured WO_3 electrodes, Electrochim Acta, 2005, 50(25–26), 5278-5291

[94] Hepel M, Luo J, Photoelectrochemical mineralization of textile diazo dye pollutants using nanocrystalline WO electrodes, Electrochim Acta, 2001, 47(5), 729-740

[95] Yang Z, Woo T K, Hermansson K, Effects of Zr doping on stoichiometric and reduced ceria: a first-principles study, J Chem Phys, 2006, 124, 224704

[96] Nguyen T B, Delorme J P, Perrichon V, Study of the redox behavior of high surface area $CeO_2–SnO_2$, solid solutions, Appl Catal A, 2003, 249, 273-284

[97] Putna E S, Bunluesin T, Fan X L, Ceria films on zirconia substrates: models for understanding oxygen-storage properties, Catal Today, 1999, 50, 343-352

[98] KC Patil, M S Hegde, T Rattan, and S T Aruna, Chemistry of nanocrystalline oxide materials, combustion synthesis, properties and application, World Scientific, Singapore (2008)

[99] M M A Sekar, S S Manoharan, K C Patil, J Mater Sci Lett 9, 1205 (1990)

[100] S T Aruna, K C Patil, Nanostructured Mater 10, 995 (1998)

[101] K C Patil, S T Aruna, S Ekambaram, Curr Opin Solid State Mater Sci 2, 158 (1997)

[102] K C Patil, S T Aruna, T Mimani, Curr Opin Solid State Mater Sci 6, 507 (2002)

[103] S R Jain, K C Adiga, V R P Verneker, Combust Flame 40, 71 (1981)

Synthesis and Characterization of Undoped TiO_2 and Pd doped TiO_2 for Reduction of Aromatic Nitro Compounds to Amines by Solution Combustion Method

Paper Published: "Development and Catalytic Application of Palladium Doped Titania ($Ti_{0.98}Pd_{0.02}O_2$) Through Low Temperature Solution Combustion Method". **ADVANCED SCIENCE LETTER**, Volume 24, Number 8, 2018, .6004-6007.
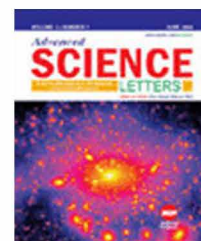
Paper Communicated: "Novel Synthesis of Palladium Doped TiO_2 **($Ti_{0.98}Pd_{0.02}O_{1.97}$)** Nano Catalyst for Selective Reduction of Aromatic Nitro Compounds to Amines". **Nature material** (Under Review).
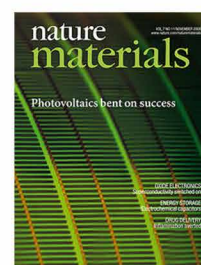
CHAPTER-2

Synthesis and Characterization of Undoped TiO$_2$ and Pd Doped TiO$_2$ for Reduction of Aromatic Nitro Compounds to Amines by Solution Combustion Method

An efficient chemo selective reduction of aromatic nitro compounds to corresponding amino analogs was achieved using palladium doped TiO$_2$ (Ti$_{0.97}$Pd$_{0.03}$O$_{1.97}$) nanoparticles. The obtained catalyst characterized by XDR and FTIR spectroscopy. The reductions are effectively carried out in the presence of aromatic nitro compounds of various other reducible functional groups such as halo, alkoxy, carbonyl, and cyanide. The reactions are worthy and high yielding (100%). The reduction of aromatic nitro compounds to aromatic amines was recognized with excellent yield by using nanoporous palladium as a sustainable catalyst and as a hydrogen source. A wide range of substrates including those bearing reducible functional groups such as aldehyde, ketone, acid, ester, amide, nitrile, halogens, even allyl, and heterocyclic was chemo selectively reduced in good to excellent yields, even on a gram scale. Reductions of the aromatic nitro compound to amines were well characterized using ^{1}H NMR, ^{13}C NMR, and FTIR spectroscopy. The stability and efficiency of the catalyst for reduction of O-Nitrobenzaldehyde and 4-Nitrophenol were repeated for 11 cycles and 9 cycles and the recovered catalyst was analyzed by XRD.

2.1 INTRODUCTION

The palladium is the cheapest and most commonly used metal and palladium-based catalysts, particularly nanoscale palladium particles, have recently drawn enormous attention due to their versatile role in organic synthesis [1-3]. The use of palladium nanoparticles in catalysis is not only industrially important [4-6], but also scientifically interesting as a result of the sensitive relationship between catalytic activity, nanoparticle size, and shape as well as the nature of the surrounding media [7]. Newly, it has received extensive attention utilizing support interactions to increase the electrocatalytic activity and stability of supported metal catalysts [8-10]. It also confirmed that the interactions could change the electronic structure of the metal catalyst, which in go changes its catalytic activity. The durability of the support materials could also influence the durability of the resultant catalyst [11]. At low-temperature treating, denote a favorable application and TiO_2-based catalyst [12-14]. Pd doped electrons can easily flow to the metal sites on TiO_2, and the role of the metal is to act as an electron sink and thus to enhance the activity. [15-16].

Aromatic amines are intermediates for dyes, agricultural, and pharmaceutical chemicals [17-18]. The common method to prepare aromatic amines is the reduction of aromatic nitro compounds [19, 20]. Nitro compounds are one of the most readily available and valuable starting materials in organic synthesis [21]. Nitro compounds are majorly used for the production of primary amines and their derivatives, such as secondary and tertiary amines, with wide applications [22-23]. It is highly e ective in the selective reduction of aromatic nitro compounds to amines [24], it is a challenge to develop catalysts for solvent-free hydrogenation of aromatic nitro compounds to

amines at atmospheric pressure of hydrogen gas. Using activated hydrogen (H) rather than hydrogen gas (H_2) would reduce the activation energy, and let the reaction proceed under mild and safe conditions. Now some hydrogen transfer reaction systems have been developed for the reduction of aromatic nitro compounds by using formic acid [25] and various alcohols [26] as the hydrogen source. TiO_2 based magnetic photocatalysts have been enjoying great research interest for their potential in photocatalysis [27-28]. The photocatalytic reduction of nitro compounds has attracted increasing attention as it holds great promise for providing an alternative to the conventional synthetic process [29-32]. Aromatic amines are synthetically important compounds in various organic reactions. Many of the amine functionalities are biologically important. Also, these compounds act as precursors for the preparation of many interesting organic molecules. Generally, these amines readily synthesized from their corresponding nitro compounds via the reduction of nitro compounds. In majority reduction of the nitro compounds are carried out under metal catalysis [33-34] or hydrogenation in the presence of transition metals in some harsh conditions of reduction, selective reduction of nitro in the presence of functionalities such as halide, ester, nitrile, etc. is very difficult [35].

In heterogeneous catalysis, under the heating condition as well as solvent-free microwave irradiation condition, hydrazine hydrate acts as an excellent hydrogen source [36-37]. The reduction of nitro always compounds a significant reaction in industry and is often employed as an ideal procedure for studies on catalyst effectiveness and recyclability. Earlier, several procedures based on PdS fixed on the solid support of Fe_2O_3, Al_2O_3, SiO_2, and CeO_2 and several other metal oxides [38-40]. Aliphatic or aromatic amines are widely used as important intermediates in the

synthesis of chemicals such as dyes, antioxidants, conducting polymers, photographic, pharmaceutical and agricultural chemicals [41] Aromatic amines can be easily transformed to other functional groups (H, F, Cl, Br, I, OH, etc.) via their diazonium salts [42]. Aromatic amines can be produced from the corresponding nitro-arenes by catalytic hydrogenation [43-49].

Hydrogenation of Aromatic nitro compound yielded high catalytic rates over Pd/MCM-41 [50] and Pt/C [51] catalyst. Raney nickel [52] and Pt/C [53] are used for the reduction of aromatic nitro compounds at high pressure of H_2. The aromatic nitro compound derivatives to the corresponding amines that are efficient, chemoselective, and compatible with a plethora of functional groups. We have to expect that the catalyst should also be effective for the reduction of aromatic nitro compounds. On the basis, we employed $Ti_{0.97}Pd_{0.03}O_{1.97}$ for nitro to amine conversion, and here, we show high catalytic activity on the reduction of nitro compounds under solvent and solvent-free condition under 1.2-1.3 bar pressure. Selective reduction of nitro compounds (Ram & Ehrenkaufer, 1984; Yuste et al., 1982; Lyle & Lamittina, 1974; Ho & Wang, 1974; Onopchenko et al., 1979) is an important synthetic tool for preparation of aromatic amines in organic chemistry. Many methods have been reported in the literature for this reduction, including homogeneous and heterogeneous catalytic hydrogenation (Welton, 1999; Wasserscheid & Keim, 2000; Sheldon, 2001; Dupont et al., 2002; Harmon et al., 1973; Johnstone et al., 1985), reduction using metals (Steines et al., 2000; Dyson et al., 1999), and electrolytic reduction (Popp & Schultz, 1962). The selective reduction of aromatic nitro compounds using iron and dilute acid (Hazlet & Dornfeld, 1944; Liu et al., 2005), or stannous chloride (Bellamy & Ou, 1984) have been reported as e cient methods. Zinc

has been used in combination with acids/bases (Vogel et al., 1989) and also with hydrogen donors (Gowda et al., 2001; Tsukinoki & Tsuzuki, 2001) for the reduction of aromatic nitro compounds.

The main applications of this catalyst are used as high rates of H_2+O_2 recombination, solvent-free reduction of aromatic nitro compounds to amines as high with olefins prepared. TiO_2 is nontoxic reducible oxides, and noble metal ions can be substituted in TiO_2.

In $Ti_{1-x}Pd_xO_{2-x}$ (x=0.01, 0.02 and 0.03) where Pd is in +2 oxidation state showed high rates of NOx reduction by CO, high rates of hydrogen-oxygen recombination and good photocatalytic activity for CO oxidation. Smaller the metal particle, large is the surface area, higher is the amount of CO absorption, and higher is the catalytic converter. Highly distributed nanoparticles of noble metals (Pt., Pd, Rh, Ru, and Au), in mesoporous supports such as Titania, alumina, silica are broadly used as catalysts in organic synthesis and petrochemistry.

The present study was developed in a reduction in aromatic nitro compounds to amine reaction method by using a $Ti_{0.97}Pd_{0.03}O_{1.97}$ catalyst. Synthesized $Ti_{0.97}Pd_{0.03}O_{1.97}$ as further used to study their palladium-catalyzed organic coupling reactions. The $Ti_{0.97}Pd_{0.03}O_{1.97}$ powdered catalyst showed much higher catalytic property of the reduction reaction with the effect of aromatic nitro compounds using different ethanol, methanol, and n-butanol. We reported the use of the powdered catalyst for different solvents with different reaction conditions.

2.2 EXPERIMENTAL

2.2.1 Materials

The present research chemicals, specifications, and suppliers were presented in Table.2.1

Table - 2.1 : List of chemicals, specification and suppliers used

Name	Specifications	Suppliers
Titanium tetra isopropoxide (Ti $(OC_3H_7)_4$)	Molar mass: 284.22 g/mol	Sigma-Aldrich
Palladium chloride ($PdCl_2$)	Molar mass: 177.33 g/mol	Sigma-Aldrich
Glycine (NH_2CH_2COOH)	Molar mass: 75.07 g/mol	Merck
Nitrobenzene ($C_6H_5NO_2$)	Molar mass: 123.11 g/mol	Merck
4-nitrophenol (4-($C_6H_5NO_3$)	Molar mass: 139.11 g/mol	Merck
4-aminoacetophenone (4-$(NH_2)C_6H_4COCH_3$)	Molar mass: 135.16 g/mol	Sigma-Aldrich
o-Nitrobenzaldehyde ($C_7H_5NO_3$)	Molar mass: 151.12 g/mol	Sigma-Aldrich
p-nitro toluene ($C_7H_7NO_2$)	Molar mass: 137.18 g/mol	Sigma-Aldrich
Benzyolenitromethane ($C_6H_5COCH_2NO_2$)	Molar mass: 165.15 g/mol	Sigma-Aldrich
4-nitroacetophenone ($O_2NC_6H_4COCH_3$)	Molar mass: 165.15 g/mol	Sigma-Aldrich

2.2.2 Synthesis of TiO_2 and $Ti_{0.97}Pd_{0.03}O_{1.97}$ Powdered Catalysts

Both un-doped TiO_2 and Pd-doped TiO_2 catalysts were synthesized using the solution combustion method. The compounds TiO_2 and $Ti_{0.97}Pd_{0.03}O_{1.97}$ can be prepared from the solution combustion method. The starting materials are Ti $(OC_3H_7)_4$, $PdCl_2$, and Glycine as fuel. For the synthesis of TiO_2 and $Ti_{0.97}Pd_{0.03}O_{1.97}$, the stoichiometric ratio of starting materials was to be taken as 9.89 mmol of TiO $(NO_3)_2$ which is prepared from $Ti(OC_3H_7)_4$, 0.31 mmol of $PdCl_2$ and 10.99 mmol of Glycine in a 300 ml capacity crystallizing dish. The compounds were fully dissolved in 15 ml of H_2O. The solution was kept in the preheated furnace at $350°$ C. The combustion takes place after dehydration and the solid product is left behind.

The chemical reaction on the synthesis of undoped TiO_2 can be written as shown in the below equation (1).

$$TiO(NO_3)_2 \text{ (aq)} + 10C_2H_5O_2N \text{ (aq)}$$
$$\rightarrow 9TiO_2(s) + 14N_2(g) + 20\,CO_2(g) + 25H_2O\,(g) \dots \dots (1)$$
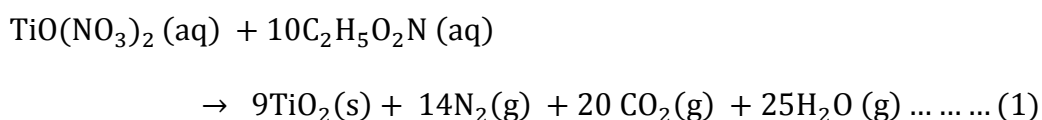
The general chemical reaction on the synthesis of Pd doped TiO_2 can be written as shown in the below equation (2).

$$9(1-x)TiO(NO_3)_2 + 10(1-x)C_2H_2NO_2 + 9xPdCl_2$$
$$\rightarrow 9\,Ti_{1-x}Pd_xO_{2-\delta} + 20(1-x)CO_2 + 14(1-x)N_2$$
$$+ (25-34x)H_2O + 18x\,HCl: x = 0.01, 0.02, 0.03 \dots \dots (2).$$
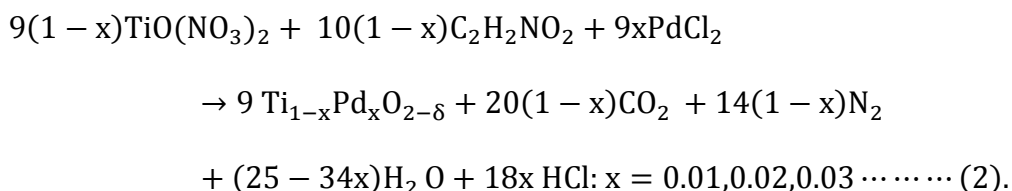
2.2.3 Experimental Set-Up for Catalytic Reduction of Aromatic Nitro Compounds.

The reduction of aromatic nitro compounds was carried out in evacuated three-necked round bottom flask and it was connected to a bladder filled with hydrogen gas. When opened to the evacuated 3 necked round bottom flask, the pressure was near to 1.2-1.3 bar pressure as measured from a monometer. Catalytic reaction was carried out using a hot plate and with around 450 rpm stirring speed. The experimental setup is shown in the fig.2.1. The product was confirmed by thin-layer chromatography. The final product was analyzed by the NMR spectroscopy, FTIR Spectrum. After completion of the reaction, the mixture was centrifuged by using a small amount of ethanol for dissolving the products and the solution was slowly decanted. The remaining solid catalyst was again centrifuged for 2 to 3 times and the catalyst was dried at 100^0C. The catalyst was reused. After 3 cycles, the catalyst was washed in alcohol and the dried catalyst was analyzed by XRD, SEM, and EDAX.
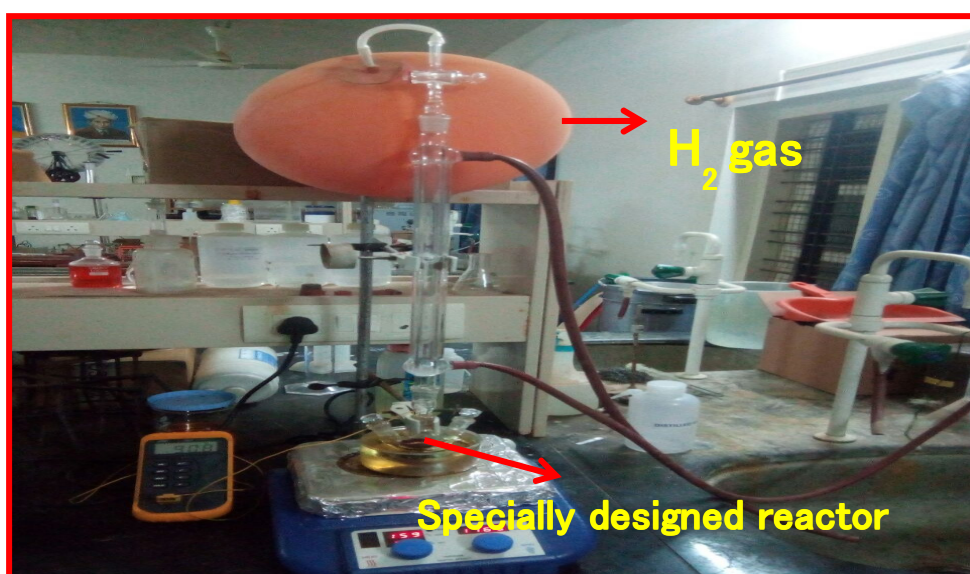
Fig. 2.1 : Experimental set-up for catalytic reduction of the nitro group in aromatic nitro compounds.

2.2.4 General Experimental Procedure.

The ^{1}H NMR and ^{13}C NMR spectra were recorded on an AMX-400 MHz spectrometer using deuterated chloroform ($CDCl_3$) as the solvent and Trimethyl silane (TMS) as internal standard and IR spectra on a Shimadzu FTIR- 8300 spectrometers. The commercially available reagents and solvents were used without further purification. The reactions were monitored by TLC plates (detection by UV light). The NMR spectra of all the compounds were recorded on Bruker ALS 300, DRX 300, DRX 400, and AV 500 MHz spectrometers in $CDCl_3$, CD_2Cl_2, $DMSOd_6$, or CD_3OD-d_4. Chemical shifts were assigned relative to the reference solvent in ppm. Infrared analyses were recorded on a Nicolet iS10 Smart ITR spectrometer equipped with an ATR diamond. Purifications were carried out by flash chromatography on silica gel (230–400 mesh; 40–63 μm). The reactions were carried out in a manual thermostated (25–30 °C) ultrasonic cleaning bath (Bransonic, Branson 2510EMT) at 42 kHz frequency.

2.2.5 Procedure for the Reduction of Aromatic Nitro Compounds Using $Ti_{0.97}Pd_{0.03}O_{1.97}$ Catalyst

A suspension of an appropriate aromatic nitro compound (10 mmol) and 50 mg of powdered catalyst in ethanol, methanol, and n-butanol in any other suitable solvent (20 mL) was stirred under H_2 gas atmosphere with ammonium formate (0.5 g), at room temperature. After the completion of the reaction (monitored by TLC), the catalyst was filtered off. The residue was extracted with chloroform or dichloromethane or ether (15 mL). The extract was washed twice with a saturated sodium chloride solution (15 mL) and then with water (10 mL). The organic layer was

dried (Na$_2$S0$_4$) and then evaporated to obtain the desired amino derivative. To get a good yield of a volatile aliphatic amine, the reaction was carried out using a condenser cooled with ice water and by immersing the reaction flask in a cold-water bath. After filtration, the reaction mixture was neutralized with HCl. The solvent was evaporated under reduced pressure. The residue was lyophilized or subjected to column chromatography by using 60-120 mesh silica gel and a suitable eluting system. Aliphatic amines were obtained as their hydrochloride salts are up to 80 % yield. Reaction treatment was carried out by dilution in ethyl acetate (10 ml), washed with 1M NaOH solution (20 ml). The aqueous phase was extracted with ethyl acetate (3 × 20 ml). The combined organic layers were dried (MgSO$_4$), filtered, and concentrated. The compounds were purified by flash chromatography on silica gel.

2.3 RESULTS AND DISCUSSION

2.3.1 Powder X-Ray Diffractometer Analysis (PXRD) and Rietveld Refined Method

The XRD pattern of undoped TiO$_2$ and palladium doped TiO$_2$ was obtained using an X-ray Diffractometer Shimadzu model: XRD 6000 with CuKα radiation in the range of 20-70° (λ=0.154nm). The XRD patterns of the undoped and palladium doped TiO$_2$ nanoparticles obtained by the solution combustion method were shown in Fig. 2.2 a) and 2.2 b) respectively. All the peaks in the XRD patterns can be indexed as anatase phases of TiO$_2$ and the diffraction data were in good agreement with JCPDS No: 21-1272. Crystallite size was obtained by Debye-Scherrer's formula given by equation

$$D=K \lambda / (\beta \cos \theta)\ldots\ldots\ldots (3)$$

Where D is the crystal size; λ is the wavelength of the X-ray radiation (λ=0.15406 nm) for CuKα; K is usually taken as 0.89 and β is the line width at half-maximum height.

The crystallite size obtained using this formula is 6.24 nm for undoped and 7.8 nm palladium doped TiO_2. This reveals that Pd ions are uniformly doped in the TiO_2 matrix. In the region of $2\theta°$=10°-85°, the shape of diffraction peaks of the crystal planes of pure TiO_2 is moderately analogous to those of Pd/TiO_2. The average crystal sizes of TiO_2 and Pd doped TiO_2 nanoparticles were calculated and also the average crystal size was not significantly altered due to the addition of the Pd^{+2}. The Rietveld refined XRD profiles of undoped and palladium doped TiO_2 are shown in Fig.2 c). The pattern is indexed to anatase TiO_2 (tetragonal) one to two atomic percent Pd metal can be detected by slow scan in the XRD. If Pd ion was substituted for Ti^{4+} ion in six coordination, there should have been a measurable increase in lattice parameters and if at all, a slight decrease in cell volume from135.6 to135.2A as indicated in Table 2.2. Therefore, Pd ion in these oxides is not in octahedral coordination. The ionic radius of Pd^{2+} ion in square planar coordination is 0.64 A, which is close to Ti^{4+} ion in octahedral coordination. Because for every Pd^{2+} ion substitution one oxide ion vacancy needs to be created for charge balance, Pd is likely to be in square-planar coordination.

Table 2.2 : Rietveld refined lattice parameters of TiO_2 and $Ti_{0.97}Pd_{0.03}O_2$ (different doping conc. of palladium 0, 0.01, 0.02 and 0.03)

Catalysts	a	c	Cell volume	R_f	R_B
TiO_2	3.779(1)	9.497(1)	153.62	2.8	2.6
$Ti_{0.99}Pd_{0.01}O_2$ (0.01 mg)	3.779(0)	9.491(1)	153.54	3.8	2.8
$Ti_{0.98}Pd_{0.02}O_2$ (0.02 mg)	3.779(0)	9.487(0)	153.48	3.9	3.1
$Ti_{0.97}Pd_{0.03}O_2$ (0.03 mg)	3.778(1)	9.473(0)	153.21	2.7	2.5
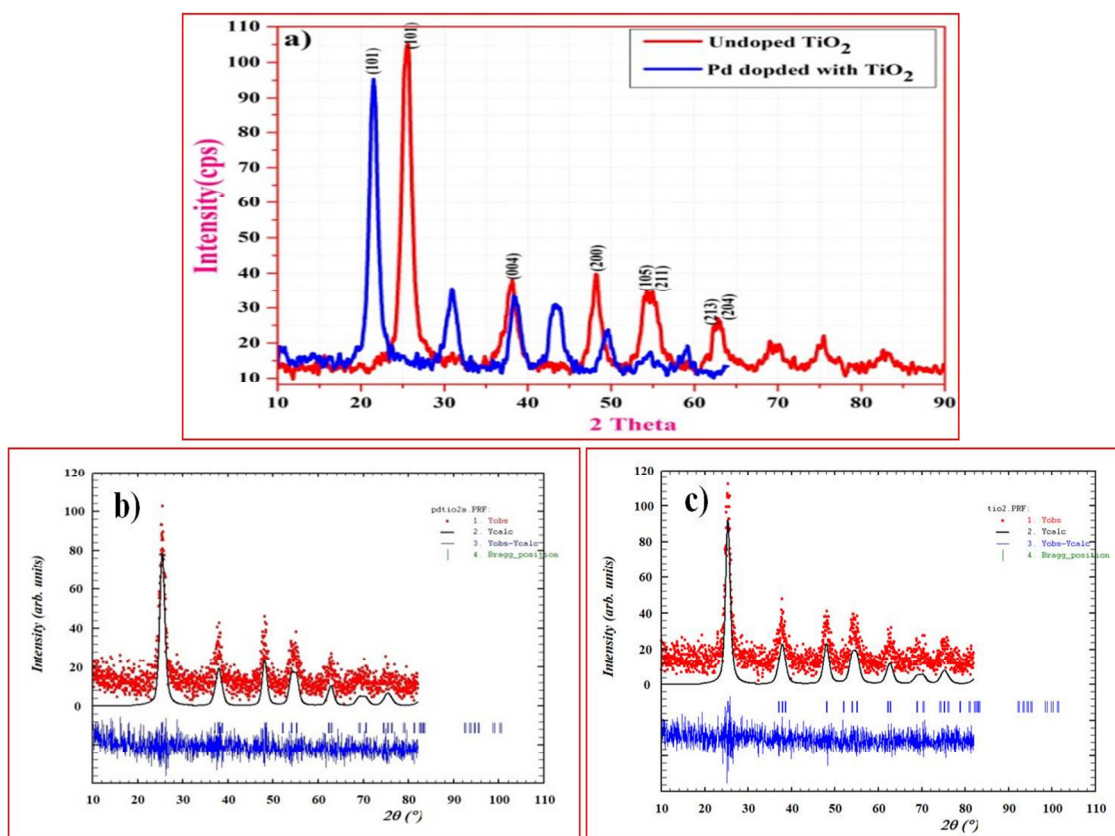
Fig.2.2 : XRD Pattern of a) Undoped TiO_2 and Palladium doped TiO_2 and Rietveld refined images of b) Palladium doped TiO_2 and c) TiO_2 nanoparticle

2.3.2 X-Ray Photoelectron Spectroscopy (XPS) Studies

The XPS of Ti (2p) on the $Ti_{0.97}Pd_{0.03}O_{1.97}$ monolith was measured before the chemical reaction was shown in the figure. Ti at the +4 state potential of Ti (2p3/2) and Ti (2p1/2) is 459.2 eV and 464.9 eV respectively. The XPS of Pd (3d) of $Ti_{0.97}Pd_{0.03}O_{1.97}$ was exposed to the aromatic oil before exposure. The coupling strength of Pd (3d5/2) and Pd (3d3/2) of $Ti_{0.97}Pd_{0.03}O_{1.97}$ coils and monolith 337.25 eV and 341.10 eV respectively. The binding energies of Pd (3d5/2) and PdO are observed in PdO at 335.1 eV and 336.4 eV, respectively [54]. The coating state of Pd in $Ti_{0.97}Pd_{0.03}O_{1.97}$ of the monolith coating is +2, and the bond strength of the Pd^{2+} ion and TiO_2 matrix is higher than that of PdO, and Pd^{2+} ion is ionic than that of PdO. The added strength Pd (3d) core of $Ti_{0.97}Pd_{0.03}O_{1.97}$ honeycomb coating is the same as $Ti_{0.97}Pd_{0.03}O_{1.97}$ powder [55]. The dependence of the C 1s is 285.56 eV, 284.3 eV, and 287.1 eV, respectively. The example shows the high number of O 1s seen in parentheses. The two peaks present in this Fig. 2.3 are expressed in O 1s and OH^- two, respectively. Attempts to limit the maximum number of O1s at about 530.5 eV and the peak at 528.5 eV are associated with OH individually.
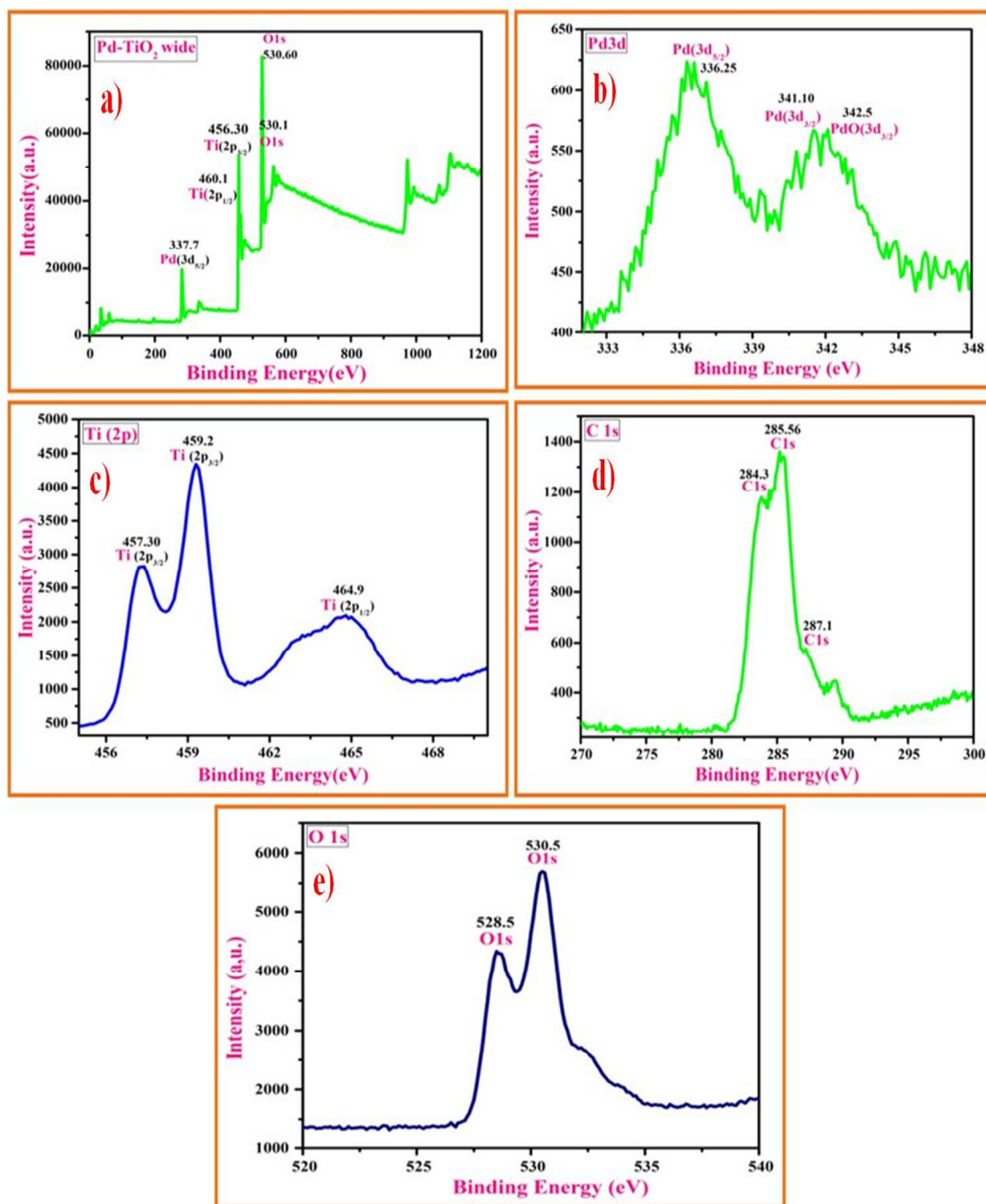
Fig.2.3 : Core level XPS of (a) Pd doped TiO_2 wide (b) Pd (3d), (c) Ti (2p), (d) C 1s and (e) O 1s in $Ti_{0.09}Pd_{0.03}O_{1.97}$-catalyst.
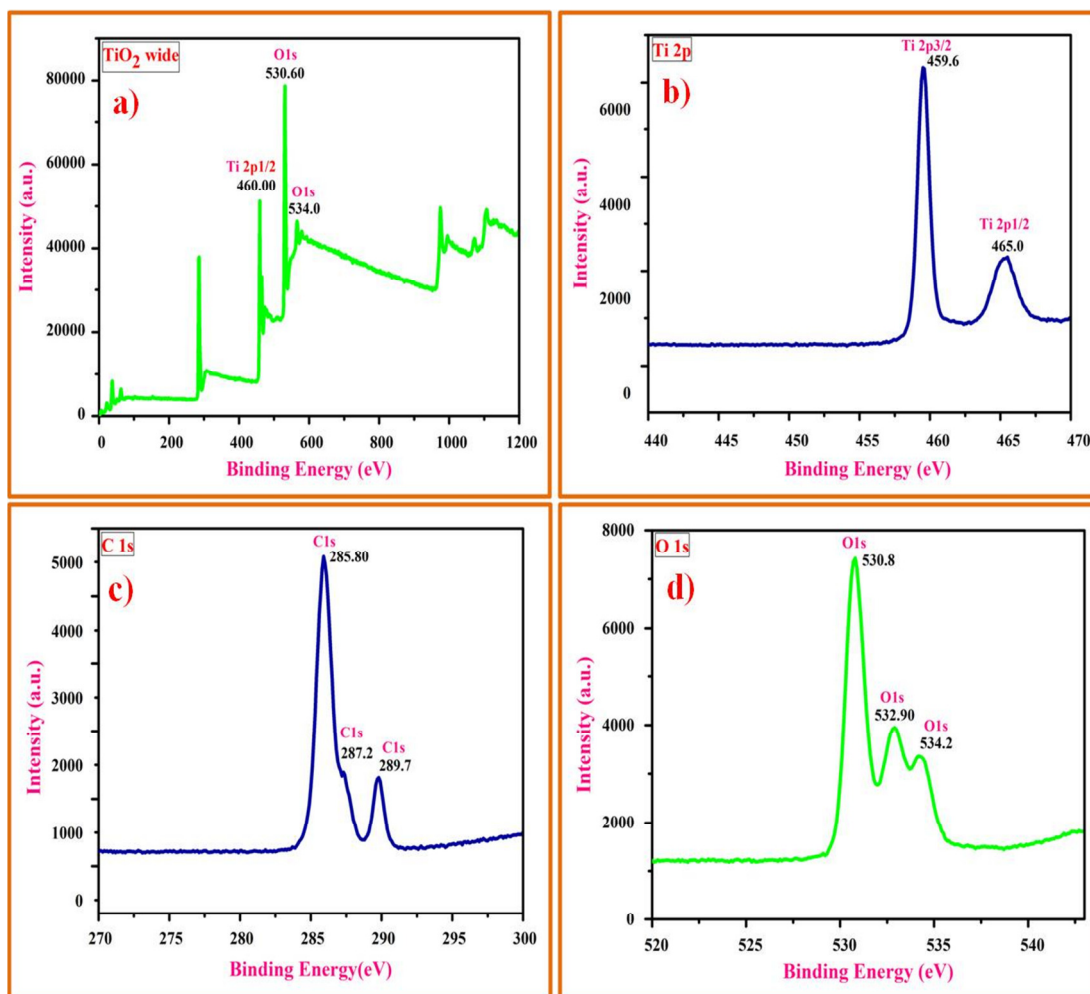
Fig.2.4 Core level XPS of (a) TiO_2 wide (b) Ti (2p), (c) C 1s and

(d) O 1s in TiO_2-catalyst.

2.3.3 Catalytic Reduction of Aromatic Nitro Compounds

Initially, $Ti_{0.97}Pd_{0.03}O_{1.97}$, the catalyst was used for hydrogenation or reduction of nitro compounds with H_2 with solvents like alcohol under mild reaction conditions. Nitroaromatic compounds like Nitrobenzene, p-nitrophenol, 4-Nitroacetophenone, etc., are taken for the catalytic reduction reaction. 50 mg of catalyst was made in a three-necked round bottom flask with 20 ml of solvent and 10 mmol of the nitro compound. H_2 gas-filled bladder was connected into the round bottom flask through a glass valve (Fig.2.1). The closed system was evacuated by pumping. The glass valve

was opened to expose H_2 gas on the reactants, and the reaction was carried out with 450 rpm stirrer speed at a constant temperature. The total pressure created inside the closed round bottom flask was the pressure developed by bladder with H_2 gas, and the pressure was around 1.2 to 1.3 bar as measured from a monometer. The final product was analyzed by GC, NMR, and IR spectroscopy.

2.3.4 Screening Studies

Screening of the aromatic nitro compounds to corresponding amine reduction reaction was started with the response of equivalent amounts of aromatic nitro compounds as starting materials. Powder Pd doped TiO_2 ($Ti_{0.97}Pd_{0.03}O_{1.97}$) catalyst was utilized in each of the screening reactions. 10 mmol (100 mg) of Aromatic nitro compounds and 50 mg of the powdered catalyst with 20ml of solvents were taken. Initially, the Solvents have been investigated where different fuels are utilized for reactions, such as ethanol, methanol, and n-butanol. We attempted to use single and single results with the resultant yield. We ended up exploring what they did. We have performed six additional results using the $Ti_{0.97}Pd_{0.03}O_{1.97}$ catalyst site, one with nitro hydrocarbons and 200 mg catalyst, the other containing 50 mg of catalyst. 2 g of Nitrobenzene Utilized as the starting element; they were closed at over 99%. Funny, the time taken for these reactions was only four hours. Finally, we decided to take 50 mg of the sample for the rest of the episode. The face of exploration of nitro to amine reduction reactions is summarized in Table 2.3

Reaction Scheme:
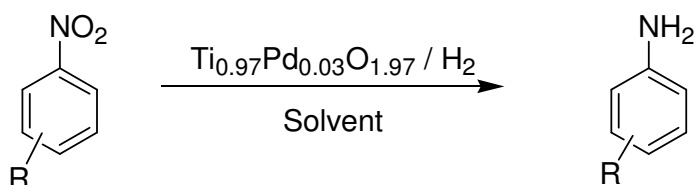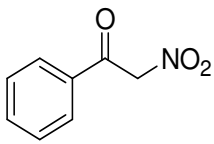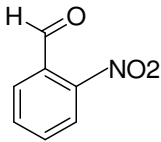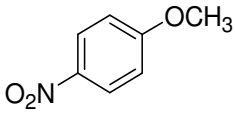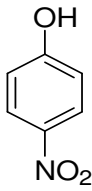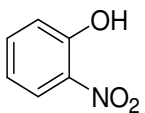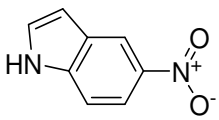
Table -2.3 : Screening of nitro to amine reductions of aromatic nitro compounds

Entry	Nitro compounds	No. of moles of starting material (mmol)	Solvent	Temp (^{o}C)	Time (hrs)	Yield (%)
1	Nitrobenzene	10	Ethanol	68	10	Nil
			n-Butanol	105	6	**100**
2	2,7-Dinitrofluorene	10	Methanol	64	10	**100**
3	4-Nitrophenol	10	Methanol	64	5	**100**
4	2,4-Dinitrophenol-hydrazine	10	n-Butanol	105	24	Nil
			Ethanol	68	48	40
			Methanol	64	24	**100**
5	4-Nitroaniline	10	Ethanol	68	5	**100**

6	 Benzyl nitromethane	10	Ethanol Methanol n-Butanol	68 64 105	24 12 5	Nil Nil **100**
7	 o-Nitrobenzaldehyde	10	Ethanol Methanol n-Butanol	68 64 105	12 12 2	Nil Nil **100**
8	 4-Nitroacetophenone	10	Ethanol	68	6	**100**
9	 p-nitrophenol	10	n-Butanol	105	3	**100**
10	 o-Nitrophenol	10	Ethanol	68	10	**100**
11	1-Nitropropane	10	Methanol Ethanol	64 68	24 24	Nil Nil
12	P-Nitro benzyl alcohol	10	Methanol Ethanol n-Butanol	64 68 105	12 24 12	Nil Nil Nil
13	 5-nitroindole	10	Methanol Ethanol	64 68	12 24	Nil 80

Reaction Conditions: 1 equivalent of Nitro compounds, 50mg of powdered catalyst, H_2 gas, 20ml of solvent, isolated yield.

In Table.2.4.starting materials, solvent, temperature, duration of reaction, and yield are summarized for the conversion of nitro to amine over In the table, starting materials, solvent, temperature, duration of reaction, and yield are summarized for the conversion of nitro to amine over $Ti_{0.97}Pd_{0.03}O_{1.97}$. Here, the corresponding amine is 100% selective product among nitroso and hydroxylamine products over $Ti_{0.97}Pd_{0.03}O_{1.97}$. At different solvents are utilized at a different temperature, 100% conversion of nitro to amine compounds was observed in various solvents are utilized in different temperature. In the absence of the catalyst, there was no conversion of aromatic compounds in the solvent medium. Here, the corresponding amine is 100% selective product among nitroso and hydroxylamine products over $Ti_{0.97}Pd_{0.03}O_{1.97}$. At different solvents are utilized at a different temperature, 100% conversion of nitro to amine compounds was observed in various solvents are utilized in different temperature. In the absence of the catalyst, there was no conversion of aromatic compounds in the solvent medium.

Reaction Scheme:
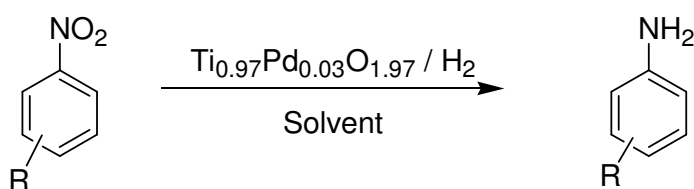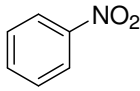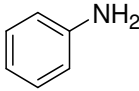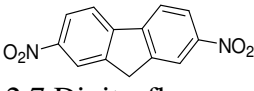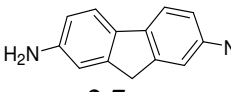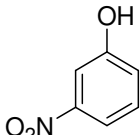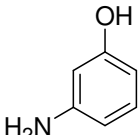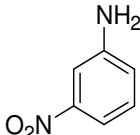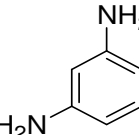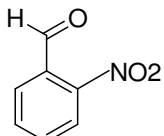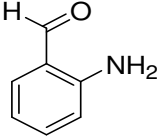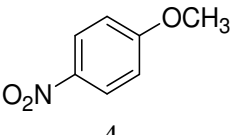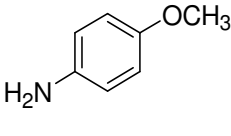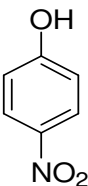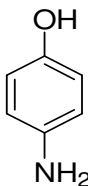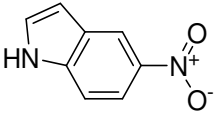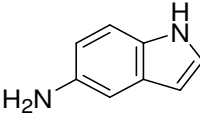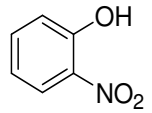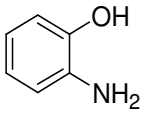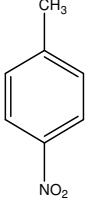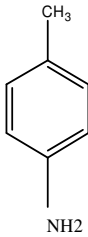
Table -2.4 : The reduction of aromatic nitro compounds with different solvents over the $Ti_{0.97}Pd_{0.03}O_{1.97}$ catalyst

Entry	Nitro compound	Product	Solvent	Temp (^oC)	Time (hrs)	Yield (%)	TOF (h^{-1})
1.	Nitrobenzene	Aniline	n-Butanol	105	6	100	91
2.	2,7 Dinitrofluorene	2,7-Diaminofluorene	Methanol	64	10	100	54
3.	3-Nitrophenol	3-Aminophenol	Methanol	64	5	100	109
4.	3-Nitroaniline	3-Aminoaniline	Ethanol	68	5	100	109
5.	o-Nitrobenzaldehyde	o-Aminobenzaldehyde	n-Butanol	105	2	100	273
6.	4-Nitroacetophenone	4-Aminoacetophenone	Ethanol	68	6	100	91

7.	OH / NO$_2$ p-nitrophenol	OH / NH$_2$ p-aminophenol	n-Butanol	105	3	100	182
8.	5-nitroindole	5-aminoindole	Ethanol	68	24	100	22
9.	OH / NO$_2$ O-Nitro phenol	OH / NH$_2$ O-Aminophenol	Ethanol	68	10	100	54
10.	CH$_3$ / NO$_2$ p-nitro toluene	CH$_3$ / NH2 p-toluidine	Ethanol	68	8	100	135

Reaction Condition: 1 Equiv. of Nitro compounds (10 mmol), 50mg of catalyst, 1.2-1.3 bar H$_2$ gas pressure, 20mL of solvent, and 450 rpm stirrer speed.

In Table.2.5 With an increase in temperature from 50 ^{0}C to 110 ^{0}C, 100% conversion of Nitrobenzene to aniline is reached within 6h, and TOF is 42, 34, 91, and 109 h-1at 70 ^{0}C respectively. TOF for reduction of p-nitrophenol to p-aminophenol is 57, 86, and 172 h^{-1} corresponding to the reactions at 50 ^{0}C, 70 ^{0}C, and 110 ^{0}C. Increase temperature from 80 ^{0}C to 130 ^{0}C, 100% conversion of 5-nitroindole to 5-aminoindole is reached in 14 h, and TOF is 43, 21, and 18 h^{-1}respectively. Ti$_{0.97}$Pd$_{0.03}$O$_{1.97}$ gave much higher TOF at nearly one atmospheric pressure of H$_2$.

Reaction Scheme:
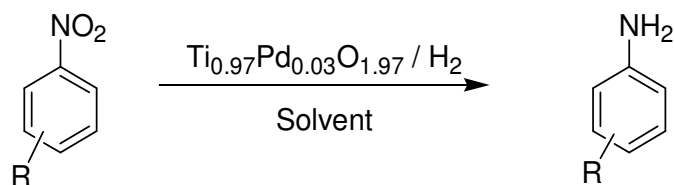
Table 2.5 : Solvent-free catalytic reduction of aromatic nitro compounds over $Ti_{0.97}Pd_{0.03}O_{1.97}$ at different temperatures is summarized in the Table. 2.5

Entry	Nitro compound	Product	Temp (^{o}C)	Time (hrs)	Yield (%)	TOF (h^{-1})
1	Nitrobenzene	Aniline	50	13	70	42
2	Nitrobenzene	Aniline	70	16	85	34
3	Nitrobenzene	Aniline	90	6	100	91
4	Nitrobenzene	Aniline	110	5	100	109
5	p-nitro phenol	p-aminophenol	50	9	100	57
6	p-nitro phenol	p-aminophenol	70	6	100	86
7	p-nitro phenol	p-aminophenol	110	3	100	172
8	5-nitroindole	5-aminoindole	80	12	36	43
9	5-nitroindole	5-aminoindole	110	24	75	21
10	5-nitroindole	5-aminoindole	130	28	100	18

Reaction Conditions: 1 Equiv. of Nitro compounds (10 mmol), 50 mg of catalyst, 1.2-1.3 bar H_2 gas pressure, and 450 rpm stirrer speed.

In Table.2.6, we have compared the solvent-free reduction of the nitro group over different catalysts 90°C. For the reaction, the weight of Pd taken in each case was the same as in 50mg of $Ti_{0.97}Pd_{0.03}O_{1.97}$. TOF of aniline formation over

$Ti_{0.97}Pd_{0.03}O_{1.97}$ is three times higher than that of reaction over $Ce_{0.97}Pd_{0.03}O_{1.97}$ catalyst. The catalytic activity for the reduction of p-aminophenol over $Ti_{0.97}Pd_{0.03}O_{1.97}$. It is 15 times higher than the response over Pd metal. PdO and Pd metal on γ-Al_2O_3 catalysts showed similar catalytic activity as demonstrated by PdO, and Pd doped CeO_2 also showed lower activity than $Ti_{0.97}Pd_{0.03}O_{1.97}$ for the reduction of p-nitrophenol. TOF for Nitrobenzene and p-nitrophenol conversion are 109 over $Ti_{0.97}Pd_{0.03}O_{1.97}$, respectively. There is a little conversion over synthesized TiO_2 and γ-Al_2O_3 catalysts. Among the catalysts for the reaction of nitroaromatic reduction, $Ti_{0.97}Pd_{0.03}O_{1.97}$ showed high TOF under solvent-free conditions.

Reaction Scheme :
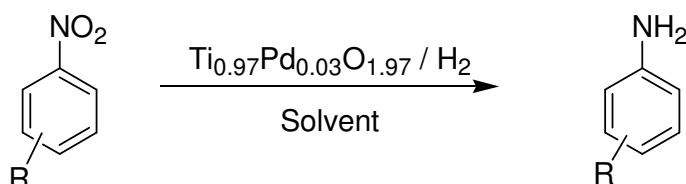
Table 2.6 Comparison of solvent-free catalytic reduction reaction with different catalysts at 100^0C temperature over $Ti_{0.97}Pd_{0.03}O_{1.97}$ catalysts Table 2.6

Entry	Nitro compound	Product	Catalyst	Time (hrs)	Yield (%)	TOF (h^{-1})
1	Nitrobenzene	Aniline	$Ti_{0.97}Pd_{\mathbf{0.03}}O_{1.97}$	5	100	109
2	Nitrobenzene	Aniline	$Ti_{0.98}Pd_{\mathbf{0.02}}O_{1.97}$	5	85	163
3	p-nitro phenol	p-aminophenol	$Ti_{0.97}Pd_{0.03}O_{1.97}$	9	100	60
4	p-nitro phenol	p-aminophenol	TiO_2	24	6	1
5	p-nitro phenol	p-aminophenol	γ-Al_2O_3[#]	24	70	1
6	p-nitro phenol	p-aminophenol	$Ce_{0.97}Pd_{0.03}O_2$	28	50	40
7	p-nitro phenol	p-aminophenol	CeO_2	24	3	1

Reaction Conditions: 1 Equiv. of Nitro compounds (10 mmol), 50mg of catalysts, 1.2-1.3 bar H_2 gas pressure, and 450 rpm stirrer speed.

Note: # Al ion as active site and weight of catalyst was 65 mg

2.3.5 FT-IR Analysis for Reduction of Nitro Compounds to Amines

The label of the following peak provided IR samples such as C-H, N-H, and C-N which is helpful to identify the functional groups of the present compound. The confirmation of compounds that comes from the FT-IR spectra of aniline, p-aminophenol, 4-aminoacetophenone, and benzyolaminomethane are shown in Fig.2.5. a) the FT-IR spectra of aniline, N-H stretching vibrations at 3578 cm^{-1} and 3387 cm^{-1} N-H bending vibration at 1525 cm^{-1} and 1067 cm^{-1}, are observed in all these compounds. C-H stretching vibrations are found in the region between 3120 cm^{-1} and 2820 cm^{-1} depending on the nature of substituent. Fig.2.5. b) the FT-IR spectra of 4-aminoacetophenone, N-H stretching vibrations at 3464 cm^{-1} and 3374 cm^{-1} and N-H bending vibration at 1599 cm^{-1} and 1397 cm^{-1}, are observed in all these compounds. C-H stretching vibrations are found in the region between 2964 cm^{-1} and 2927 cm^{-1}. Fig.2.5. c) the FT-IR spectra of 4-aminophenol, FT-IR spectra of aniline, N-H stretching vibrations at 3658 cm^{-1} and 3341 cm^{-1} N-H bending vibration at 1510 cm^{-1} and 1475 cm^{-1}, are observed in all these compounds. C-H stretching vibrations are found in the region between 3280 cm^{-1} and 2854 cm^{-1}. Fig.1.5. d) The FT-IR spectra of benzyolaminomethane, N-H stretching vibrations at 3355 cm^{-1} and 3066 cm^{-1} and N-H bending vibration at 1721 cm^{-1} and 1451 cm^{-1}, are observed in all these compounds. C-H stretching vibrations are found in the region between 2959 cm^{-1} and 2931 cm^{-1}.
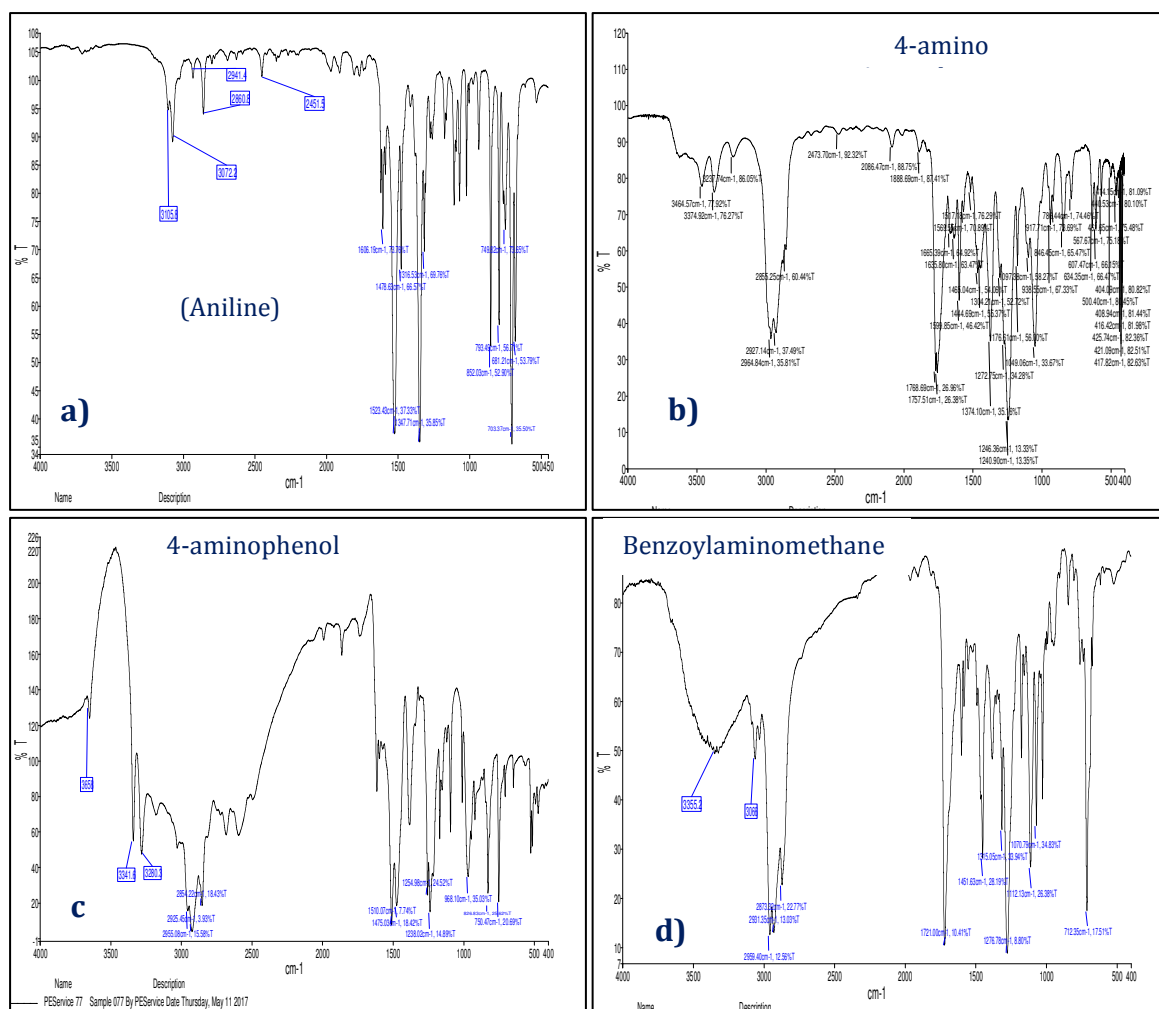
Fig.2.5 : FT-IR spectra of a) aniline b) p-aminophenol c) 4-aminoacetophenone

d) Benzyolaminomethane

2.3.6 NMR Studies

2.3.6.1 Aniline-Substrate: Nitrobenzene $\delta 6.762$-7.310 (m, Ar-H); $\delta 6.891$ (m, Ar-H); $\delta 3.713$ (s, NH$_2$), ^{1}H NMR (400 MHz/ CDCl$_3$) δ ppm): (Fig.6 a), 7.26 (2H, t, J=8.62 Hz) 6.77 (1H, t, J=8.20 Hz), 6.76 (2H, d, J=7.64 Hz), 3.71 (2H, br., s).

^{13}C NMR (100 MHz/CDCl$_3$) δ ppm: (Fig.6 b), 161.4, 148.2, 121.1, 118.0.

2.3.6.2 P-Aminophenol-Substrate: P-Nitrophenol: ^{1}H NMR (400 MHz/ CDCl$_3$) δ ppm): (Fig.7 a), $\delta 8.362$ (s, OH); $\delta 6.469$ (m, Ar-H); $\delta 4.395$ (s, NH$_2$); $\delta 3.388$ (m,

$CDCl_3$); δ2.505 (s, C_2H_5OH)

^{13}C NMR (100 MHz/$CDCl_3$) δ ppm: (Fig.7.b) 143.9, 140.4, 126.3, 115.5, 76.5.

2.3.6.3 P-Phenylenediamine-Substrate: P-Nitro Aniline: ^{1}H NMR (400 MHz/ $CDCl_3$) δ ppm): (Fig.8 a), δ6.346 (m, Ar-H); δ3.957 (s, NH_2); δ3.389 ($CDCl_3$);

^{13}C NMR (100 MHz/$CDCl_3$) δ ppm: (Fig.8.b) 138.6, 134.7, 129.7, 116.7, 76.6.

2.3.6.4 O-Phenylenediamine-Substrate-nitroaniline: ^{1}H NMR (400 MHz/ $CDCl_3$) δ ppm): (Fig.9 a), δ7.250 (s, $CHCl_3$); δ6.689-6.737 (m, Ar-H); δ3.336 (s, NH_2)

^{13}C NMR (100 MHz/$CDCl_3$) δ ppm: (Fig.9.b) 142.2, 134.2, 127.1, 116.8, 76.8.

2.3.6.5 O-Aminobenzaldehyde-Substrate: O-Nitrobenzaldehyde: ^{1}H NMR (400 MHz/ $CDCl_3$) δ ppm): (Fig.10 a), 9.92 (1H, s), 7.59 (2H, d, J=8.42 Hz) 6.40 (2H, d, J=7.88 Hz), 3.50 (2H, br., s). ^{13}C NMR (100 MHz/$CDCl_3$) δ ppm: (Fig.10.b) 190.0, 150.0, 129.5, 125.0, 115.5.

2.3.6.6 P-Toluidine-Substrate: P-Nitotoulene: δ6.996 (d, 2H, Ar-H); δ6.645 (d, 2H, Ar-H); δ3.478 (s, 2H, NH_2); δ2.279 (s, 3H, CH_3); δ0.052 (m, C_2H_5OH)

^{1}H NMR (400 MHz/ $CDCl_3$) δ ppm: (Fig.11.a) 6.996 (2H, d, J=7.42 Hz), 6.6 (2H, t, J=6.20 Hz), 3.47 (2H, br., s), 2.27 (3H, s)

^{13}C NMR (100 MHz/$CDCl_3$) δ ppm: (Fig.11.b) 143.9, 129.8, 127.8, 115.4, 20.5.
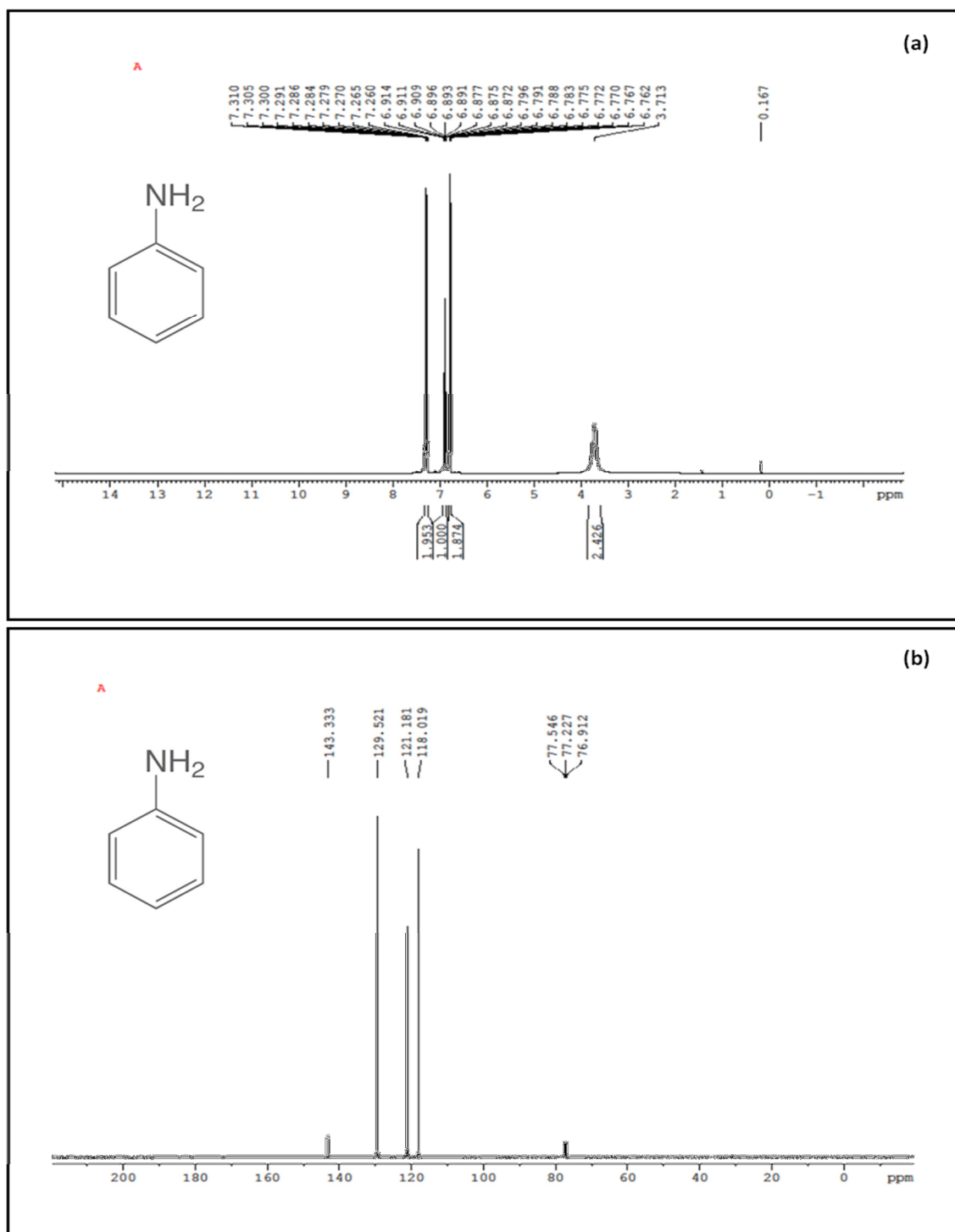
Fig.2.6. a) ^{1}H NMR and b) ^{13}C NMR spectra of Aniline
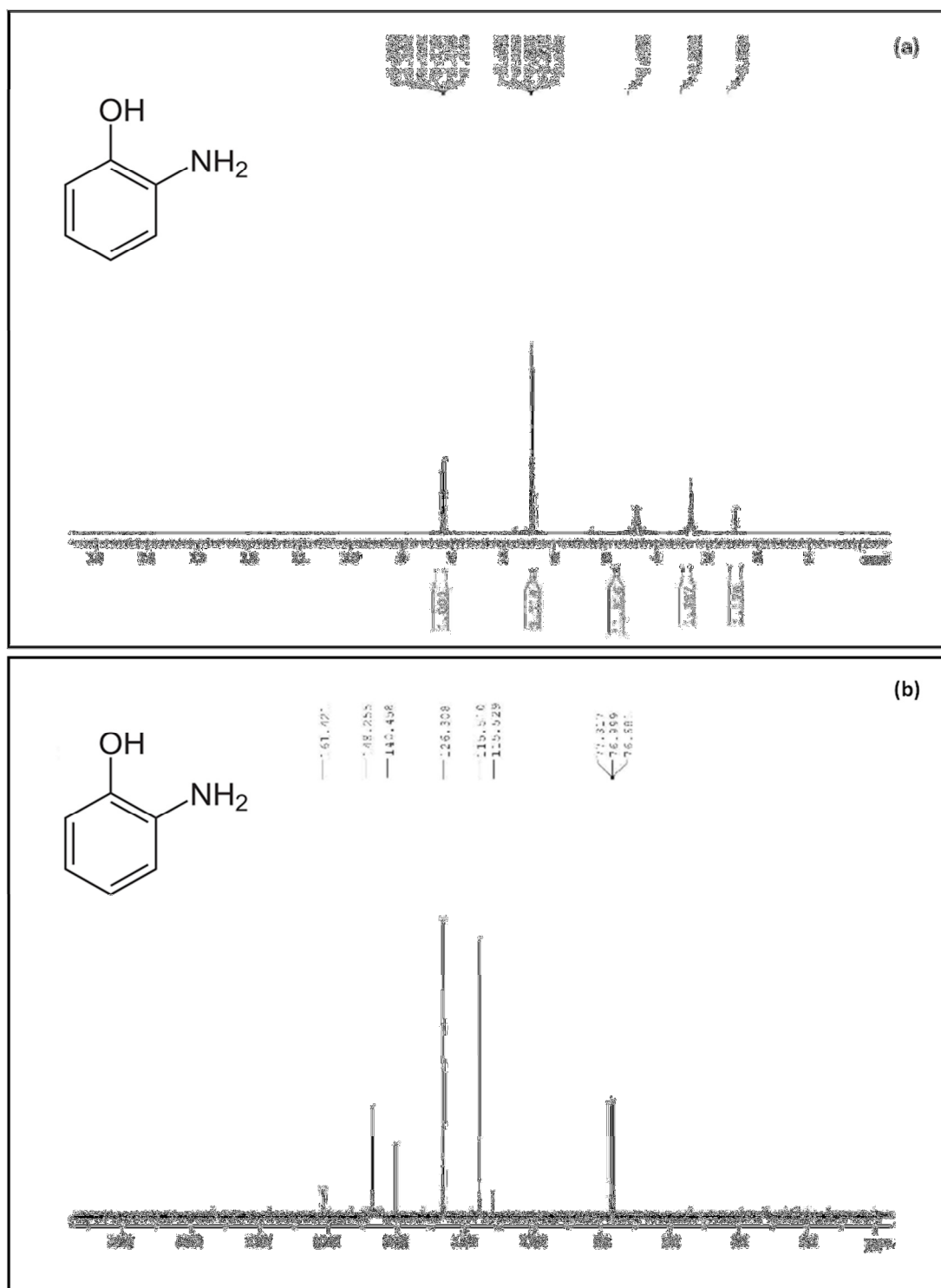
Fig.2.7. a) ^{1}H NMR and b) ^{13}C NMR spectra of p-Aminophenol

Fig.2.8. a) ^{1}H NMR and b) ^{13}C NMR spectra of o-Phenylenediamine
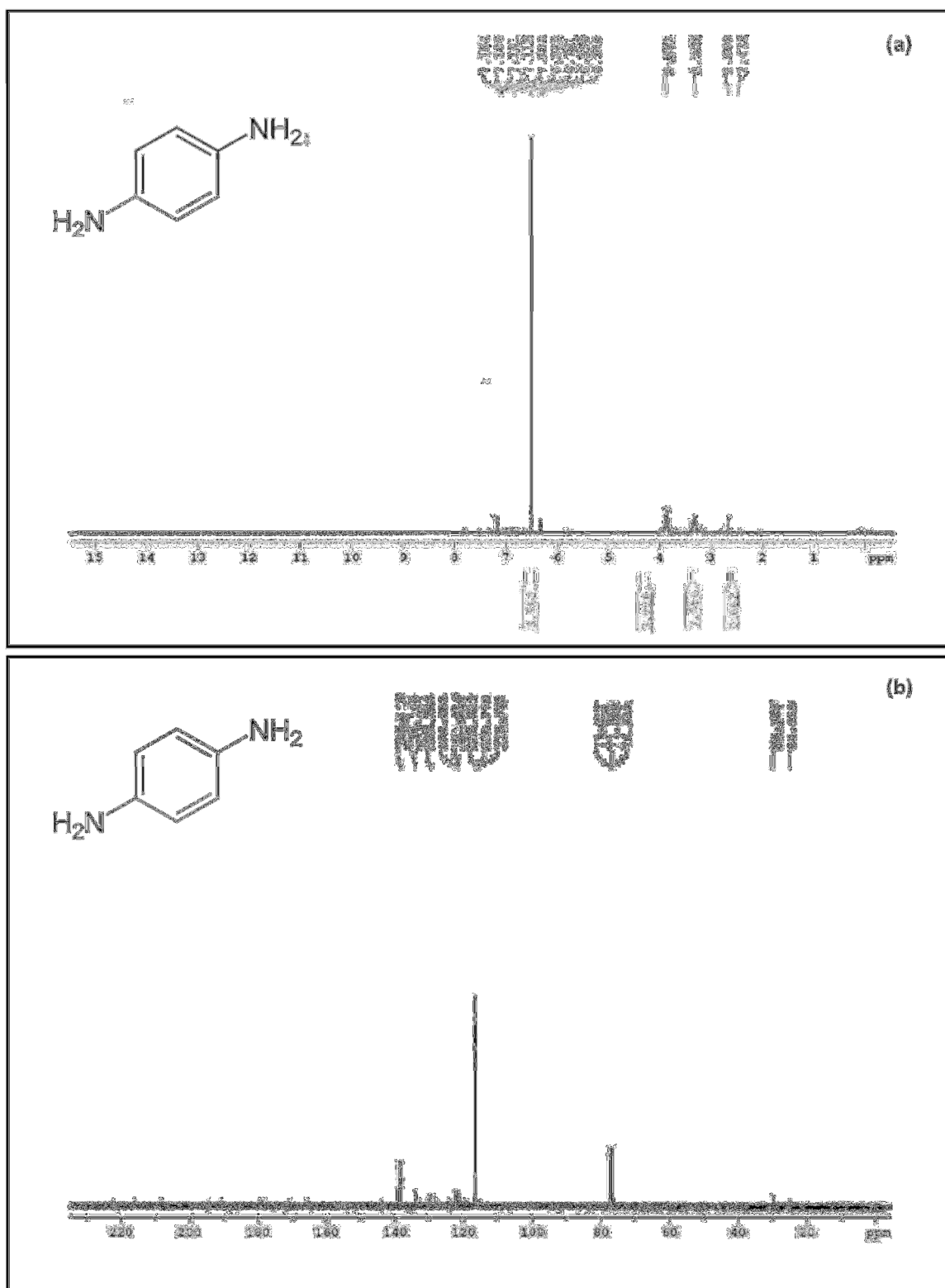
Fig.2.9 a) ^{1}H NMR and b) ^{13}C NMR spectra of p-Phenylenediamine
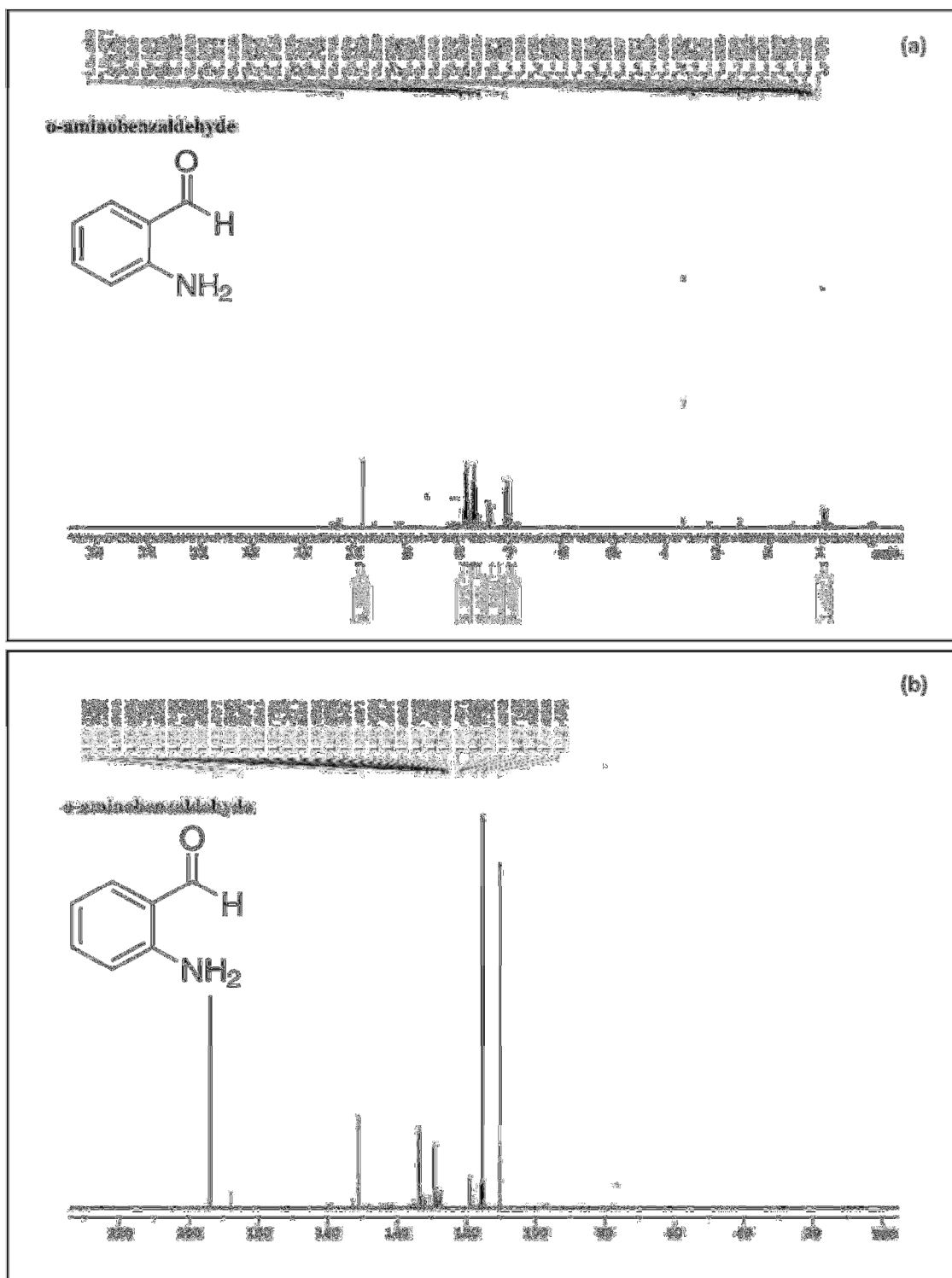
Fig.2.10 a) ^{1}H NMR and b) ^{13}C NMR spectra of o-amino benzaldehyde
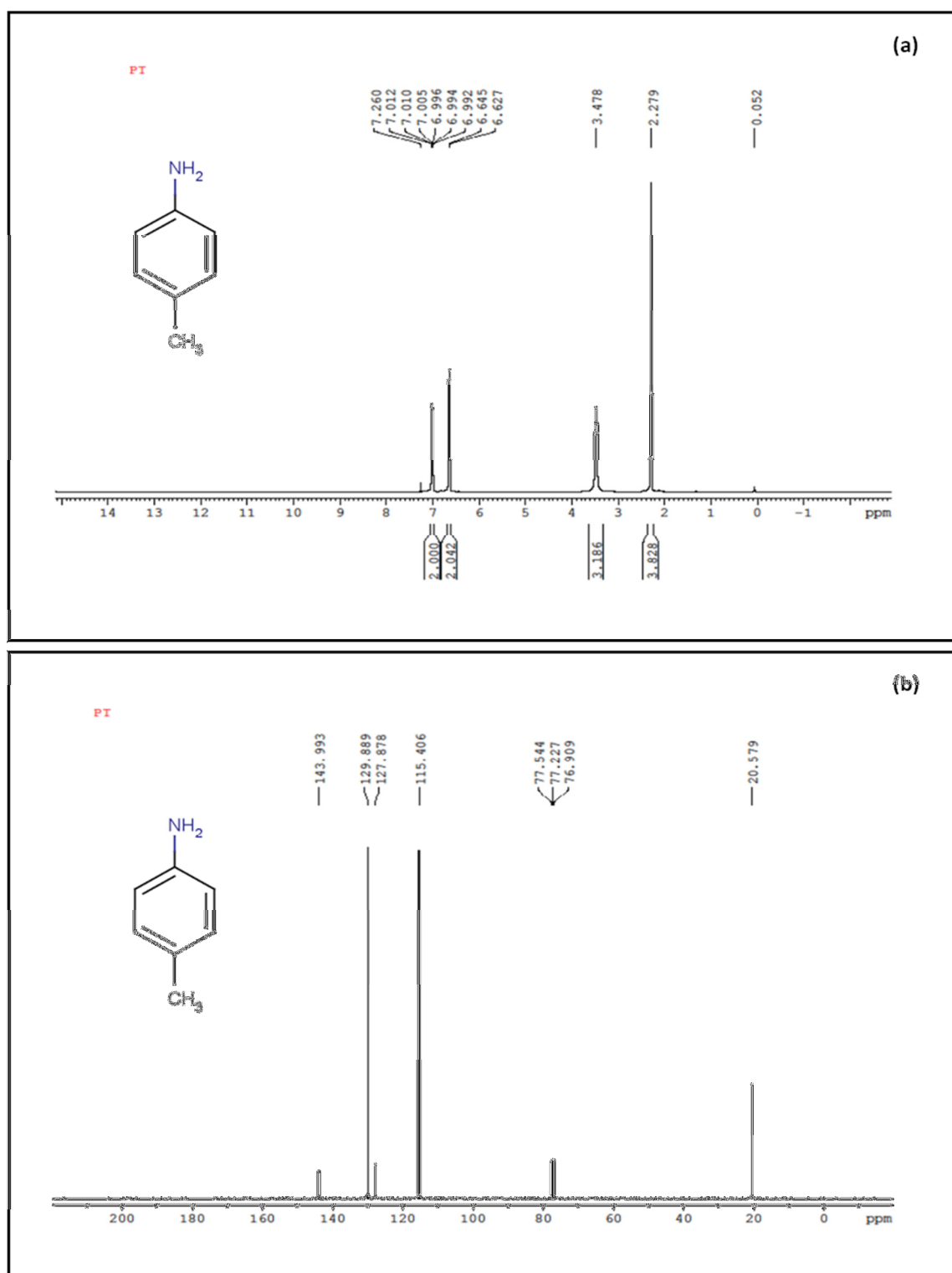
Fig.2.11 a) ^{1}H NMR and b) ^{13}C NMR spectra of p-toluidine

2.3.7 Recycling and Reusability of $Ti_{0.97}Pd_{0.03}O_{1.97}$ Catalyst

2.3.7.1 Reuse of Catalyst for Reduction of O-Nitrobenzaldehyde and 4-Nitrophenol

To check the stability and efficiency of the catalyst, the experiment was repeated for 11 cycles in the presence of palladium as shown in Fig.2.12. The catalyst was collected from the reactor in the first cycle with the coupling product yield 100%. The yield of the 11th cycle decreased slightly when compared with the first cycle probably due to the conglomeration of particles and loss of the catalyst as shown in fig. In addition to that, washing with water after separation reduced the activity of the catalysts, and filtering also leads to the loss of some catalyst material.

Parameter maintained	No of Cycles	% Yield
	1	100
Reaction completed: 01:30 hr	2	100
Reaction condition: 105°C	3	100
Nitro compound: O-	4	100
Nitrobenzaldehyde	5	100
(MW-151.12 g/mol) (1.5112g	6	100
weight)	7	100
(Catalyst weight 96.2 mg)	8	100
Solvent: n-Butanol (25ml)	9	100
	10	100
	11	99
	12	98
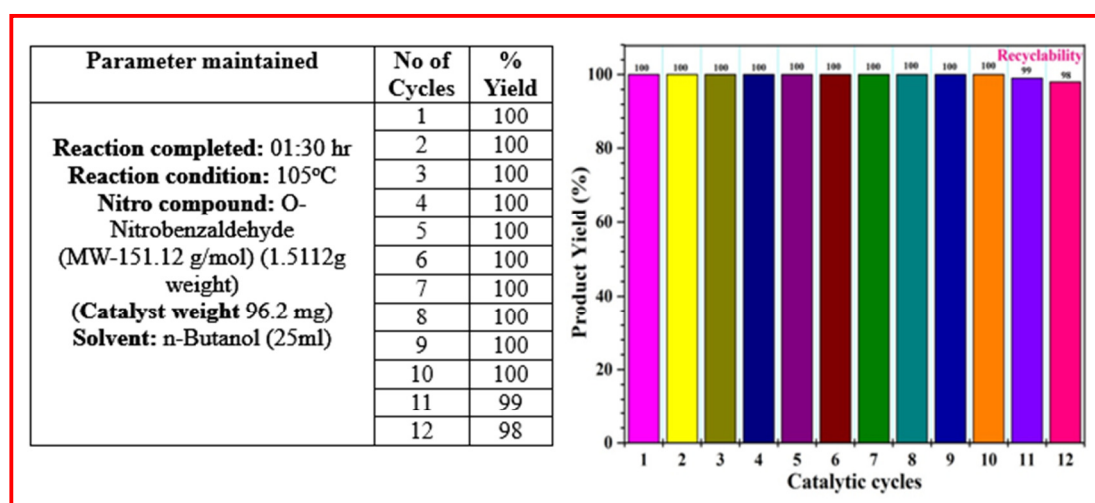
Fig.2.12 : Recycling of catalyst for the reduction reaction of o-Nitrobenzaldehyde.

The deactivation of the catalysts was studied by using the $Ti_{0.97}Pd_{0.03}O_{1.97}$ catalyst for nine cycles of the reduction reaction as shown in Fig.2.13. After the first cycle, the catalyst was collected by the decantation way, and the dried catalyst was utilized again for the second cycle. Up to 9 cycles for the reduction of p-nitrophenol

are summarized in the below table. The recovery of the catalyst is more than 98%, and even after the 9th cycle, 100% conversion has occurred within 2:30 h. At least up to 9th cycles, there was no degradation.

Parameters maintained	No of cycles	%Yield	Chart
Reaction condition: 105°C Temperature, Nitro compound: 4-Nitrophenol (MW-139.11 g/mol) Catalyst weight is 92.3 mg Solvent: n-Butanol (Bp=117.7°C) (25 ml) Reaction completed: 2:30 hr.	1. 2. 3. 4. 5. 6. 7. 8. 9.	100 99 99 99 99 99 99 98 98	
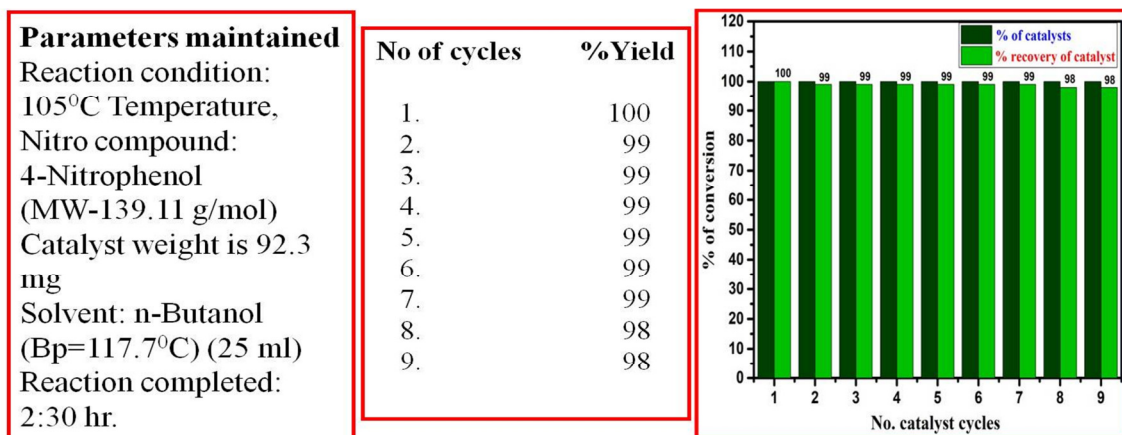
Fig.2.13 : Recycling and reusability of catalyst for the reduction reaction of 4-Nitrophenol.

2.3.7.2 Structural Analysis Completed In Catalyst

The catalyst was completely converted into aromatic nitro compounds to amines. After 11th cycles of o-Nitrobenzaldehyde and 9th cycles of p-Nitro phenol reduction over $Ti_{0.97}Pd_{0.03}O_{1.97}$ are shown in Fig. 2.14 a), o-Nitrobenzaldehyde b) p-Nitro phenol. The catalyst was analyzed for its structure by XRD. In Fig.2.14 c); the XRD pattern of the spent catalysts was shown in a) before b) after the reduction reaction of nitrobenzene.
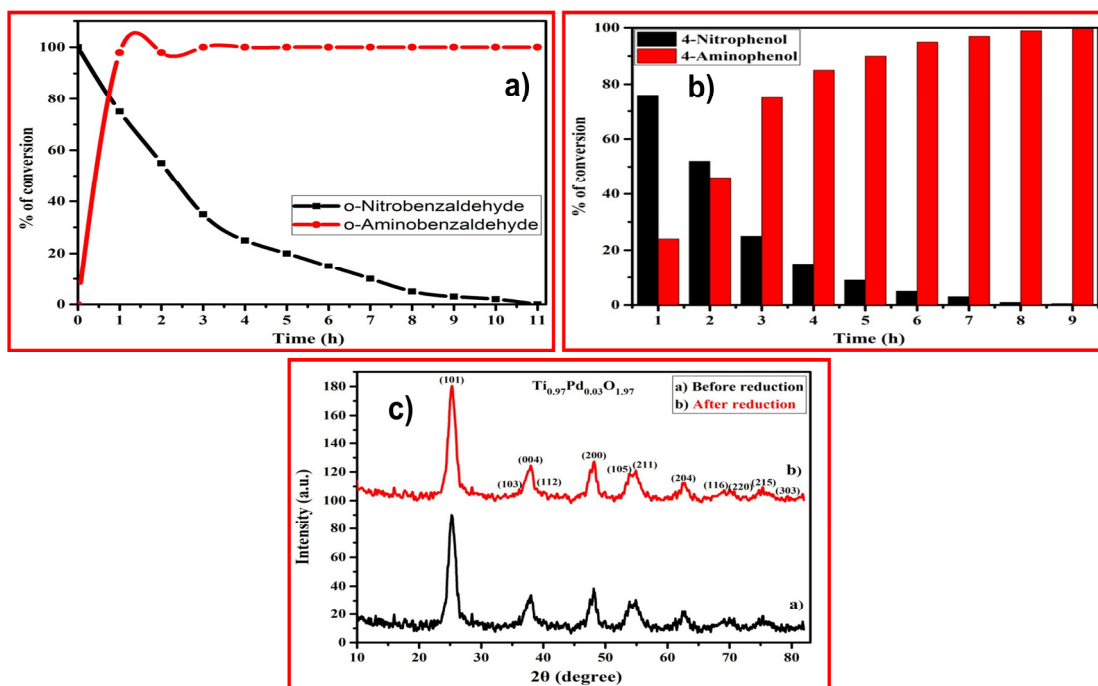
Fig. 2.14 : a) The plot of % conversion of o-Nitrobenzaldehyde of
o-Aminobenzaldehyde b) 4-nitrophenol to 4-aminophenol at 105 ^{0}C vs. Time in an
hour c) Powder XRD of $Ti_{0.97}Pd_{0.03}O_{1.97}$ on a) before and
b) after the reduction of nitrobenzene.

2.4 Conclusion

$Ti_{0.97}Pd_{0.03}O_{1.97}$ is an excellent catalyst for the reductions of the aromatic nitro
compound to amine, avoiding the formation of toxic hydroxylamine by-product.
100% selectivity of the amine has shown by the $Ti_{0.97}Pd_{0.03}O_{1.97}$ catalyst with high
rates of a catalytic reaction. Pd doped TiO_2 is revealed in high catalytic activity on the
solvent and solvent-free reductions of the aromatic nitro compound in 1.2-1.3 bar
pressure of H_2. The reduction of aromatic nitro compounds to aromatic amines was
realized with excellent yield by using nanoporous palladium as a sustainable catalyst
and as a hydrogen source. The above results indicated that the Pd doped TiO_2 shows
that superior catalytic performance.

Reference:

[1]. E. Negishi, Wiley, Chichester, UK, 2000.

[2]. J. Tsuji, John Wiley & Sons, Ltd, Chichester, UK, 2004.

[3]. K. Esumi, R. Isono, T. Yoshimura, Langmuir. 2004, 20, 237.

[4]. N. Toshima, Y. Wang, Adv. Mater. 1994, 6, 245.

[5]. A.J. Bard, Science 207. 1980, 139.

[6]. Willner, R. Maidan, D. Mandler, H. Durr, G. et al. Am. Chem. Soc., 1987, 109, 6080.

[7]. Y. Mizukoshi, K. Okitsu, Y. Maeda, et al, J. Phys. Chem. B. 1997, 101,7033.

[8]. Y.H. Qin, H.H. Yang, X.S. Zhang, P. Li, et al, Int. J. Hydrog. Energy. 2010, 35, 7667-7674.

[9]. Z. Zhang, J. Liu, J. Gu, L. Su, L. Cheng, Energy Environ. Sci. 2014, 7 2535 2558.

[10]. C. Zhang, L. Xu, N. Shan, T. Sun, J. Chen, Y. Yan, ACS Catal. 2014, 1926-1930.

[11]. Y. Shao, J. Sui, G. Yin, Y. Gao, Appl. Catal. B-Environ. 2008, 79, 89-99.

[12]. H. Dislich, E. Hussmann, Thin Solid Films. 1981, 771, 29-139.

[13]. H. Dislich, J. Non-Cryst. Solids. 1984, 63, 237-241.

[14]. B.E. Yoldas, T.W. O'Keeffe, Appl. Opt. 1979, 18, 3133-3138.

[15]. K.T. Ranjit, T.K. Varadarajan, et al, J. Photochem. Photobiol. A Chem. 1996, 96A 18-185.

[16]. S. Yuan, Q. Sheng, J. Zhang, F. Chen, M. Anpo, W. Dai, Catal. Lett. 2006, 107, 19-24.

[17]. R. S. Downing, P. J. Kunkeler, H. van Bekkum, Catal. Today 37, 121(1997)

[18]. E. L. Pitara, B. N. Zemba, J. Barbier, et al, J. Mol. Catal. A: Chem. 144, 199(1999)

[19]. F.Yang, Y.Cao, Z.Chen, X.He, L.Hou, Y.Li, NewJ.Chem.42 (2018)2718–2725,

[20]. Z.Wang, Q.Chen, Chemistry Select3 (2018)1108–1112,

[21]. N. Ono, The nitro group in organic synthesis, John Wiley & Sons, 2003.

[22]. A. Corma, P. Serna, Science 313 (2006) 332-334.

[23]. H. Yang, S.J. Bradley, A. Chan, et al, J. Am. Chem. Soc. 138 (2016) 11872-11881.

[24]. F.D.Bellamy, K.Ou, Tetrahedron 25 (1984) 839–842.

[25]. I.Sorribes, G.Wienhofer, C.Vicent, et al, Angew.Chem.Int.Ed.51 (2012) 7794–7798,

[26]. R.V.Jagadeesh, G.Wienhöfer, F.A.Westerhaus, et al, Chem. Eur. J. 17 (2011)14375–14379.

[27]. H. Yao, M. Fan, Y. Wang, G. Luo, W. Fei, J. Mater. Chem. A 3 (2015)17511-17544.

[28]. Y. Tang, G. Zhang, C. Liu, S. Luo, et al, J. Hazard. Mater.252–253 (2013) 115-122.

[29]. B. Weng, S. Liu, N. Zhang, Z.R. Tang, Y.J. Xu, J. Catal. 309 (2014) 146–155.

[30]. N. Zhang, M.Q. Yang, S. Liu, Y. Sun, Y.J. Xu, Chem. Rev. 115 (2015) 10307–10377.

[31]. W. Wu, G. Liu, Q. Xie, S. Liang, H. Zheng, et al, Green Chem. 14 (2012) 1705-1709.

[32]. S.K. Pahari, P. Pal, D.N. Srivastava, et al, Chem. Commun. 51 (2015) 10322-10325.

[33]. L Wang, P. Li, Z. Wu, J. Yan, M.Wang, Y.Ding, Y. Synthesis 13, (2003), 2001-2004.

[34]. G.A Herepoulos, S.Georgakopoulos, B.R.Steele, Tetrahedron Lett. 46, (2005), 2469- 2473.

[35]. K.Nomura, J. Mol. Catal. 130, (1998), 1-28.

[36]. C.Zhang and Y.Wang. I. J. Chem. 45 (2006), 510-511. 7. B.H.Han, D.H Shin, R.Lee Hyun, B.H Ro. Bull. Korean Chem. Soc., 1989, 315.

[37]. S. Ravikanth, V.G Reddy, S. Rao, et al, Synth. Commun. 2002, 32(18): 2849-2853.

[38]. S. Cheong, J. D. Watt, R. D. Tilley, Nanoscale, 2010, 2, 2045.

[39]. S. Horinouchi, Y. Yamanoi, T. Yonezawa, et al, 2006, 22, 1880.

[40]. H. Kobayashi, M. Yamauchi, et al, M. Takata, J. of Am. Chem. Society, 2010, 132, 5576.

[41]. Downing, R. S.; Kunkeler, P. J.; Bekkum, H. Catal. Today. 1997, 37, 121-136; (b) One, N. Wiley-VCH: New York, 2001; (c) Suchy, M.; Winternitz, P.; Zeller, M. World (WO) Patent 91/00278, 1991.

[42]. F. Korte, Methodicum Chimicum, Thieme, Stuttgart (1975).

[43]. Lara P, Philippot K (2014): An Overview. Catal Sci Technol 4: 2445-2465.

[44]. Kasparian AJ, Savarin C, Allgeier AM, Walker SD (2011). J Org Chem 76: 9841-9844.

[45]. Corma A, Gonzalez-Arellano C, et al (2009). Appl Catal A: Gen 356: 99-102.

[46]. Wua H, Zhuo L, He Q, Liao X, Shi B (2009). Appl Catal A: Gen 366: 44-56.

[47]. Takasaki M, Motoyama Y, Higashi K, et al, et al. (2008). Org Lett 10: 1601-1604.

[48]. Corma A, Serna P, Concepción P, Calvino JJ (2008). J Am Chem Soc 130: 8748-8753.

[49]. Corma A, Serna P (2006). Science 313: 332-334. 15. Chen Y, Wang C, Liu H, Qiu J, Bao X (2005). Chem Commun (Camb): 5298-5300.

[50]. M. Chatterjee, A. Chatterjee, H. Kawanami, et al, Adv. Synth. Catal.354, 2009 (2012)

[51]. F. Zhao, S. Fujita, J. Sun, Y. Ikushima, M. Arai, Catal. Today 98, 523 (2004)

[52]. H. Becker, W. Schmidt, U.S. Patent, 4,287,365 (1981)

[53]. W. C. Craig, W. C. Craig, U.S. Patent, 3,474,144 (1969)

[54]. Lunxiang, J. Liebscher, Chem. Rev. 2007 (107) 133–173.

[55]. X. Huang, K. W. Anderson, D. Zim, L. Jiang, A. Klapars, S. L. Buchwald, J. Am. Chem. Soc. 125 (2003) 6653 -6655.

Synthesis and Structural Characterization of Undoped CeO$_2$ and Pd Doped CeO$_2$ for Photo Catalytic Studies under Sunlight and UV-light irradiation

Paper Published: "Synthesis and Structural Characterization of Undoped CeO$_2$ and Pd Doped CeO$_2$ for Photo Catalytic Studies under Sunlight and UV-light irradiation". **International Journal of Advanced Science and Technology,** 29, (2020), 1436-1453.

CHAPTER-3

Synthesis and Structural Characterization of Undoped CeO$_2$ and Pd Doped CeO$_2$ for Photo Catalytic Studies under Sunlight and UV-light irradiation

The main objective of the analysis is concentrated on the preparation and fabrication of doped and undoped CeO$_2$ nanoparticles by solution combustion technique to taken glycine as fuel. The correct morphology of the doped metal compounds was studied by Scanning electron microscopy (SEM). The composition of ceria (CeO$_2$) and palladium substituted Ceria (Ce$_{0.98}$Pd$_{0.02}$O$_2$) was confirmed from the powder X-ray Diffractometer (PXRD). The functional groups were analyzed by Fourier transfer infrared spectroscopic analysis, XRD, RR, UV–Vis, and XPS. The Photocatalytic properties of CeO$_2$ and palladium doped CeO$_2$ (Ce$_{0.98}$Pd$_{0.02}$O$_2$) nanoparticles (NPs) were studied using the radiation conjugation of red (CR) under UV light and sunlight exposure. Based on the XRD analysis, CeO$_2$ and Pd doped CeO$_2$ NPs were formed as crystal structures. CeO$_2$ and Pd doped CeO$_2$ showed excellent Photocatalytic activity by degrading more than 92% of the CR color in the intervals of 120 min under UV light and sunlight.

3.1 INTRODUCTION

In the current study, we can develop a regular solid catalyst wherever the catalyst may be a unique phage solid having a definite structural and its potential to distinguish the active area of the catalysts for the chemical process. The palladium metallic element is the least expensive and most typically used metal. CeO_2 absorbs lightweight within the close to ultraviolet radiation and small light within the visible region. Further, Cerium dioxide (CeO_2) composite materials were used as a cost-effective, chemical change catalyst, economical chemical reaction catalysts, distinctive oxidation-reduction property, oxygen storage capability (OSC), environmental catalysts for the natural and synthetic process to pull down of assorted volatile organic compounds to the removal of contaminates from carbon dioxide [1-3]. Palladium based catalysts significantly nanoscale metallic element particles have recently drawn massive attention because of their versatile role in organic synthesis [4-5]. The employment of Pd in catalysis not only in industrial [4-6] but also the catalytic activity, size, shape, form, yet as the nature of close to the surrounding media [7]. CeO_2 has been wide investigated as support in three-parts of catalysts for exhaust gas treatment from vehicles [8-9], water gas shift catalysts [10-11], electro-oxidation catalyst [12], oxygen particle in a compound fuel cells [13], sprucing chemical, mechanical and planarization technique [14], the molecular, structural compounds of semiconductor devices [15], ultraviolet difficulty materials [16]. Metal oxides became the most productive palladium supports for heterogeneous catalytic chemical change action due to accessibility, low production costs, and photo induction hole pairs on the surfaces of a compound that could be harvest to spice up electron transfer and their chemical reactivity [31]. Newly, the intense extended

electrochemical catalytic action and the stability of supported metal catalysts [17-19]. Additionally confirmed that the communications could be modified with the structure of the catalyst, that go change in chemical actions of catalysts, the sturdiness of the carried materials may additionally control the durability of the resultant catalyst [20]. At the low-temperature treating (350^0 to 450^0), it denotes a favorable application and CeO_2 based catalyst [21-23]. The synthesis of ceria and palladium doped ceria is most useful for the high oxygen storage capability. The synthesized doped metal oxides are characterized by PXRD, SEM, Most applications of this catalyst are employed as high rates of H_2+O_2 recombination, solvent-free reduction of aromatic nitro compounds to amines as high with olefins ready [30]. CeO_2 could be nontoxic reducing oxides, and metal ions are substituted in CeO_2. In $Ce_{1-x}M_xO_{2-x}$ (x= 0.01, 0.02 and 0.03) wherever metallic element palladium having +2 oxidation state showed high rates of nitro to amine reduction and sensible picture chemical change activity for CO reaction. Smaller the metal particle, higher is that the quantity of CO absorption and better is that the chemical change conversion. Nanoparticles of high-quality metals (Pt, Pd, Rh, Ru, and Au) hold titanium, alumina, and chemicals. These catalysts are often associated with natural compounds, petrochemistry [30]. The synthesis of CeO_2 nanoparticles in a variety of uses, and growing important because it applied for fuel and solar cells, metal oxides, semiconductor devices, and phosphor [24-25]. This chapter reported on the molecular structure and characterization of CeO_2 and Pd Doped CeO_2 nanoparticles using a molecular method among the pollutants. Congo red (CR) is most widely used as a pollutant in industries. The destruction of red sunlight is an effective and unique method for the elimination of waste and safe water. Along with the finite element

properties, the photocatalysis system using the semiconductor has attracted considerable attention since it provides environmental and economic features [32-34]. Cerium oxide (CeO_2), a Photocatalytic solvent, has attracted considerable interest from researchers because of its electrical, optical, and chemical properties [35, 36]. CeO_2 is an important component in the chemical and photochemical resistance method, the light absorption in the UV region (extraction, 385-700 nm). Unfortunately, large quantities of CeO_2 [37–38] are severely restricted by the large bandgap (3.2 eV). Machine correction tools (e.g., TiO_2, ZnO, CeO_2, SnO_2, NiO, etc.) are of particular interest to the electronic media because of their unique electronic properties, diagnostic properties, and transmitting travel features. And porosity [39]. Usually, Photocatalytic systems use semiconductors such as TiO_2, WO_2, and ZnO as UV detectors [40-42]. CeO_2 was another active ingredient that is used in the UV light field. The efficiency of the ceria is accompanied by several advantages such as its high bandgap (3.2-eV) [43], high sensitivity [44], high-frequency domain [45], potential high oxygen concentration [44] and the ability to respond [45]. However, the narrow band of CeO_2 (3.0–3.4 eV) has been restricted to activity. The photoexcited electron/ion coupler during light irradiation [46–48].It is important to prevent this process from the use of metal ions, which can produce impurities in the CeO_2 group configuration for car compensation and reduce the redox bond rate as well as facilitate the redox reaction on the surface of the photocatalysts. [49-51]. Palladium ion-based ionization as a potential catalyst for Pd^{2+}/Pd^{3+} and Pd^{+} / Pd^{2+} levels, which can act as a low-energy ion for electron or hole-based catalysts. The position of Fermi level is present and where they live [52], the work was intended to convert CeO_2 fibers using Pd ion using different percentages to perform the same methods as water,

impregnation, and calcinations method. The use of XPS, XRD, FESEM/ EDS, spectroscopy, spectroscopy, and CeO_2 spectroscopy due to the Pd dopant were studied by experimental data, spectroscopy, and IR measurements. Sampling, the development of visible, non-toxic, and chemical compounds under long-light emission. The activity of Pd on CeO_2 for both un-doped ceria and palladium doped ceria materials were analyzed in terms of lattice parameters, average crystalline size, and small internal strains. Within the present work, CeO_2 and palladium doped CeO_2 ($Ce_{0.98}Pd_{0.02}O_2$)nanoparticles were prepared by solution combustion methodology, glycine as fuel and the final product was well characterized by PXRD, Scanning microscopy, Rietveld refinement method(RRM), Fourier transformation of infrared spectrum analysis (FT-IR), Ultraviolet-visible spectrum analysis (UV).

3.2 EXPERIMENTAL METHOD

3.2.1 Materials

$(NH_4)_2Ce$ $(NO_3)_6$, NH_2CH_2COOH, metallic element Palladium chloride $PdCl_2$ was purchased from Merck. The combustion technique prepared ceria (CeO_2) and Pd-doped ceria catalysts, Congo red.

3.2.2 Synthesis of Cerium Dioxide (CeO₂) Nanoparticles

The starting materials are ceric ammonium nitrate and glycine as fuel. Synthesis of CeO_2, the stoichiometric ratio of starting materials were to be taken as 9.89 mmol of ceric nitrate $(NH_4)_2Ce(NO_3)_6$ and 10.9 mmol of glycine in a 300ml capability crystallization salt in a container, the reactants were dissolved in 15 ml of H_2O, and the aqueous solution was introduced into the preheated chamber at 350°C. The solution ignited to burn with a flame takes place once dehydration is completed to get

the voluminous reliable product is obtained. The solid product was chosen for structural characterization.

$$5Ce(NH_4)_2(NO_3)_6 + 12C_2N_4H_6O_2 \rightarrow 5CeO_2 + 24CO_2 + 44N_2 + 36H_2O \dots (1)$$
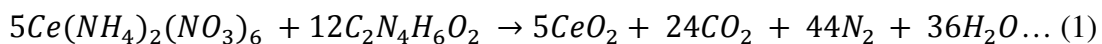
3.2.3 Synthesis of Palladium Doped Ceria (Ce$_{0.98}$ Pd$_{0.02}$ O$_2$).

The Palladium doped ceria catalyst was synthesized using the combustion method. The compound Ce$_{0.98}$Pd$_{0.02}$O$_2$ can be prepared from the solution combustion method. The starting materials are (NH$_4$)$_2$Ce (NO$_3$)$_6$, Palladium chloride PdCl$_2$, Glycine NH$_2$CH$_2$COOH as fuel. For the synthesis of Ce$_{0.98}$Pd$_{0.02}$O$_2$ by taking the stoichiometric ratio of beginning materials were to be taken as 9.89 mmol of (NH$_4$)$_2$Ce(NO$_3$)$_6$, 0.21mmol of PdCl$_2$ and 10.99 mmol of glycine in a 300ml capability of crystallization borosilicate salt container (dish). These three compounds were wholly dissolved in 25 ml H$_2$O, and the solution was brought in to preheated chamber at 350°C. The solution burns with flame once dehydration is completed to an obtained solid product. The reliable product was taken for the structural characterization, and we have record X-ray diffraction techniques and the Rietveld refinement method. Solution combustion synthesis for Ce1-xPdxO2 can be written as follows:

$$9(1-x)(NH_4)_2Ce(NO_3)_6 + 24(1-x)C_2H_5NO_2 + 9xPdCl_2 \rightarrow 9Ce_{1-x}Pd_xO_{2-\delta} +$$
$$96(1-x)N_2 + 48(1-x)CO_2 + (96-114x)H_2O + 18xHCl \dots\dots (2)$$
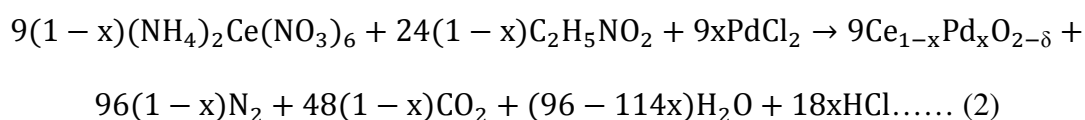
3.2.4 Evaluations of Photocatalytic Activities

The adsorbents were investigated by the dissolution of the Rome hair filter (CR) (10 mg / L) under visible UV irradiation. All reactions were performed at room

temperature with average air temperature. 60 mg of catalyst was dissolved in 100 mL shampoo. Before irradiation, the cells were placed in a dark environment, and the magnetic stirred for 30 min until they reached the adsorption-desorption level. From this, the photographic reaction began with the introduction of visible light in the system. 5mL of the solution was taken at time intervals and centrifuged to remove the particles, and the results of the irradiation were determined using a UV-vis spectrophotometer. The photocatalytic activity of the reagents evaluated the interference of the seawater. The photocatalytic reaction efficiency was calculated using Equation (1).

$$\text{Degradation Capacity (DE \%)} = C_0 - C_t / C_0 \times 100 \ \ldots\ldots \text{ (3)}$$

Where 'C_0' is the initial concentration and 'C_t' or photo concentration or time constant. (Optical resolution for CR $\lambda = 498$ nm).

3. Result and Discussion

3.1 Powder X-Ray Diffraction Analysis (PXRD)

XRD pattern of CeO_2, palladium doped CeO_2 were recorded to X-ray Diffractometer. The radiations vary 20-700 (λ=0.15nm). The XRD peaks of the CeO_2 and ($Ce_{0.98}Pd_{0.02}O_2$) nanoparticle obtain and the structures were characterized by PXRD, and the structure was refined by the Rietveld refinement technique. The Rietveld refinement methodology and, therefore, the program is employed to recognize the different phases present within the solid compound. The XRD patterns are index as anatase phase of *CeO_2*, and additionally, the physical phenomenon data were in good a correspondence with JCPDS Number.340394. The average crystal size was obtained by Scherrer's formula:

Crystalline size (D) =K λ/ ($\beta \cos \theta$).... (4)

D is the size of the crystal in nm; λ is the wavelengths of the X-ray (λ=0.154 A^0 in nm) for Cu Kα; K is the crystal form is 0.9, θ is the brag's angle, and β is the 0.5 high dimension at half-maximum height. The Rietveld refined patterns of CeO_2 and $Ce_{0.98}Pd_{0.02}O_2$ as shown in Fig. 3.1 c) & d). The profile is indexed to anatase tetragonal shape of CeO_2 increases 1 to 2 atomic percentage of palladium metal may be detected by the slow scan. If the Palladium metal particle was substituted for the Ce^{4+} particle showed six coordination centers. The Rietveld refinement information was given by equation (4).

$$\beta = (U \tan2\theta + V \tan\theta + W)1/2..... (5)$$

Crystalline size obtained each of the strategies together. The parameter, Rf, Rbragg, $\chi2$ area unit, summarized the below Table -3.1. The lattice parameter (a), of CeO_2, was 5.411 (JCPDS.No.21-1272). The lattice parameter (a) of nanocrystalline CeO_2 is slightly lower than palladium doped CeO_2 (5.411). Typical analysis of the catalysts was shown in Fig.3.1 a) that showed experimental and calculated values of powdered XRD patterns obtained by the refinement of CeO_2 and palladium doped CeO_2. The parameters (Rf, Rbragg, $\chi2$) showed decent accordance between the Rietveld refined and determined XRD patterns for cuboids of CeO_2. The refined lattice parameter value of CeO_2 and palladium doped CeO_2 are 5.5 nm (A^0) and 3.7 nm (A^0). The cell volume of CeO_2 confirming that the cuboids structure. The powder samples were further confirmed by the refinement of the diffraction patterns with the Rietveld method. Fig. 3.1 c) and d), shows the Rietveld refinement method. The improvement could be a methodology within the profile that shows the potency of

scanning measurements of the particles permit to estimate an approximate structural

model for the vital CeO_2 and palladium doped CeO_2 structures.

Table - 3.1 : Structural Parameter of CeO_2 and $Ce_{0.98}Pd_{0.02}O_2$.

Catalysts	Lattice parameter (a)	Rf	R Bragg	$\chi 2$	Size (nm)	Rietveld refinement size (nm)
CeO_2	5.410(1)	0.51	0.71	1.14	5.9	5.5
$Ce_{0.98}Pd_{0.02}O_2$	5.411(1)	0.81	1.08	1.39	3.1	3.7
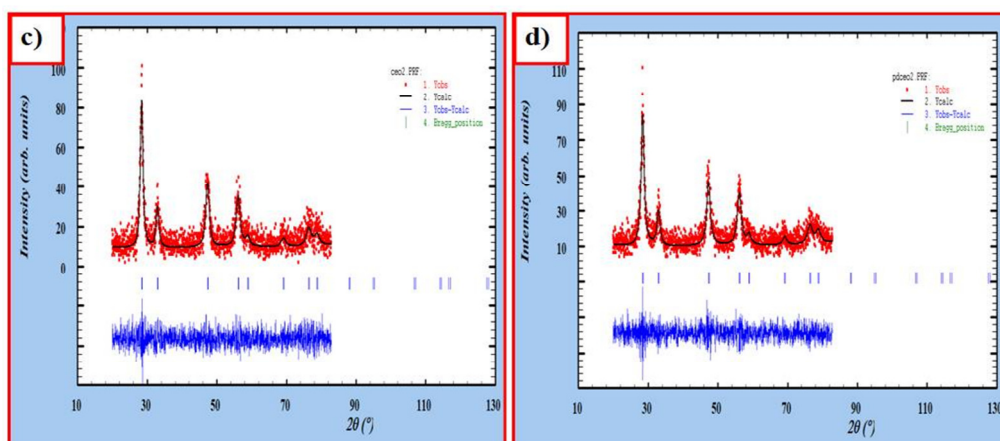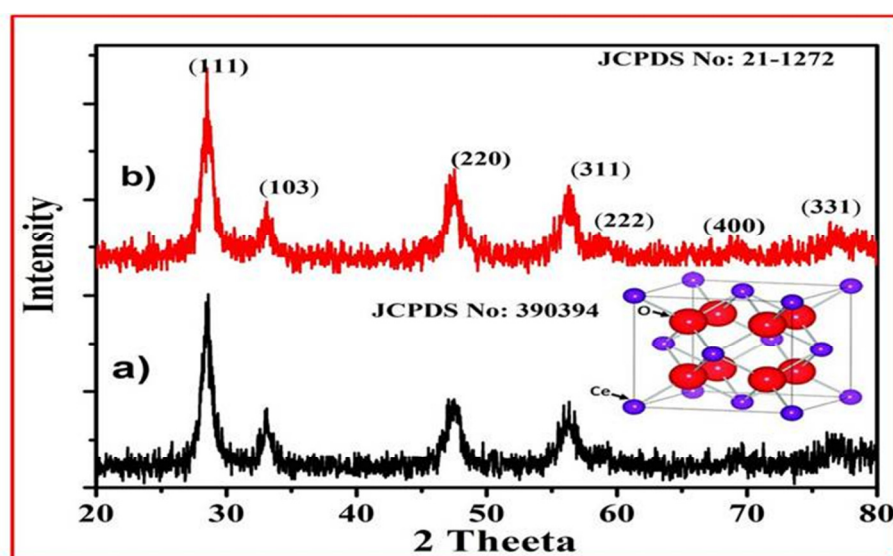
Fig.3.1 : XRD Pattern and of Rietveld refined structures of a),c) CeO_2 and b), d)

$Ce_{0.98}Pd_{0.02}O_2$

3.2 Scanning Electron Microscopic Analysis (SEM)

The Scanning electron microscopy pictures of CeO_2 and metallic element of palladium doped CeO_2 is ready to show, the interpret nanoparticles structures additionally may be seen in grain size ~ 1µm and also two-dimensional figure showed, the evidence of the nanoparticles is very little accumulation and a two-dimensional Fig.3.2, showed morphology. The SEM analysis of $Ce_{0.98}Pd_{0.02}O_2$ catalyst doesn't have any impact on the morphology and structure of the CeO_2 nanoparticles. The SEM analyses showed top homogeneity at time intervals, the prepared palladium doped CeO_2 samples surface area increasing the hardening temperature. These results show that the morphology of particles changes to the spherical kind with less quantity by increasing temperature. The SEM analysis of the typical crystal size of tempered nanocrystals is regarding ~ 20nm.
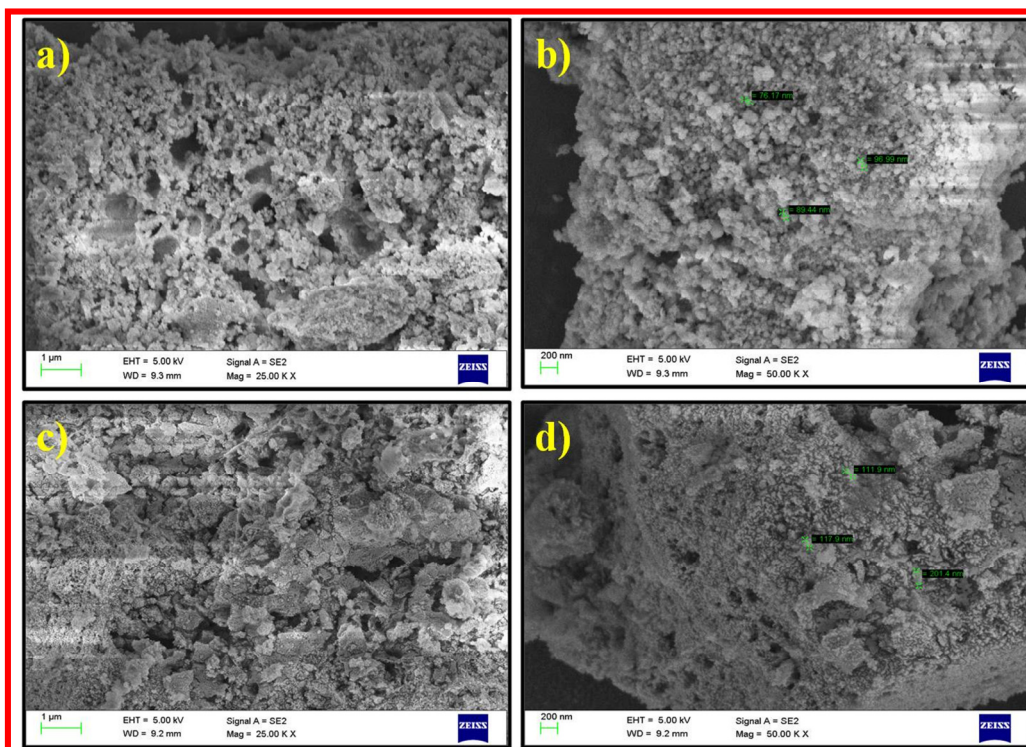
Fig.3.2 : SEM images of a), b) CeO_2 and c),d) Palladium doped CeO_2

3.3   Energy Dispersive X-Ray Analysis (EDAX)

The typical EDAX spectra of synthesized CeO_2 and Pd doped CO_2 catalyst is shown in Fig. 3.3. In the synthesized CeO_2 and Pd dope, CO_2 catalysts having an atomic percentage of Ce and O were found to be 89.84 % and 10.16%, respectively. However, for the transition metal ion Pd^{2+}, doped CeO_2 nanoparticles, the atomic percentage of Ce, Pd, and O were found to be 82.24%, 0.18%, and 17.58%. The cerium percentage increased, and whereas the oxygen percentage also increased, this is due to the doping effects.

Table - 3.2 : Elemental composition of CeO_2 and $Ce_{0.98}Pd_{0.02}O_2$.

Element (Wt. %)	O	Ce	Pd
CeO_2	10.16	89.84	-
Pd doped CeO_2	17.58	82.24	0.18
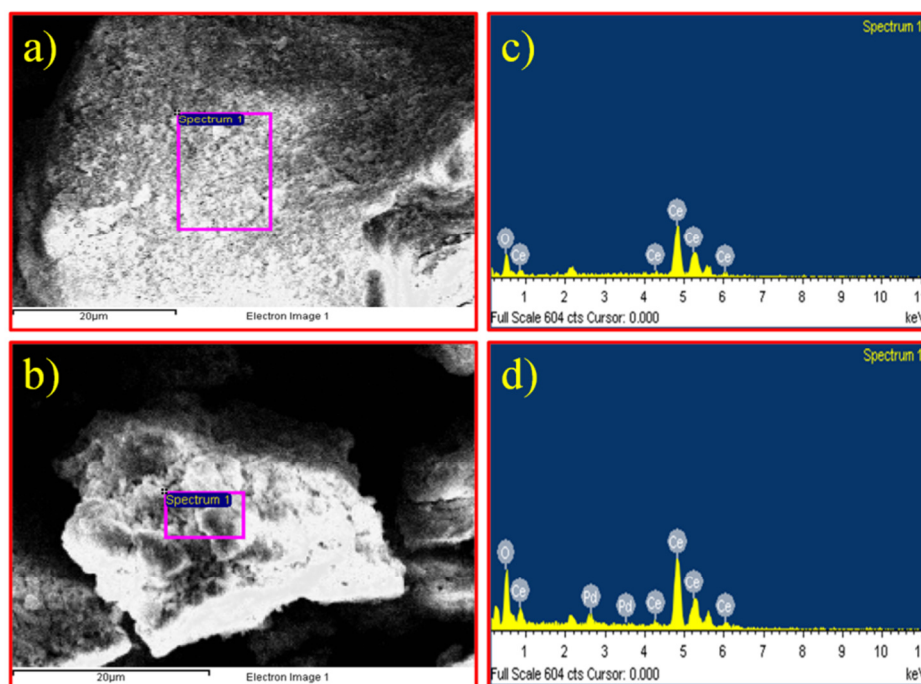
Fig.3.3. EDAX images of a), c) CeO_2 and b), d) Palladium doped CeO_2

3.4. Fourier Transformation-Infrared Spectroscopy Analysis (FT-IR)

The Fourier transformation-infrared spectra are used to recognize the functional group, study the vibration of atoms and molecules of CeO_2 and palladium doped CeO_2 shown in Fig. 3.4 a) and b). Each Fourier transformation infrared spectra from Fig. 3.4 a), and c) it denotes 4-fold cerium coordination in vitreous matrix.3 absorbed peaks were discovered at 3426, 1622, and 1089. In Fig. 3.4 a) and b), showed vibration bands: 1622 cm^{-1} (HOH), 366 cm^{-1} correlation to Ce-O bond vibration, when increase temperature, the intensity vibration bands due to Ce-O bonds can increase the unit area made higher outlined. At a similar time, vibration band is present in water molecules, and structure can be diminished. The same profile is obtained for metal palladium doped CeO_2 as shown within the Fig.4 a).The synthesized FTIR spectrum of CeO_2 nanoparticles among the vary 500-4000 cm^{-1} that establish chemical bonds furthermore practical terms among the chemical element. The large, broadband showed at 3415 cm^{-1} was assigned due to the O-H vibration in OH groups. The absorption peak around 1464 cm^{-1} is designated in the bending wave of C-H stretching. The critical peak at 500 cm^{-1} corresponds to the Ce-O stretching vibrations [26, 27].
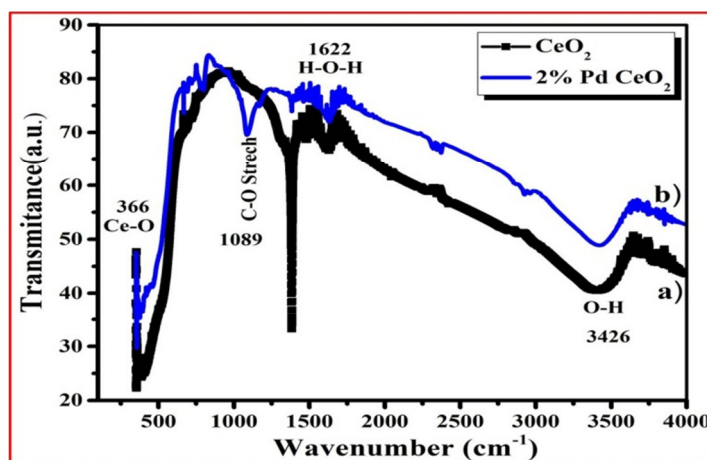
Figure.3.4. FTIR spectra of a) CeO_2 and b) Palladium doped CeO_2

3.5   X-Ray Photoelectron Spectroscopy (XPS) Studies

XPS analysis of CeO_2 higher rates is observed in Fig.3.5 due to Ce3d, Ce4d, O1, and C1. Figure.3.1.5. Shows how the Ce3d header is integrated into a different state, in addition to the XPS experimental data. The XPS of CeO_2 on the surface is shown to be two Ce3d and tetravalent Ce4d sulfur soils and can be solved with five $Ce3d^{5/2}$, $Ce3d^{3/2}$ spin-orbit double bonds [76, 77, 78-83]. Different levels of C1s were measured throughout the experiment; specifically, each XPS system observed increasing C1s levels at 285.07, 286, and 291.2 eV across all measurements and the combined power of all spectra averaged 285 eV for the C1s. O 1s deconvoluted spectra are shown in Fig. 3.5. The bands added to the O1s show three thresholds at 530.5, 530.7, and 532.8 eV. The two bands have higher frequencies at 530.5 eV and 530.7 eV respectively [76, 77, 84-86]. The third triplet peak at 532.8 eV has high oxygen/hydroxyl species similar to that reported in the present paper [87-89].
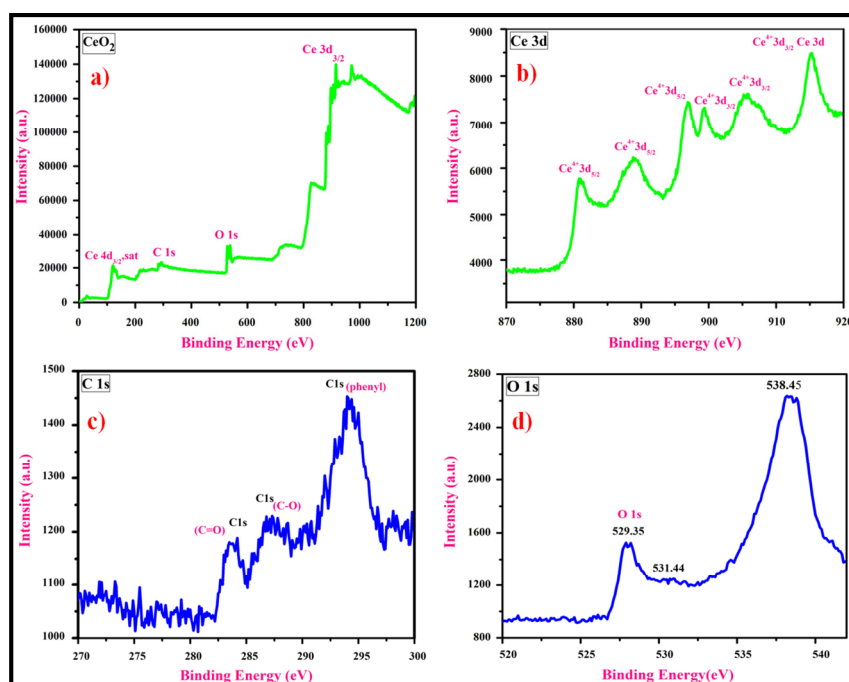
Fig.3.5 : XPS images of CeO_2 nanoparticles
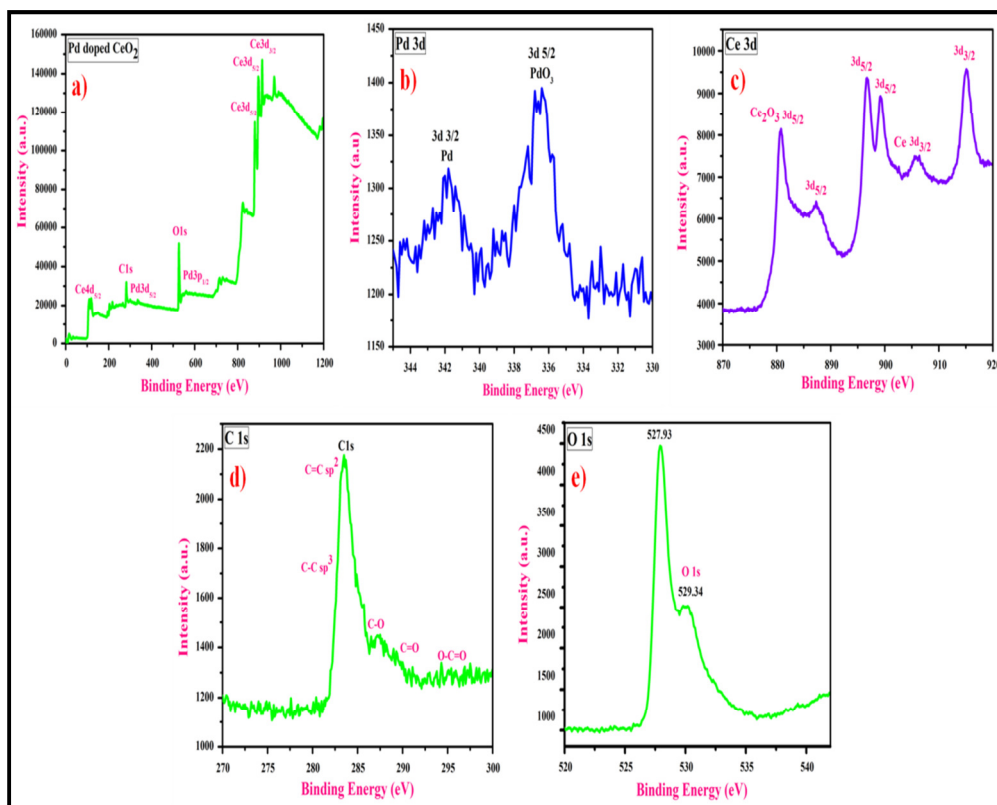
Fig. 3.6 : XPS images of Pd doped CeO_2

In Fig. 3.6. The XPS spectra of Pd doped CeO_2 were determined by measuring the concentrations of Ce3d, Pd3d, O 1s, and C 1s. XPS level Pd (3d) XPS was expressed in 2% Pd doped CeO_2 ($Ce_{0.98}Pd_{0.02}O_2$). Pd ($3d^{5/2}$) power was found to be correlated at 336.3 eV, which is higher than Pd^{2+} ($3d^{5/2}$) energy in association with PdO [90] less than the potential of Pd^{2+} ($3d^{5/2}$) and 338 eV and $PdCl_2$ [91]. So Palladium in 2+ oxidation state at ($Ce_{0.98}Pd_{0.02}O_2$). The (3d) XPS levels are shown in fig.6. From different levels of Ce (3d), we found that 10% Ce is in the 3+ state. Ce4d spectra of Ce4 show a two-dimensional peak with the energy of 896 and 912 eV. In an additional peak at 887 eV and 905, eV is given to some Ce^{3+} ion activity related to oxygen generation [92]. These results demonstrate that the smoking states of Ce (IV) and Ce (III) are in preparations. The Ce3d region is expressed by splitting the $Ce3d^{5/2}$ and $Ce3d^{3/2}$. The XPS of the Pd 3d region appears to be doubled at 336.3 eV, and

343.89 eV is the Pd^{2+} effect [93]. Another energy associated with 341.2 eV was connected to Pd^0 $3d^{3/2}$, which also shows that Palladium elements are in the background. The low affinity for BE can be attributed to the relationship between palladium and cerium oxide in their analysis [94]. Due to the orbit coupling, Pd 3d films are divided into two $3d^{5/2}$ and $3d^{3/2}$ electrons, respectively. Two pairs of pegs were drawn and repeated, representing two Pd species. A couple may be more likely to be assigned to the Pd type, whereas a more stable couple may be present in the Pd (II) species. It is interesting to count on binding affinity for Pd species is higher compared to PdO or PdO [95]. In total, the Pd 3d level of the XPS shows that the absorbance energy of 336.4 eV is assigned to the Pd electron, and injected with the combined energy of 336.8 eV, corresponding to the PdO. The reflectance spectra of the O 1s show a similar peak in the potential energy (BE) of 529.9 eV of the oxygen atom in the cerium oxide. The presence of several O1s during the potential of 530 eV is due to the presence of oxide [96]. As shown in Figs. The O1s of the sample is divided into two groups. The peak at 530.9 eV is in the oxygen lattice, while the peak at 531.8 eV is chemisorbed oxygen [97]. In the C1s regions, the most affected signals were followed by sp^2 hybridization, with a BE of 285.97eV, follow by weak sp3, CeO, C-O, and O-C-O [98, 99]. This signal is 283.49eV is air pollution [100]. The characteristic feature of the C1s region is the high potential $C-C-sp^2$ hybridization, and the coupling is 283.98eV.

3.6. UV-Visible Absorption Studies

The synthesized CeO_2 and Palladium doped CeO_2 were examined by UV-Visible spectro-photometer in (Fig.3.7) Excellently-definite sharp-edged transmitted

peak located at 329 nm. The transmitted peak moves toward the shorter wavelength to a higher wavelength. It indicates the slim, single particle size distribution obtained during this fabrication technique. Ultraviolet-Visible spectra showed no alternative peak connected with impurities and structural defects that confirmed that the synthesized nanoparticles square measure pure CeO_2. The absorption wavelength seems at concerning 329 nm for CeO_2 nanoparticles [29].The variation within the absorption peaks for comfortable and mixed chemical compound nanoparticles area unit because of the smaller size of nanoparticles [30].
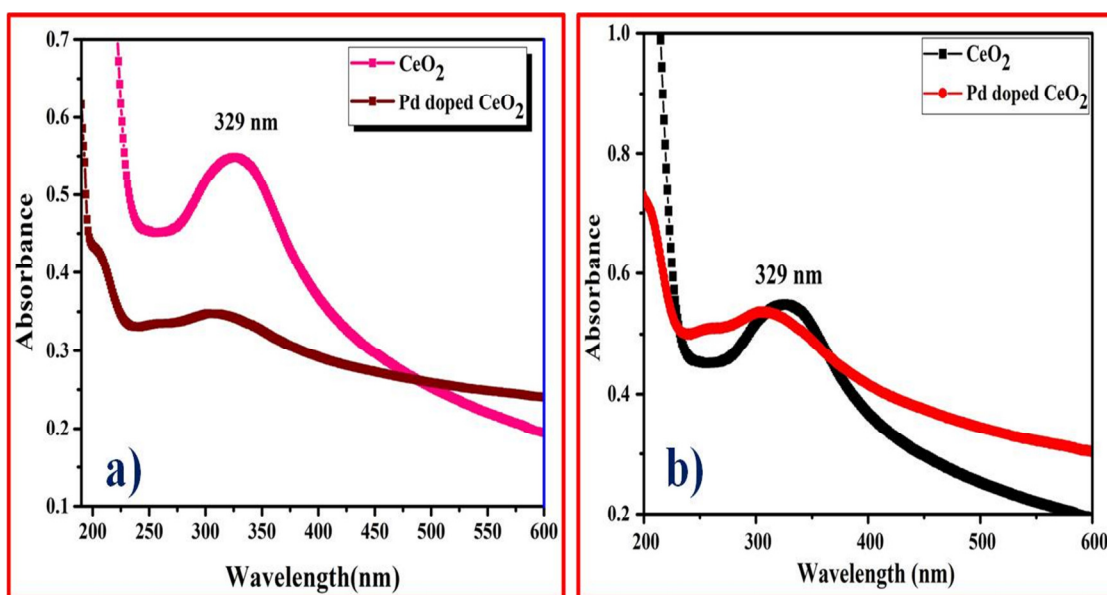
Fig. 3.7 : UV-absorption spectra of a), b) Solid and Liquid

CeO_2 and Palladium doped CeO_2

3.7 Photocatalytic Studies

3.7.1 Photocatalytic Activity of Congo Red

Hydrophobicity of the gradient CR dye in the presence of nanocomposite material provides an essential lightening effect to changes in the concentration and duration of irradiation. (Fig. 3.8). Displays the optical fluctuations of the resulting

CR fluorescence. The effect of irradiation in the presence of CeO_2 and Pd doped CeO_2 nanocomposite leads to a reduction in water content. Photoelectron spectra of both catalysts were investigated, along with their performance comparison. It is found during the acceptance period that the amount of confirmation will decrease during the irradiation period. It showed the absorption of the dye was decreased in the presence of CeO_2 and that of the nanoparticles of Pd doped CeO_2 under UV light. The red light at 497 nm (fig.3.1.8) decreased significantly during the irradiation period, with the restriction of the color ending within 120 min for CeO_2, while Pd doped CeO_2 exhibited degradation. The color lost at the end of 120 min (figure 8). The peak was significantly lost during the irradiation period, indicating that a complete photoelectron had taken place to destroy the chromophore of the dye. Compared to the visible UV (sunlight) exposure of the red Congo colon, the photocatalytic ability of donors to damage red Congo significantly reduced extraction after irradiation. The final results concluded the activity of CeO_2 aggregates was much lower than that of Pd doped CeO_2, which indicates that Ce^{+4}, has a higher molecular weight than Pd^{2+}.
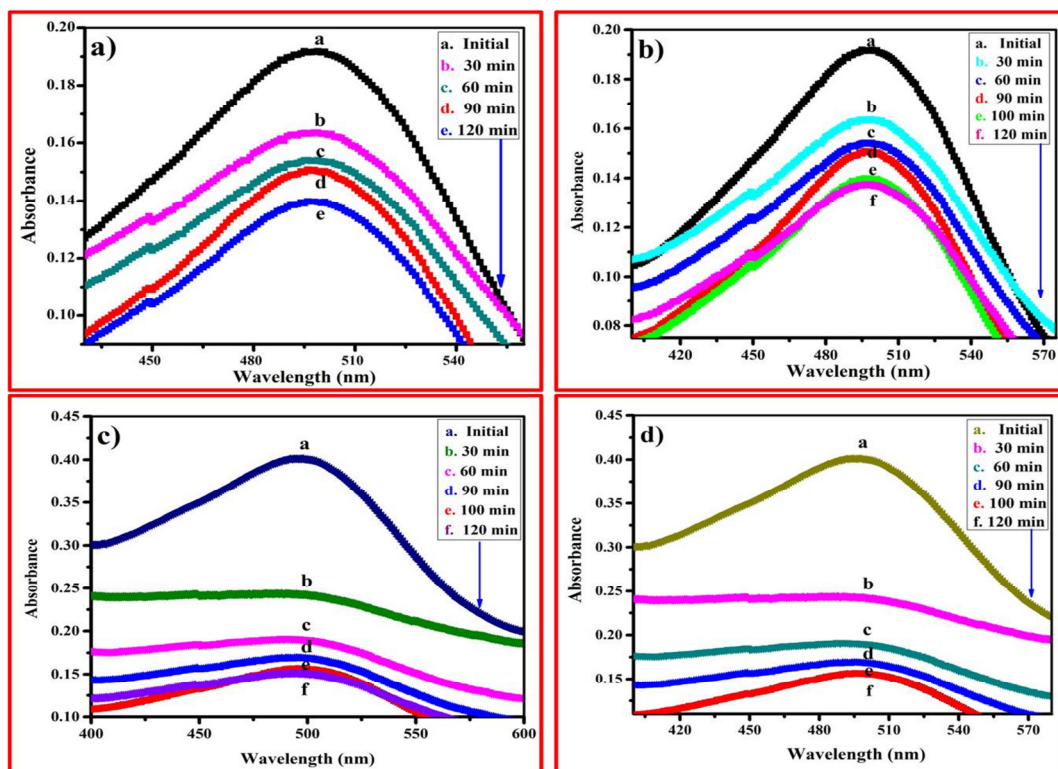
Fig. 3.8 : Absorption spectra of CR dye in the presence of a) and b) CeO_2 and c) and d) Pd doped CeO_2 under exposure to UV light and visible light at different irradiation time intervals.

3.7.2 Evaluation of Photocatalytic Activity

Photo degradation was performed on CR, a common antibiotic for UV irradiation in photocatalytic experiments of undoped CeO_2 and Pd doped CeO_2 catalysts. To illustrate, photodegradation of CR of CeO_2 and Pd doped CeO_2 in a non-catalytic manner was done. The photodegradation time course of the CR and the various inputs provide the experimental results shown in Fig. 3.9. These results indicate that the CR system is stable under visible and UV irradiation without any bandwidth. When catalysts were added to the CR dye solution, the photocatalytic degradation rate of CeO_2 reached approximately 94% within 120 minutes of irradiation, less than that of Pd doped CeO_2 that could reach 86% of the total decomposition. Fig. 3.9. Image displays the destruction of the red-brown Congo of the

sediments under the dark, presence of CeO_2, and Pd doped CeO_2 catalysts. From the results, CeO_2 and Pd doped CeO_2 nanocomposite showed excellent photocatalytic activity of CeO_2, Pd doped CeO_2 nanocomposite. CeO_2 unlocked showed 94%, with Pd doped CeO_2 catalyst shows 86% of degradation Congo red of water is cooled after 120 min. There was no photodegradation observed in the absence of a catalyst. The result revealed that the CeO_2 nanocomposite exhibited better photocatalytic activity.
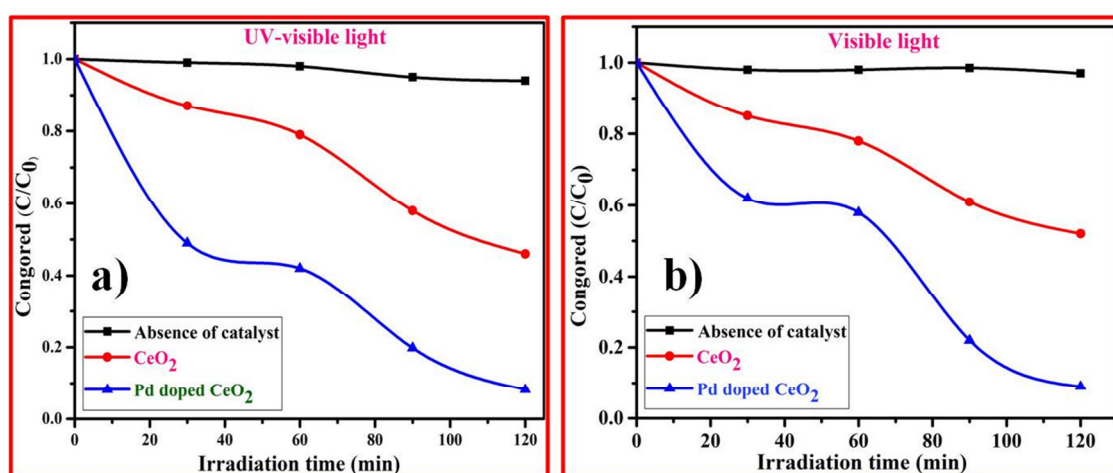
Fig. 3.9 : The photocatalytic degradation of CR dye in absence and presence over different photocatalysts a) UV-light b) Sunlight

The Contribution of Congo red and undoped CeO_2 to Pd doped CeO_2. To estimate the characteristics of suppliers, the degradation rate of the CR dye was calculated in Table 3.3 It is, therefore, excluded from the study that CeO_2 effluent was found to be better than Pd doped CeO_2. The pure act was obtained by quantifying Congolese and red color images using CeO_2 and Pd doped CeO_2 NPs. The two most common types of lighting are sun and UV-light. The experiments were performed by diffusing 60mg of CeO_2 and Pd doped CeO_2 Nps in 100ml of red pepper extract of 20ppm Congo. The photocatalytic degradations of Congo

red for 120 min are higher in UV light (92%) than in sunlight (85%). This is because the UV light is high (low waves or high energy), so light can penetrate rapidly and result in a large number of radicals, which increase in the rate of photocatalytic damage of Congo red.
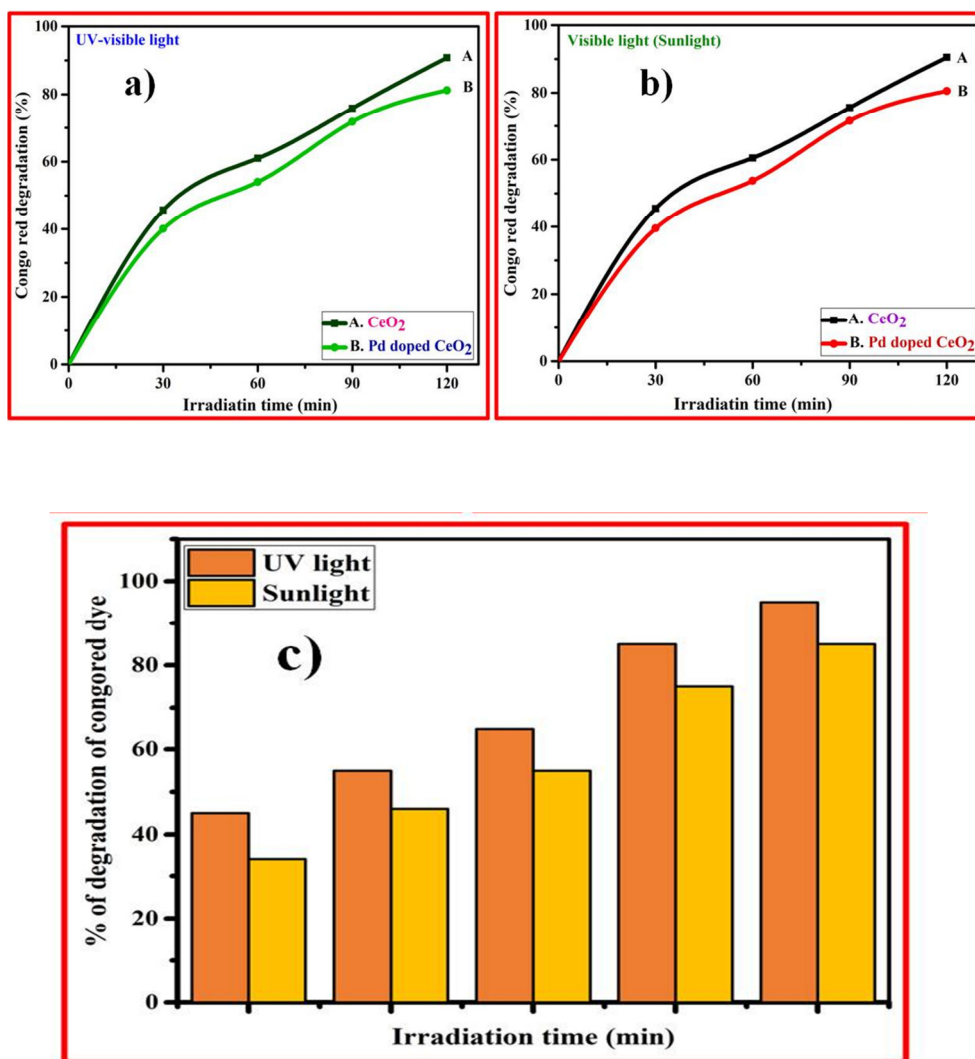
Fig. 3.10: Degradation percentage (%) capacity of a) UV light b) sunlight c) comparative study of UV light and Sunlight

Table 3.3 : Percentage (%) degradation of Congo red dye

Light Sources	Catalysts	Weight of catalysts	Degradation time	Degradation (%)
UV-light	CeO_2	60 mg	120 min	94
Sunlight	$Ce_{0.98}Pd_{0.02}O_2$	60 mg	120 min	86

3.7.3 Effects of Catalyst Weight

The catalyst quantities for CR dye in 20 ppm were 60 mg, Reduction of dose increases with supplier rate and indicates significant reductions in doses of up to 60 mg; This might be too several potent sites present when the load is 60 mg, which increases in photons, resulting in increased photodegradation. Behind the level results in no significant change observed in photodegradation because of the problem of annealing increases with increasing concentration leading to a reduction in light intensity and a reduction in photodegradation.

3.7.4 Effects of Initial Dye Concentrations

The results of the first CR were evaluated on the efficiency of photodegradation by a concentration of 20 ppm. The decrease in photoluminescence after daylight is 20 ppm, and when that is reduced, this is due to the inhibition of photocatalyst active sites and reduced photon interactions at these sites. The increased concentration of hair follicles leads to an increase in the use of artificial insemination in photos. However, the reduction of photocatalytic degradations is due to the low levels of oxygen produced by the sun. On the other hand, increasing the intensity of hair loss, the photodegradation efficiency decreased, so that fewer sites were active in

the sample, and as a result, photodegradation efficiency decreased.

3.7.5 Reusability

Determination and ability to connected are essential for their practical application. The sample was determined by repeating a five-photon photodegradation experiment of the same method, and the results of this model are shown. The achievement results showed a slight decrease in photodegradation performance at each time point and no distortion that resulted in the completion of the fifth phase, which showed the positive energy of the analyst. The reconstitution of CeO_2 nanocatalyst is investigated by the degradation process of staining; the activities of the reactor decreased gradually during the fifth cycle in 85 % after 90%, and this may be due to the removal of the ion from the superior particle. The catalysts separate and recover when the centrifuge responds. CeO_2 nanocatalysts that are retrieved due to oxidative damage can be resumed. The percentage of loss was nearly equal for the first three cycles showed in Fig. 3.11, and it began to decline slightly in the fourth series, and that may have been due to management control during the recovery process. The percentage of degradations of dye from CeO_2 nanocatalysts is slightly higher than Pd doped CeO_2. The above results demonstrate that the complementary nanoparticle CeO_2 exhibit excellent photocatalytic activity. The photocatalytic mechanism of CeO_2 as follows:-

$$CeO_2 + \text{visible-light} \rightarrow CeO_2 \ (e^- + h^+) \dots \dots (6)$$
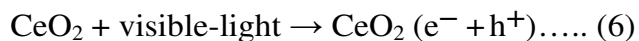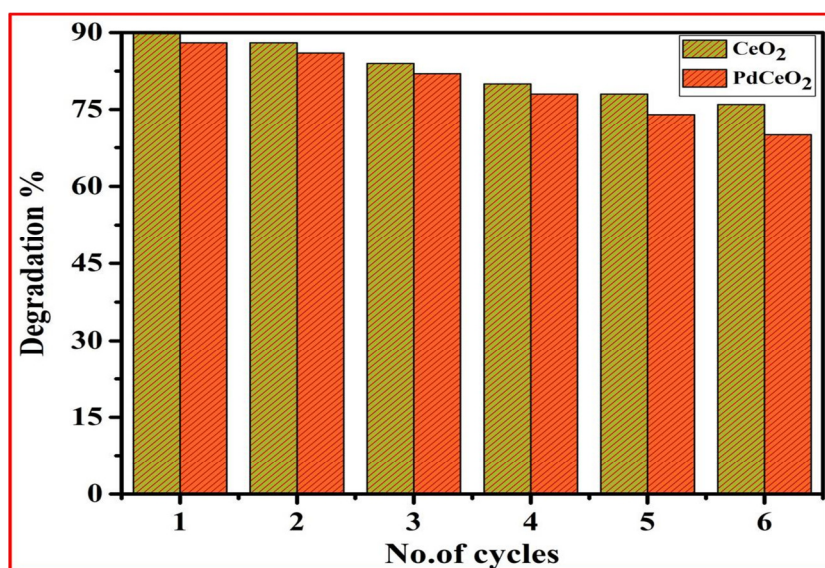
Fig.3.11 : Recycling of catalysts by using CR

3.8 CONCLUSION

From the PXRD discovered the standard crystalline size of CeO_2, $Ce_{0.98}Pd_{0.02}O_2$ catalysts were obtained at 5.9 nm and 3.1nm. The synthesized nanoparticles having polygonal shape structure; this structure showed that the $Ce_{0.98}Pd_{0.02}O_2$ catalyst doesn't change morphology. The FTIR structure exhibited the presence of Ce-O stretching bonds of CeO_2. The CeO_2 nanoparticles showed powerful UV-visible absorption at 329 nm with bandgap was resolution relating 3.26 eV, the polygonal shape morphology with uniform distribution of particles. In Fig.a) and b).The SEM analysis showed morphology CeO_2 and $Ce_{0.98}Pd_{0.02}O_2$. The $Ce_{0.98}Pd_{0.02}O_2$ catalyst doesn't affect the morphology and arrangement of the CeO_2 nanoparticles. This reveals the $Ce_{0.98}Pd_{0.02}O_2$ was a critical application for element oxygen storage capability, element uptake measurements, CO reaction studies, and reduction catalyst in coupling reactions. The pure act was obtained by quantifying Congolese and red color images using CeO_2 and Pd doped CeO_2 NPS. The two most common types of

lighting are sun and UV-light. The experiment was performed by spreading 60mg of CeO_2 and Pd doped CeO_2 Nps in 100ml of red pepper extract of 20ppm Congo. From Table one, it can be observed that the photocatalytic degradations of Congo red for 120 min is higher in UV light (93%) than in sunlight (85%). This is because the UV light has high energy (low waves or high energy), so that light can penetrate rapidly and produce large quantities of free radicals, which increase the rate of photocatalytic destruction of Congolese red dye.

References

[1]. Darroudi M, Sarani M, et al., (2014) Ceram. Int. 40:2863-2868.

[2]. Devaraja P B, Avadhani D N, et al, (2014) Spectrochim. Acta Part A.121:46-52.

[3]. Dhananjaya N, Nagabhushana H, et al., (2012) Spectrochim. Acta Part A.96:532-540.

[4]. Negishi E, (2000) Wiley, Chichester. The UK.

[5]. Tsuji J, John Wiley & Sons, Ltd, Chichester, UK, 2004.

[6]. Willner, Maidan R, Mandler D, Durr H, et al, Am J. Chem. Soc. 1987, 109, 6080.

[7]. Mizukoshi Y, Okitsu K, Maeda Y, A, et al, Phys J. Chem. B. 1997, 101,7033.

[8]. Qin Y H, Yang H, Zhang X S, Li P, Ma C A, Int. Hydrog J. Energy. 2010, 35, 7667-7674.

[9]. Zhang Z, Liu J, Gu J, Su L, Cheng L, Energy Environ. Sci. 2014, 7 2535-2558.

[10]. Shido T, Iwasawa Y, Catal J. 141 (1993) 71.

[11]. BunluesinT, Gorte R J and GrahammG W, Appl. Catal. B: Environ., 15 107 (1998).

[12]. Xc C and Kang P, Shen, Chem. Commun.,2238 (2004)

[13]. Xc C and Kang P, Shen, Chem. Commun.,2238 (2004)

[14]. Mogensen, N, Sammes M, and Tompsett G A, Solid State Ionics, 129, 63 (2000)

[15]. Wang Z L, and Feng X D, Phys J. Chem. B,107,13563 (2003)

[16]. Miki T, Ogawa T, Haneda M, Kakuta N, (1990) Phys J. Chem., 94:6464.

[17]. Qin Y H, Yang HH, Zhang X S, Li P, Ma C A, Int. Hydrog J. Energy. 2010, 35, 7667-7674.

[18]. Zhang, J, Liu J, Gu, Su L, Cheng L, Energy Environ. Sci. 2014, 7 2535-2558.

[19]. ShidoY, Iwasawa J, Catal. 141 (1993) 71.

[20]. Bunluesin, Gorte R J and Grahamm GW, Appl. Catal. B: Environ., 15 107 (1998)

[21]. XcCand Kang P, Shen, Chem. Commun.,2238 (2004)

[22]. ZhangC, XuL, Shan N, Sun T, Chem J, Yan Y, ACS Catal. 2014, 1926-1930.

[23]. Shao Y, Sui J, Yin G, Gao Y, Appl. Catal. B-Environ. 2008, 79, 89-99.

[24]. Yoldas B E, O'Keeffe T W, Appl. Opt. 1979, 18, 3133-3138.

[25]. Ranjit KT, Varadarajan T K, et al, Photochem J. Photobiol. A Chem. 1996, 96A 18-185.

[26]. Zhang Z, Kleinstreuer C, Donohue J F, and Kim C S, Aerosol Sci.J 36 (2005)

[27]. McDevitt T and Baun W L, Spectrochimica Acta 20 (1964) 799-808

[28]. Rema Devi BS, Raveendran R and et al. J.Physics Vol.68, No.4, April(2007) 679687

[29]. Change, et al, Appl.phys.Lett 80, (2002) 127.

[30]. Obaiah G O, Shivaprasad K H, Mylarappa M, et al., (2018) Advanced Science Letters.24: 6004-6007(4)

[31]. Obaiah G O, Shivaprasad K H, Mylarappa M, et al.,(2018) Materials Today: Proceedings 5:22466–22472.

[32]. K. Maeda, K. Domen, J. Phys. Chem. C 111 (12) (2007) 4749–4755.

[33]. Y. Inoue, Energy Environ. Sci. 2 (4) (2009) 364–386.

[34]. A. Kudo, Y. Miseki, Chem. Soc. Revis. 38 (1) (2009) 253–278.

[35]. T.J. Fisher, M. Wang, Y. Ibrahim, B. et al, Mater. Lett., 178 (2016) 71-74.

[36]. A. Primo, T. Marino, A. Corma, R. Molinari, H. Garcia, J. Am. Chem. Soc., 133(18) (2011) 6930-6933.

[37]. Magesh, G., Viswanathan, B., Viswanath, R. P. & Varadarajan, T. K. Indian J. Chem. B Org. 3, 480–488 (2009).

[38]. Truffault, L. et al. Mater. Res. Bull. 45, 527–535 (2010).

[39]. V. Addorisio, S. Esposito, and F. Sannino, J. Agric. Food Chem., 2010, 58, 5011–5016.

[40]. A.K. Aboul-Gheit, D.S. El-Desouki, R.A. El-Salamony, Egypt. J. Inst. Pet. 23 (2014) 339–348.

[41]. W. Shen, Z. Li, H. Wang, Y. Liu, Q. Guo, Y. Zhang, J. Hazard Mater. 152 (2008) 172–175.

[42]. S.W. Kim, H.-K. Kim, H.W. Choi, D. H. Yoo, E.J. Kim, S.H. Hahn, Nanosci. Nanotechnology. 13 (2013) 7053–7055.

[43]. R.G. Toro, G. Malandrino, I.L. Fragala, R. Lo Nigro, M. Losurdo, G. Bruno, J. Phys. Chem. B 108 (2004) 16357–16364.

[44]. S. Kanakaraju, S. Mohan, A.K. Sood, Thin Solid Films 305 (1997) 191–195.

[45]. C.S.O. Avellaneda, M.A.C. Berton, L.O.S. Bulhoes, Sol. Energy Mater. Sol. Cell. 92 (2008) 240–244.

[46]. D. Channei, B. Inceesungvorn, N. Wetchakun, S. Ukritnukun, A. Nattestad, J. Chen, S. Phanichphant, Sci. Rep. 4 (2014) 1–7.

[47]. A. Akbari–Fakhrabadi, R. Saravanan, M. Jamshidijam, R.V. Mangalaraja, M.A. Gracia, J. Saudi Chem. Soc. 19 (2015) 505–510.

[48]. N. Sabari Arul, D. Mangalaraj, T. Whan Kim, P. Chi Chen, N. Ponpandian, P. Meena, Y. Masuda, J. Mater. Sci-Matter. El. 24 (2013) 1844–1650.

[49]. S. Jayapalan, K.S. Ranjith, S. Padmanapan, D. Mangalaraj, R.T. Rajendrakumar, Mat. Sci. Semicon. Proc. 26 (2014) 218–224.

[50]. L. Truffault, Mater. Res. Bull. 45 (2010) 527–535.

[51]. J.M.A. Almeida, P.E.C. Santos, L.P. Cardoso, C.T. Meneses, J. Magn. Magn. Mater. 327 (2013) 185–188.

[52]. S. Ye, K. Ullah, L. Zhu, Z.D. Meng, Q. Sun, and W.C. Oh, B J. Korean Ceram. Soc. 50 (2013) 251–256.

[53]. S.A. Ansari, M.M Khan, M.O. Ansari, S.Kalathil, J.Lee, M.H. Cho, RSC Adv. 4 (2014) 16782-16791.

[54]. W. Deng, D. Chen, J. Hu, and L. Chen, RSC Adv. 5 (2015) 80158-80169

[55]. A. Umar, R. Kumar, M.S. Akhtar, G. Kumar, S.H. Kim, J.Colloid.Interf.Sci. 454 (2015) 61–68

[56]. S. Ansari, M. Khan, M.O. Ansari, S. Kalathil, J. Lee1, and M.H. Cho, RSC Adv. 4 (2014) 16782-16791

[57]. J. Ko, J.H. Kim, and C.B. Park, J. Mater. Chem. A, 2013, 1,241

[58]. C. Mao, Y. Zhao, X. Qiu, J. Zhu, and C. Burda, Phys. Chem. Chem. Phys. 10 (2008) 5633–5638.

[59]. G. Zhang, J. Ao, Y. Guo, Z. Zhang, M. Shao, L. Wang, L. Zhou and J. Shao, RSC Adv.4 (2014) 20131-20135

[60]. Y. Li, Q. Sun, M. Kong, W. Shi, J. Huang, J. Tang, X. Zhao, J. Phys. Chem. C 115 (2011) 14050–14057.

[61]. A.D. Liyanage, S.D. Perera, K. Tan, Y. Chabal, K.J. Balkus Jr, ACS Catal. 4 (2) (2014) 577–584.

[62]. S.A. Ansari, M.M. Khan, M.O. Ansari, S. Kalathil, J. Lee, M.H. Cho, RSC Adv. 4 (2014) 16782–16791.

[63]. D. Channei, B. Inceesungvorn, N. Wetchakun, S. Phanichphant, A. Nakaruk, P. Koshy, C.C. Sorrell, Int. 39 (2013) 3129–3134.

[64]. S. Mansingh, D.K. Padhi, K.M. Parida, Int. J. Hydrogen Energy. 41 (2016) 14133–14146.

[65]. P.Li, W. Zhang, X.Zhang, Z. Wang, X.Wang, S. Ran, Y. Lv, Mat. Res. 21 (2018) 1–6.

[66]. S. Mansingh, D.K. Padhi, K.M. Parida, Int. J. Hydrogen Energy. 41 (2016) 14133–14146.

[67]. P.Li, W. Zhang, X.Zhang, Z. Wang, X.Wang, S. Ran, Y. Lv, Mat. Res. 21 (2018) 1–6.

[68]. V. Binas, D. Venieri, D. Kotzias, G. Kiriakidis, J. Materiomics. 3 (2017) 3–16.

[69]. D. Channei, S. Phanichphant, A. Nakaruk, S.S. Mofarah, P. Koshy, C.C. Sorrell, Catal. 45 (2017) 1–23.

[70]. M. Zhang, X. Yu, D. Lu, J. Yang, Nanoscale Research Letters. 8 (2013) 543–552.

[71]. L. Yue, X.M. Zhang, J. Alloys Compd. 475 (2009) 702-705.

[72]. D. Ma, Y. Zhao, J. Zhao, Y. Li, Y. Lu, D. Zhao, Microsoft. 83 (2015) 411–421.

[73]. K.H. Kim, S.K. Ihm: a review, J. Hazard. Mater. 186 (2011) 16–34.

[74]. P. Ji, J. Zhang, F. Chen, M. Anpo, Appl. Catal. B: 484, Environ. 85 (2009) 148–154.

[75]. B. Subash, B. Krishnakumar, R. Velmurugan, M. Swaminathan, M. Shanthi, Catal. Sci. 488 Technol. 2 (2012) 2319–2326.

[76]. Rema Devi B S, Raveendran Rand Av Vaidyan. Pramana –J.Physics Vol.68, No.4, April(2007) 679687

[77]. ZhangF, et al, Appl.phys.Lett 80 ,(2002) 127.

[78]. E.J. Preisler, O.J. Marsh, R.A. Beach, T.C. McGill, J. Vac., Sci. Technol. B 19 (2001) 1611.

[79]. V. Fernandes, I.L. Graff, J. Varald, L. Amaral, P. Fichtner, D. Demaille, Y. Zheng, W.H. Schreiner, D.H. Mosca, J. Electrochem. Soc. 159 (2012) K27.

[80]. D.R. Mullins, S.H. Overbury, D.R. Huntley, Sur. Sci. 409 (1998) 307.

[81]. V. Chauvaut, V. Albin, H. Schneider, M. Cassir, H. Ardelean, A. Galtayries, J. Appl. Electrochem 30 (2000) 1405.

[82]. E. Beche, P. Charvin, D. Perarnau, S. Abanades, G. Flamant, Sur. Inter. Anal. 40, (2008) 264.

[83]. Y. Zhou, J.M. Perket, J. Zhou, J. Phys. Chem. C 114 (2010) 11853.

[84]. F. Pagliuca, P. Luches, S. Valeri, Sur. Sci. 607 (2013) 164.

[85]. B. Hirschauer, M. Gothelid, E. Janin, H. Lu, U.O. Karlsson, Appl. Sur. Sci. 148 (1999) 164.

[86]. C.G. Kim, J. Vac., Sci. Technol. B 18 (2000) 2650.

[87]. M.A. Henderson, C.L. Perkins, M.H. Engelhard, S. Thevuthasan, C.H.F. Peden, Surf. Sci. 526 (2003) 1.

[88]. M.B. Hugenschmidt, L. Gamble, C.T. Campbell, Surf. Sci. 302 (1994) 329.

[89]. Y. Lykhach, V. Johanek, H.A. Aleksandrov, S.M. Kozlov, M. Happel, T. Skala, P. StPetkov, N. Tsud, G.N. Vayssilov, K.C. Prince, K.M. Neyman, V. Matolin, J. Libuda, J. Phys. Chem. C 116 (2012) 12103.

[90]. M. Brun, A. Berthet, and J. C Bertolini, J. Electron Spectrosc. Relat. Phenom., 104, 55 (1999)

[91]. T. Baidya, A. Gupta, P. A. Deshpande, G. Madras, and M. S. Hegde, J. Phys. Chem. C, 113, 4059 (2009).

[92]. C. Zhang, J. Lin, Phys. Chem. Chem. Phys. 13 (2011) 3896–3905.

[93]. Q. Zhang, X. Wu, M. Gao, H. Qiu, J. Hu, K. Huang, S. Feng, Y. Yang, T. Wang, B. Zhao, Z. Liu, Inorg. Chem. Commun. 94 (2018) 43–47.

[94]. M. Peuckert, J. Phys. Chem. 89 (12) (1985) 2481–2486.

[95]. C.D. Wagner, W.M. Riggs, L.E. Davis, J.F. Moulder, G.E. Muilenberg, 1979, p. 111.

[96]. M. Wang, D. Fang, N. Wang, S. Jiang, J. Nie, Q. Yu, G. Ma, Polymer 55 (2014) 2188–2196.

[97]. W. Zhang, Q. Zhang, B. Yu, L. Zhao, Quality & Quantity 49 (2015) 1023-1038.

[98]. J.Cao, L.Song, J.Tang, J.Xu, W.Wang, Z.Chen, Appl.Surf.Sci.274 (2013) 138–143.

[99]. A.A.Siller-Ceniceros, M.E.Sánchez-Castro, D.Morales-Acosta, J.R.Torres-Lubian, E.G. Martinez, F.J.Rodríguez-Varela, Appl. Catal. B Environ.209 (2017) 455–467.

[100]. S.M.Senthil Kumar, J.Soler Herrero, S.Irusta, K.Scott, J.Electro anal.Chem.647 (2010) 211–221.

A Potential Use γ-Al$_2$O$_3$ Coated Cordierite Honeycomb Doped Ti$_{0.97}$Pd$_{0.03}$O$_{2-\delta}$ Catalyst for Selective High Rates in Coupling Reactions and Their Recyclable Properties

<div align="right">

CHAPTER-4

</div>

A Potential Use γ-Al$_2$O$_3$ Coated Cordierite Honeycomb Doped Ti$_{0.97}$Pd$_{0.03}$O$_{2-\delta}$ Catalyst for Selective High Rates in Coupling Reactions and Their Recyclable Properties

In the current research, The Pd-catalyze amination reactions of aryl halides have attracted much attention in recent years. Aim of review demonstrates a fundamental mechanism recently in the catalysis of one type of Buchwald-Hartwig Amination reaction. The results of FTIR, XRD, RR, scattering spectroscopy (EDS), and the analysis demonstrated the success of nanocatalyst. A scan of electron microscopy (SEM and TEM) was used to study nanocatalyst analysis. Furthermore, the Ti$_{0.97}$Pd$_{0.03}$O$_{1.97}$ catalyst was applied to Buchwald - Hartwig C – N Coupling Reaction with several functional components. The reaction of several arylamines was carried out using the effect of an aryl halide with amine used by a Pd doped TiO$_2$ catalyst. The catalyst Ti$_{0.97}$Pd$_{0.03}$O$_{1.97}$ showed useful catalytic activity in C-N coupling reactions and is reusable at this reaction at least five times without significant reduction of its Pd doped catalyst; Ti$_{0.97}$Pd$_{0.03}$O$_{1.97}$ was coated for cordierite monolith by a series of stepwise sequences. The coating on cordierite is nano-crystalline, as observed from the XRD study. The crystalline catalyst for C – N bonding was used for the synthesis of aryl halides and amines. C-N products were synthesized using ^{1}H NMR, ^{13}C NMR, and FTIR spectroscopy. This diagram shows a high selectivity in the C-N coupling. Turn over frequency (TOF) was detected twice for each high-dosage reaction.

4.1 INTRODUCTION

The Alumina magnesia Silicate ($Mg_2Al_4Si_5O_{18}$) composition of cordierite ceramic honeycomb shows tremendous thermal shock resistance and high-temperature resistance at 1200°C, and it was used for varies applications for good mechanical force as well as low thermal expansion coefficient, and it is also have been in different shapes such as block, cylinders, and plates. Cordierite fuel cells have been used in various ways, such as brake support, catalytic converter, hot gas, and air pressure, as well as have been removed from the water source. The homogenous catalytic activity has been used to make black palladium supported, less stable, and its applicants are less sensitive and are used for more expensive and hazardous donors, an important role in low percentages [1–4]. The cordierite monolith was designed for the application of their optical properties to produce a high volume of gas in contact with active additives, high geometry, low pressure, high operating power, short diffusivity, high thermal stability, low humidity. The expansion assemblies and water resistance [5-6]. There is a level of cordierite monolith needed to cover the layer of concrete, which increases the surface area and is used to connect with chemicals. This is known to be supported by a coating system. The Al_2O_3 is then coated with a monolith [7-8]. Palladium ion covers the surface of solid material, and it might be possible to stabilize the actives of palladium type and cure faults. The optical sensors used in the field include the focus of attention on the physical properties of the product, their low cost, and the use of electronic surveillance systems, and the other is higher. [9-10]. Palladium and palladium doped NPs are used in catalysis and are not only important for function [11-12] but also scientifically known for the relationship between catalytic behavior, particle size, and diffusion patterns, and information was

surrounding [13]. The Recovery and removal of emerging problems is common observable property. The Large structures (dendrimers) have been developed by the synthesis of Palladium [14] and Palladium with anti-copolymer micelles [15].TiO$_2$ catalysts provide good visualization and low-dose treatment [16-18]. Coating powder and monolith are recommended for a variety of functional applications using a coating on ceramic monoliths, sol-gel coating, colloidal coating, and other coating materials. A summary of the ceramic monoliths of Luca and Campbell [19] has also been published, as well as Lachmann et al. and various methods [20–23]. In the study by Nijhuis et al. [24], the conversion of doped monolith catalysts revealed a suitable pump. Boger et al. [25] have been considered for the high-efficiency human catalytic activity and the usefulness of aromatic hydrocarbons in the chemical industry. Beau seigneur et al. [26] was employed for different systems in the colloidal coating method. We have coating 0.03% of Pd on cordierite honeycomb in the sol-gel coating technique; this method was used for removing materials from aqueous solution. A solution was containing washout materials which were used as supportive catalyst materials. The Silica coated on monolith from the sol-gel coating method has been developed by Zwinkels et al. [27] and a similar method for the catalyst using sol of catalyst. The slurry coating was carried out the comparably larger size to macropores of the monolith catalyst supported materials. A detailed alumina slurry coating on monolith has been discussed by Blachou et al. [28]. The coating of silica on monolith developed by Zwinkels et al. [27] in sol-gel coating and a similar method was used for the preparation of Pd doped TiO$_2$ catalyst. C-N coupling (Buchwald–Hartwig) amination reaction was employed over the Ti$_{0.97}$Pd$_{0.03}$O$_{1.97}$ catalyst coated monolith. It shows the high catalytic activity of organic coupling reactions. Pd catalyzed the

Buchwald and Hartwig individually proposed amination of aryl halide [29] procedures. Several conditions of reaction have been higher for Buchwald–Hartwig amination reaction; it is used as a beneficial and synthetically significant way for synthesizing aryl and hetero aryl amines. Compare with a different approach to C-N generation [30]. The Pd reactive reactants in the reaction do no longer include tremendously in reactive materials [31]; it may be lead to safety problems. Pd catalyzed N-arylation reactions have been done in several attempts to locate appropriate catalyst systems under different conditions due to the importance of the recovery of the Pd metal. The Buchwald–Hartwig coupling reactions have been considered in different kinds of heterogeneous Pd substituted catalyst systems [32-38]. The preparation of aromatic amines in the general method has emerged as an extremely in the bond formation of the Pd-catalyzed C−N coupling reaction [39-41]. Heterogeneous Pd catalysts used as an extraordinarily useful strategy in organic synthesis have emerged in the synthetic area through the Pd-catalyzed organic reactions [42-44]. Development of palladium-catalyzed systems showed in high performance of a catalytic activity in organic reactions, and it is used for sustainable development, and environmentally kindly reaction conditions of Buchwald–Hartwig Combined reactions are seen as a condition of educational research in industrial settings [45-47]. High Palladium-catalyzed reactions are shown to be related to the functional capacity of many pharmacists; it provides the highest performance and enables and assists in process development for analog synthesis [48, 49]. Palladium-mediate cross-linking of aryl halides in NH contains a compound called the Buchwald's-Hartwig amination reactions that is proposed to be a good mediator for CN synthesis and its management and biological control for total arylamines [50]. In

particular, palladium-catalyzed arylamination became important and widely used for the production of the C - N bond [51].When circular systems affect the lower surface area due to nanoparticle formation, there is stability with a poisonous bite, and it was the highly variable preparation.

In the present C-N coupling study was mainly focused on the synthesis of 3% palladium doped Titania by using a solution combustion method, Glycine as a fuel. Synthesized $Ti_{0.97}Pd_{0.03}O_{1.97}$ as further used to study their palladium-catalyzed organic coupling reactions. Pd^{2+} ion substituted TiO_2, $Ti_{0.97}Pd_{0.03}O_{1.97}$ catalyst coated monolith catalyst showed much higher catalytic properties of the C-N couple reactions with the effects of aryl halides and amines using different solvents, bases, and oxidants. We reported the use of honeycomb cordierite monolith support for coating Pd^{2+}ion active catalyst for C-N coupling (Buchwald and Hartwig) reactions using Toluene as a solvent with different reaction conditions.

4.2 EXPERIMENTAL

4.2.1 Materials

Cordierite ceramic honeycomb, γ-Al_2O_3, Titanium tetra isopropoxide (Ti $(OC_3H_7)_4$), Titanyl nitrate $(TiO(NO_3)$, Palladium chloride $(PdCl_2)$ and Glycine (NH_2CH_2COOH) were purchase from Merck. Aryl halides (Iodobenzene and Bromobenzene) and amines (aniline) were used as purchased without further purification, TLC plates.

4.2.2 Synthesis of $Ti_{0.97}Pd_{0.03}O_{1.97}$ powder catalyst

In this study, the catalyst $Ti_{0.97}Pd_{0.03}O_{1.97}$ was synthesized by the solution combustion method.   A solution of $TiO(NO_3)_2$ (9.89 mmol), which was prepared from titanium tetra isopropoxide, $PdCl_2$ (0.31 mmol), and NH_2CH_2COOH (10.99 mmol) were taken in a 300 mL crystallizing dish. The mixture was kept in a 350 $^{\circ}$C preheated muffled furnace, and the combustion of starting materials took place, followed by dehydration. The mixture was held inside the furnace for more than 20 min to burn all the carbon contents. Then the dish was removed from the furnace and allowed to cool and collected the catalyst powder. The catalyst was ground in a pestle and mortar and characterized by powdered XRD. The combustion reaction was given by equation (1):

$$9(1-x)TiO(NO_3)_2 + 10(1-x)C_2H_2NO_2 + 9xPdCl_2$$

$$\rightarrow 9\,Ti_{1-x}Pd_xO_{2-\delta} + 20(1-x)CO_2 + 14(1-x)N_2$$

$$+ (25-34x)H_2O + 18x\,HCl: x = 0.01, 0.02, 0.03 \cdots\cdots\cdots (1).$$
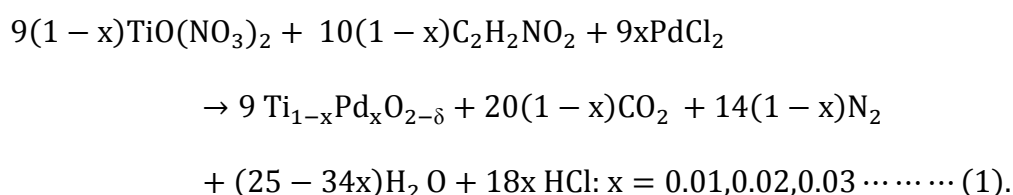
4.2.3 Procedure for Alumina ($\gamma-Al_2O_3$) coated honeycomb monolith

Before coating on the monolith, $\gamma-Al_2O_3$ is insulation and monoliths to enhance the surface area, and it held on to TiO_2. The reaction was carried out by a hot furnace by taking 16 mmol of $Al(NO_3)_2$ and 9 mmol of Glycine. The model of the object was made, and a thin film was added to the flask and placed in a furnace, after 15 minutes, the monolith was removed from the furnace and set to cool down. The process remains unchanged until the thickness of the coating $\gamma-Al_2O_3$ is increased up to 2 to 2.5% of the weight of the cordierite monoliths.

4.2.4 Growing γ-aluminates on cordierite honeycomb by solutions of combustion methods.

Take 1.4 cm breadth, 2.6 cm long cordierite coated monolith with 200 cell / inch^2. γ-Al$_2$O$_3$ was coating and water-soluble cordierite with aluminum nitrate Al(NO$_3$)$_2$ and Glycine (NH$_2$CH$_2$COOH). The dry ceramic monolith is dipped in the solution and fired at 400 ^{O}C [15]. The coating is formed by the repeated drying process—reactions and chemicals in ceramic oil below in (2).

$$2\ \text{Al(NO}_3) + 3NH_2CH_2COOH \xrightarrow[400^0C]{} \gamma - Al_2O_3 + 6CO_2 + 9N_2 + 9H_2O \cdots\cdots\cdots (2).$$
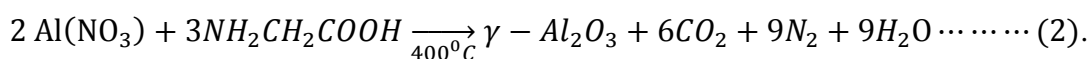
4.2.5 Coating of Ti$_{0.97}$Pd$_{0.03}$O$_{1.97}$ nanocatalyst over Alumina coated cordierite monolith

Ti (OC$_3$H$_7$), PdCl$_2$, and C$_2$H$_5$NO$_2$ are theoretically employed for Ti$_{0.97}$Pd$_{0.03}$O$_{1.97}$. It is a difficult task to the coating of 3%, Pd doped TiO$_2$ (Ti$_{0.97}$Pd$_{0.03}$O$_{1.97}$) catalyst, 9.7 mmol of TiO (NO$_3$)$_2$, 0.3 mmol of PdCl$_2$ and 11 mmol of Glycine were dissolved in water to make an aqueous solution. $\gamma-$Al$_2$O$_3$ coated cordierite honeycomb is dipped into the solution and rapidly heated at 400 ^{0}C, respectively. Dip-dry-firing is repeated to 2-3% of catalyst weight was increased for honeycomb weight. The importance of the catalyst loaded in cordierite monolith is around 110 mg; amounting to 1 % monolith weight in the study was shown in fig.4.1. The chemical reaction on the surface of $\gamma-$Al$_2$O$_3$ coated ceramic monolith honeycomb can be written in the below equation (3).

Follow the equation as (3).

$$9(1-x)\text{TiO(NO}_3)_2 + 10(1-x)\text{C}_2\text{H}_2\text{NO}_2 + 9x\text{PdCl}_2$$

$$\rightarrow 9\,\text{Ti}_{1-x}\text{Pd}_x\text{O}_{2-\delta} + 20(1-x)\text{CO}_2 + 14(1-x)\text{N}_2$$

$$+ (25-34x)\text{H}_2\text{O} + 18x\,\text{HCl}: x = 0.01, 0.02, 0.03 \cdots\cdots\cdots (3).$$
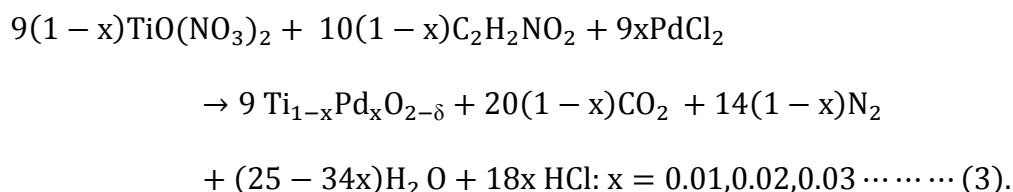
The $\text{Ti}_{0.97}\text{Pd}_{0.03}\text{O}_{1.97}$, the propellant supporter, was designed as described in the experimental part and then used in the experiment. The parameters of the system are evaluated by conserving the capacitors. The effects of the palladium doped TiO_2 catalyst were demonstrated in the formation of anionic catalyst products, as shown in Table.4.1. The $\text{Ti}_{0.97}\text{Pd}_{0.03}\text{O}_{1.97}$ catalyst showed high activity in selectivity and bonding. Pd-catalyzed C-N is synthesized as a common method for the preparation of aromatic amine. [52-54].

Table-4.1: Coating of Al_2O_3 and $\text{Ti}_{0.97}\text{Pd}_{0.03}\text{O}_{1.97}$ catalyst on honeycomb.

Sl. No.	Honeycomb (g)	Honeycomb + Al_2O_3 (g)	Honeycomb + $\text{Ti}_{0.97}\text{Pd}_{0.03}\text{O}_{1.97}$ (g)	Weight of $\text{Ti}_{0.97}\text{Pd}_{0.03}\text{O}_{1.97}$ in Honeycomb (mg)
1	2.5327	2.8090	2.9052	97.2
2	2.5954	2.8449	2.7326	182.9
3	2.5703	2.3529	2.7326	161.3
4	2.5562	2.6126	2.8196	262.4
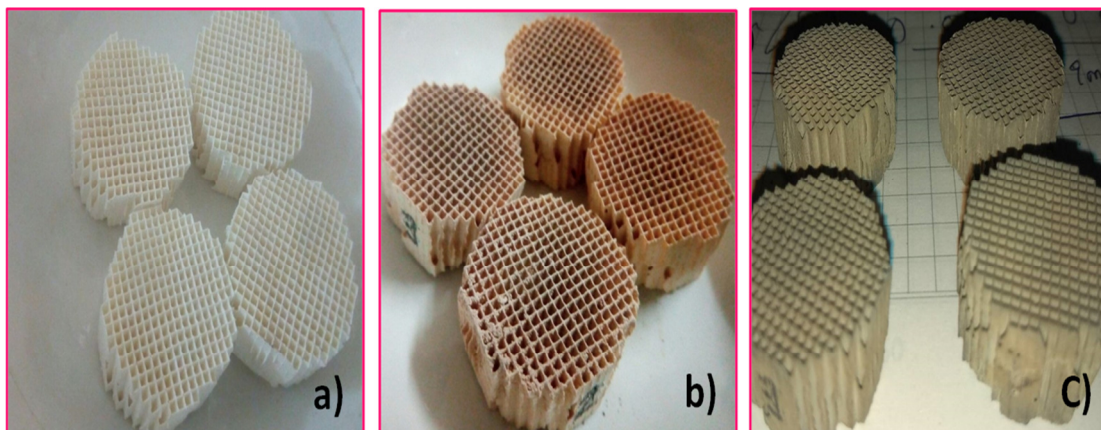
Fig.4.1. Photographs of (a) Alumina coated honeycomb monolith, (b) top view and side view of catalyst coated monolith, respectively, (c) catalyst coated honeycomb after several cycles of reactions.

4.2.6 General Experimental procedure for Buchwald-Hartwig Coupling reactions

The solution contains aryl halide (2.5 mmol), amine (0.6 mmol), K_2CO_3 (3.0 mmol), and Pd doped TiO_2 catalyst (0.03%) using toluene (10 mL). The mixture was incubated at a temperature of 110 ° C and reached 08–18 h. TLC was used to check the final product of the reaction. First, the solvent is used to remove the solvent and purify it with $MgSO_4$, which is then purified. This good product is always produced after antibiotics. The Chromatography was used for further measurements, and all of these products are measured in GC. The reaction mixture was heated to 110 °C for 12 hours as iodobenzene (2 mol), amine (2.4 mol), dipropyl amine ($C_6H_{15}N$) (3 mol), and oxidant (0.03 mol %) and toluene (10 mL) of tert-butyl hydroperoxide (T_BH_7Ox). This mixture was heated, stirring with the Celite (silica) bed in hot conditions. The study showed a 90% effect on the GC test. Subsequently, the filtrate was used for the reaction without adding, the stoichiometric composition, and the reaction condition

allowed. After 12 hours, the GC reaction with the reaction mixture showed that there was no% before the reaction. After the reaction period, 5 ml of ethyl acetate was added to the reaction mixture and stirred for 5 min. After this period, centrifugation separates the burning machine. In other systems, the refined oils use EtOH (ethanol) and dried under a vacuum. Then, the restored pump is used for another run. the coupling reaction was used for different instruments are shown in fig.4.2.

Fig.4.2 Photograph of a) C-N coupling reaction setup b) UV cabinet c) Rota evaporator d) Celite bed.

4.3 RESULTS AND DISCUSSION

4.3.1 Powder X-ray Diffractometer analysis (PXRD)

Catalyst $Ti_{0.97}Pd_{0.03}O_{1.97}$ developed by the solution combustion method of boiling $TiO(NO_3)_2$, $PdCl_2$, and (NH_2CH_2COOH) at 350 ^{0}C. The Pd replaced TiO_2 crystallizing damage. The XRD and Rietveld of XRD for three atoms% Pd and TiO_2 are given in Fig.4.3. No quantities of PdO or Pd iron are available separately. The lattice angle is = 3.796 Å and c = 9.534 Å which is close to the pure TiO_2 values, a = 3.796 Å and c = 9.533 Å. Pd^{2+} is 0.64Å close to that of Ti^{4+} (0.605 Å). The morphological data of $Ti_{0.97}Pd_{0.03}O_{1.97}$ are 2.5 cm thick and overlaid with $Mg_2Al_4Si_5O_{18}$. We can see (101) the output of the XRD output in section 25.3∘ , and the difference between the closed monoliths is shown in Fig. 4.3. Each Monolith has a clearly defined path. Therefore, the higher surface area is exposed to reactors. The color of the plaster is brown. The thickness of the crystals is 8 ± 2 nm calculated by the half-wavelength (101) of the solid line (Fig.4.3) using the Scherrer's method (d = $0.9\lambda / \beta \cos\theta$) and the powder and surface are also. a. The same size is expected because the half-width of (101) is the same. On a water-resistant surface, a coating of the coated monolith (HC) is applied. The complete catalytic reaction of HC catalyst is present in the solvent. The balcony and argon type are written above your query. Stay in the 110 ^{o}C hot water bath. The conversion speed of the catalyst is high and then separates the reaction mixture and solvent from the HC catalyst
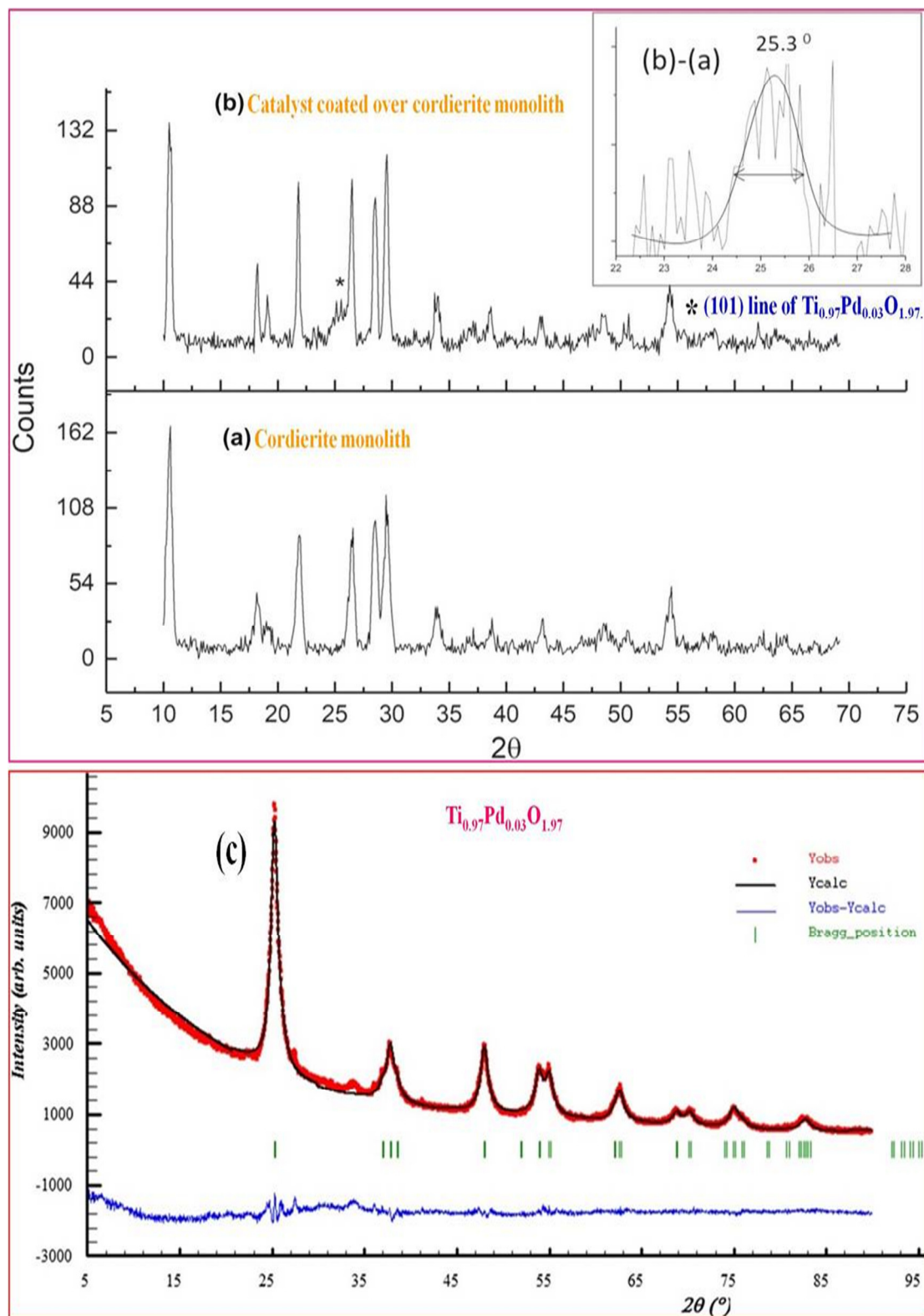
Fig.4.3. Powder XRD patterns of (a) cordierite monolith, (b) catalyst coated over cordierite monolith, c) Rietveld refined pattern of the $Ti_{0.97}Pd_{0.03}O_{1.97}$ catalyst.

4.3.4 Fourier transforms Infrared spectroscopy (FT-IR) analysis

The free N-H absorption in secondary amine has been reported to be in the region of 3385 cm. The significant fall in the frequency observed is due to association by intermolecular H-bonding in the solid phase spectrum. The frequency change of this order might well arise from a change of state due to the possibilities of interactions of hydrogenic vibrations in neighboring molecules in the solid-state. It is not possible to do more than indicate the approximate range of 3400-3100 cm°' for associated absorptions of this type. Accordingly, we find three N-H absorptions, which are all weak at 3120, 310, and 3180 cm° in the spectrum of diphenylamine in Fig.4.4 b). The N-H deformation absorption is usually very weak in secondary amines. In table.4.2.

Table.4.2 Characteristic Infrared Absorption Region (cm^{-1}) of Diphenylamine.

Sl	Region (cm)	Nature of bands	Frequency
1	< 3300	Strong and sharp	C-H present
2	3400-3100	Broad absorption	N-H present (aromatic)
3	1236-1050	Intense-band	C-C or C-N present
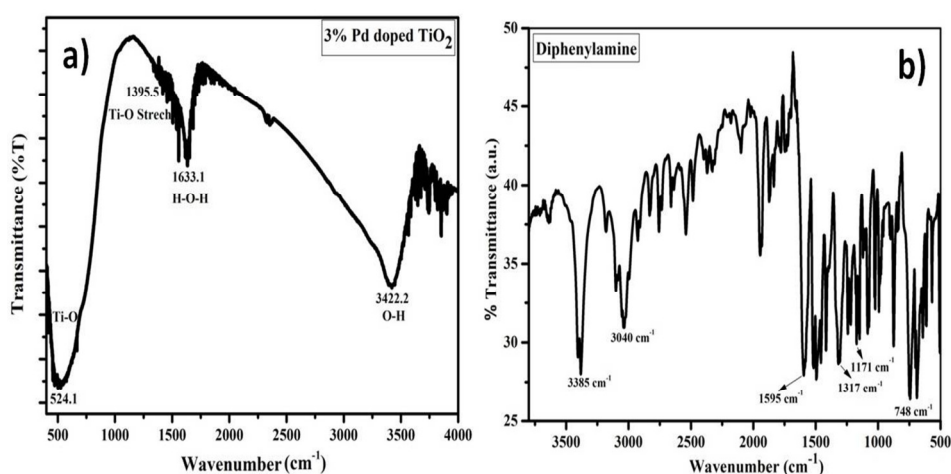
Fig.4.4 a). FT-IR Spectra of a) $Ti_{0.97}Pd_{0.03}O_{1.97}$ catalyst b) diphenylamine

The FT-IR spectra of Pd doped TiO_2 are shown in Fig. 4.4 a). FT-IR sample from point to the combination of two-dimensional structures in the vitreous matrix. The larger range appears in 3854-3751 cm^{-1} is given by the different functions of –OH and the numbers 1767 and 1781 cm^{-1} are O-H stretching guns. The rat is thought to be ~ 2341 cm^{-1} as a result of the species having a CN chain, and the same group 1185-1163 cm^{-1} may be related to the nitrogen oxide species. The Ti-O and O-Ti-O fluorescence emission spectra are derived from a wide range of wavelengths between 400 and 800 cm^{-1}. When a TiO_2 ion is added to the surface of the TiO_2, the catalytic phase changes and, at the same time, a new extraction effect occurs. The broadband can be dropped to 3412.2 cm^{-1} with waterproofing. The peak at 1631 cm^{-1} is due to the moving sound of the droplets indicating the presence of water-solids.

4.3.5 C-N coupling reaction flask

The cylinder has a diameter of 3.6 cm and has a height of 13 cm, and also, the height from the ground is 1.5cm. The length of the beads should be reduced to the request for breaking two separate sections and a small gap. The surface panel contains a magnetic lock and reactions of mixtures. On a waterproof surface, a coating of coated oil (HC) is applied. The complete catalytic reaction of HC catalyst is present in the solvent. The balcony and argon type are written above your query. Stay in the 110°C hot water bath. The conversion speed of the catalyst is high and then separates the reaction mixture and solvent from the HC catalyst.

Fig.4.5 : Photographs of a) the reaction mixture and coated honeycomb catalyst. b) Specially designed reaction flask (reactor) for the C-N coupling reaction.

4.3.6 Procedure for the C-N coupling reaction

The result was measured in 25 mL around the bottom fl medium. Iodobenzene (200 mg, 1 equivalent), aniline (1.5 equivalent), the donor (15 mg) and K_2CO_3 (1.5 equivalent) were dissolved in 25 mL around the flask medium. 3 mL of DMF was added. Their reaction was kept at room temperature at 110∘C. TLC monitors their activities. The reaction was performed three times with diethyl ether and water. The percentage of the substrate was determined using gas chromatography. The C – N test reaction was presented with a customized reaction. Aryl halides (2 g, 1 equal), Aniline (1.5 in equivalent), and base (1.5 in equivalent) do their thing. A catalyst coating monolith is included in the survey. The reaction was carried out under argon at 110°C. TLC investigated its reaction. After the reaction was performed, the couple diethyl ether was removed and washed three times with water to remove the solvent in the base. The monolith coating is removed from the solvent, washed with water to remove the solvent. Then, wash the unheated n-hexane and dry in a warm oven for 2 h at 200°C. An extra two cartridges were searched for the other two in response to the

C-N reaction. The top ingredients used are animal ether and ethyl acetate. The ratios were expressed using TLC to their size. A couple of sample presentations were identified as ^{1}H NMR, ^{13}C NMR, IR, and multicenter.

4.3.7 Screening studies

An experimental study of the C-N synthesis of bromobenzene and iodobenzene (aryl halide) has been proposed. The powdered powder was used in each reaction to recover .0.98 mmol (200 mg) bromobenzene and 1.5 anilines. 3.7 mol containing 15 mg of catalytic Pd^{2+} ion was used. First, tests are performed where the solvent is added individually to the reaction. Except for reaction with DMF as a solvent, all other reactions with different solvents are given atoms. The reaction time for toluene blocking was 90 min at 110^0C temperature using K_2CO_3 (1.5 sizes) as the base. We tried the inactive response and got the results. Then we use our standard 1.5 sets in different settings such as CS_2CO_3, t-BuONa, K_2CO_3, and $C_6H_{15}N$. Their interaction with $C_6H_{15}N$ and K_2CO_3 was restricted to the original seeds, including the copolymers (oxidant) $K_2S_2O_8$ and $T_BH_7O_X$, such as $C_6H_{15}N$. The next step in the analysis is warming up; the reaction was performed at 80◦C, 60◦C and at room temperature, and the extract was kept low so we decided that toluene should be kept as a melting point, with temperature $C_6H_{15}N$ as 1.5, and C-N bond as reaction value of 110^0C. We tested the response at 1 and 1.5 equivalents for K_2CO_3 and yielded less than about 1.5 of the base. We performed two reactions using a monolith catalyst pump, a monolith coating, and a 100 mg catalyst, the other containing 50 mg of catalyst. 2 g of iodobenzene was used as the starting material. Both the reactions ended with a yield of over >90%. It is important to note that the time taken for these two reactions is only 4 hours. The stable, catalytic reaction gave a quick reaction when comparing the

reaction with the powdered oil. Finally, we decided to cover 50 mg of monolith cordierite for the further reaction was summarized in Table 3.
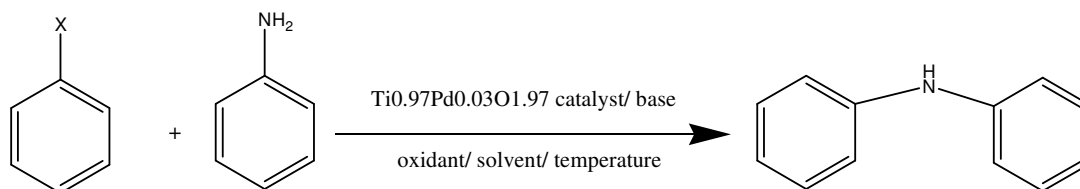
Where X= I, Br….etc

Table.4.3. Screening of the reaction.

Entry	Base	Oxidant	Solvent	Temp (^{0}C)	Time (hrs)	Yield (%)
1	K_2CO_3	-	DMF+H_2O	100	24	23 [a]
2	K_2CO_3	Ag_2O	DMF+H_2O	100	48	-
3	K_2CO_3	$K_2S_2O_8$	DMF+H_2O	100	24	56 [a]
4	K_2CO_3	$K_2S_2O_8$	Toluene+H_2O	120	24	53 [a]
5	K_2CO_3	$K_2S_2O_8$	Ethenol+H_2O	120	24	-
6	K_2CO_3	$K_2S_2O_8$	Toluene	120	24	54 [a]
7	K_2CO_3	$K_2S_2O_8$	DMF	110	24	67 [a] d
8	t-BuONa	$C_4H_6CuO_4$	Toluene	120	48	-
9	K_2CO_3	$K_2S_2O_8$	Toluene	120	48	46 [a,f]
10	t-BuONa	$K_2S_2O_8$	Toluene	120	12	55 [a,f]
11	K_2CO_3	-	MeOH+H_2O	100	24	-
12	CS_2CO_3	-	Toluene	110	48	-
13	t-BuONa	$K_2S_2O_8$	DMF	110	24	35 [a]
14	t-BuONa	$K_2S_2O_8$	Toluene	120	24	42 [a]
15	t-BuONa	$K_2S_2O_8$	Toluene	120	48	80 [b,b,c]$_1$ d
16	t-BuONa	$K_2S_2O_8$	Toluene	120	48	40 [a]
17	t-BuONa	$K_2S_2O_8$	Toluene	120	48	37 [a]
18	t-BuONa	$K_2S_2O_8$	Toluene	120	48	56 [a]
19	K_2CO_3	$K_2S_2O_8$	Toluene	120	24	60 [b,e]

20	t-BuONa	$K_2S_2O_8$	Toluene	120	48	$56^{b,e}$
21	t-BuONa	$K_2S_2O_8$	Toluene	120	48	$78^{b,b,c}{}_2$ d
22	$C_6H_{15}N$	$T_BH_7O_X$	Toluene	110	04	$90^{b,b,c}{}_3$ d
23	-	$T_BH_7O_X$	Toluene	110	48	-

Reaction conditions: 1 equivalent (200 mg) of Bromobenzene[a], Iodotoulene[b,] and Iodobenzene[b, b, c]$_1$, [b, b, c]$_2$, and [b, b, c]$_3$. **1.5** equivalent of Aniline[b], **1.5** equivalent of the base, **1** equivalent of oxidant, **3** mL of solvent, **c_1 and c_2-50mg** powder catalyst coated over monolith (5 weight % of powder catalyst), and **c_3-100mg** of catalyst coated over monolith (10 weight % of powder catalyst), the temperature at 110^0C, under Ar atmosphere. All are GC yield. **d** Isolated yield, **d_{100}** mg of catalyst coated over catalyst. **$e_{0.5}$** equivalent of the base, **f_1** equivalent of base.

C-N coupling reaction between iodobenzene and aniline is carried out in the presence of $C_6H_{15}N$ base with different solvents are summarized in table 4. Reaction with Toluene gave >90% yield, and DMF solvent gave <45% by using the base $C_6H_{15}N$, dioxane solvent doesn't have any yield react with $C_6H_{15}N$ base
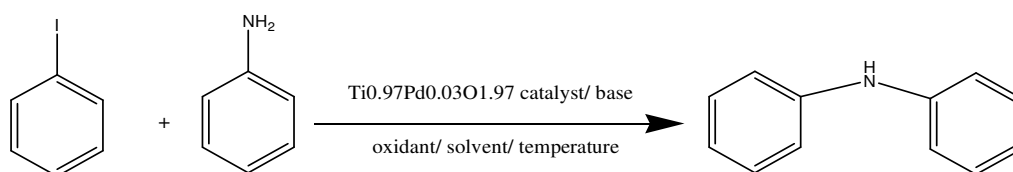
Table.4.4 Effect of solvents on C-N coupling over $Ti_{0.97}Pd_{0.03}O_{1.97}$ Coated monolith.

Entry	Base	Solvent	Yield (%)
1	$C_6H_{15}N$	Toluene	**>90**
2	$C_6H_{15}N$	DMF	<45
3	$C_6H_{15}N$	Dioxane	Nil

In table 3. Shows the effect of bases on the C-N coupling reaction over $Ti_{0.97}Pd_{0.03}O_{1.97}$ Coated monolith. Different bases such as $C_6H_{15}N$, t-Buona, and K_2CO_3 bases were taken for the comparison. The C-N coupling reaction in the presence of $C_6H_{15}N$ as a base showed >90% conversion and t-Buona, K_2CO_3 showed around 80% and 70% yield in the Toluene solvent at 110-120°C, reaction condition
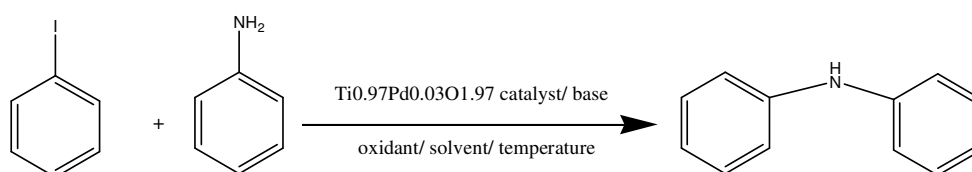
Table.4.5 : Effect of bases on C-N coupling over $Ti_{0.97}Pd_{0.03}O_{1.97}$ Coated monolith.

Entry	Solvent	Base	Yield (%)
1	Toluene	$C_6H_{15}N$	**>90**
2	Toluene	t-BuoNa	**80**
3	Toluene	K_2CO_3	71

The below table showed the effect in the presence and absence of different oxidants, bases, and solvents on the C-N coupling reaction over $Ti_{0.97}Pd_{0.03}O_{1.97}$ Coated monolith. , in the presence of $T_BH_7O_X$ as oxidant with $C_6H_{15}N$ as base and Toluene as solvent condition gave   >90% of yield and $K_2S_2O_8$ as an oxidant with K_2CO_3, t-BuoNa as bases gave >65%, >75% respectively.
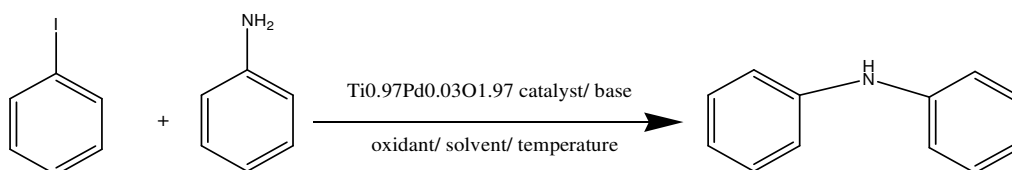
Table.4.6 : Effect the presence and absence of different oxidants, bases, and solvents on the C-N coupling reaction over $Ti_{0.97}Pd_{0.03}O_{1.97}$ Coated monolith.

Entry	Base	Oxidant	Solvent	Yield (%)
1	K_2CO_3	$K_2S_2O_8$	DMF	**>65**
2	t-BuONa	$K_2S_2O_8$	Toluene	**>75**
3	t-BuONa	-	Toluene	Nil
4	$C_6H_{15}N$	$T_BH_7O_X$	Toluene	**>90**
5	$C_6H_{15}N$	-	Toluene	Nil
6	K_2CO_3	-	$DMF+H_2O$	. >20
7	CS_2CO_3	-	Toluene	Nil
8	K_2CO_3	Ag_2O	$DMF+H_2O$	Nil
9	K_2CO_3	$T_BH_7O_X$	Dioxane	Nil

In the absence of bases with the presence of different oxidants with different solvents are carried out, the C-N coupling reaction gave a less amount of yields, such as 57% and 27% yield, respectively.
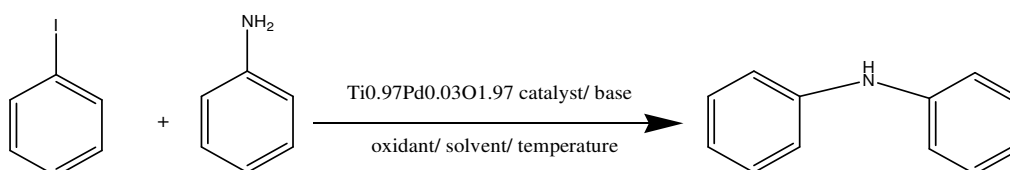
Table.4.7 : The effect in the presence of oxidant and absence of base on C-N coupling over $Ti_{0.97}Pd_{0.03}O_{1.97}$ Coated monolith.

Entry	Oxidant	Solvent	Yield (%)
1	$T_BH_7O_X$	Toluene	57
2	$K_2S_2O_8$	Toluene	27

The study was conducted to study the possibility of Buchwald-Hartwig catalyzing the reaction standard set at 110 ° C. The product was observed in the presence of species, the reaction performed well and yielded the identical product with 93% yield. The concentration dropped as low as 0.03 mol%. To determine if an increase in the polarity of the pores results in any difference in the yield, the input product varies from 0.01 mol% to 0.3 mol%. However, there was no significant improvement in the yield of the extract. To determine the best catalysts, the reaction was performed with various solvents such as H_2O, toluene, 1,4-dioxane, p-xylene, and hexane in the best conditions. In water and hexane reactions do not proceed at all, while among others, toluene gives the most productive yield. As a rule, the most common response was found to be t-BuONa (between Na_2CO_3, K_2CO_3, and Cs_2CO_3).

4.3.8 Substrate scopes

The yields of aryl halides and Amines were used for the replacement of CN behavior listed in Table 2. We have used the best conditions which are equivalent to aryl halide (2 g), 1.5 particle size amines, 1.5 equivalent $C_6H_{15}N$ as a table containing $T_BH_7O_X$ oxidant with 20 ml of Toluene as a solvent. Nearly 50 mg of catalysts and cordierite monolith were coated with any reaction to the catalyst. The aryl iodide derivatives showed good reactivity at the amines providing electrical excitability and diffraction contributions. All products are isolated and found to be transported by ^{1}H NMR. The host has been widely accepted for the use of amines and amines. The reaction with aryl iodide was inhibited by yielding a positive yield compared with aryl bromide.

4.3.9 C-N coupling of aniline with aryl iodides and aryl bromides
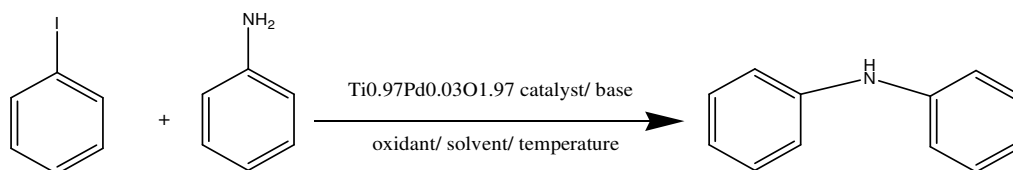
Table.4.8 : The substrate scope of the reaction.

Entry	Aryl halides	Amines	Product	Time (h)	Yield (%)	TOF (h^{-1})
1				4	93	5.90
2				8	90	2.86
3				12	72	1.52
4				5	65	4.32
5				7	80	2.90

Reaction condition: 1 equivalent (2g) of aryl halide, 1.1 equivalent of aniline, 1.5 equivalent of $C_6H_{15}N$ as a base, 20mL of Toluene as a solvent, 50mg catalyst coated over honeycomb monolith, the temperature at $120^{\circ}C$, under Ar atmosphere. All are

isolated yield. TOF = [(No. of moles of product/ No. of moles of the active site of catalyst)]/time in hours.

This complete reaction is given in bold. To demonstrate the goodness of the Pd doped TiO_2 catalyst, the C-N reaction (Buchwald Hartwig) was performed using deactivated (electron-rich) aryl iodides and bromides. The results are summarized in the table. The data showed that the product was shown to be highly effective (75-93%) for a reaction time of 8-18 hours. Aryl iodides (I, Br) inhibit electron transporters and give similar products with high affection (92-96%), while aryl iodides have the same electron yield (75-84%). Ortho replaces aryl halides with low yield (62-66%) and aniline. However, iodobenzene exhibits better performance than bromobenzene external products such as white or yellow wine that are usually water-soluble. The products were identified as melting solvent, ^{1}H-NMR, and ^{13}CNMR, and agreed with the addition literature, for the conversion and recombination between aniline and iodobenzene after the reaction; the reaction mixture was dissolved. To isolate the detergent, rinse with acyl acetate and then dry it before purification. It was found that the propeller did not stop working well until the third round. To test the validity of the search, EDX and FE-SEM analyzes were performed after the third cycle. These data clearly prove that the manufacturer maintains the integrity of the Pd test obtained from the thermal test to determine whether the Pd is involved by any solid substance. No. Upon completion of the reaction, the bed is rotated through the Celite bed so that the unwanted agent can stay behind the bed. The filtrate was reactivated for a new reaction, using the reaction mixture the same size as before, with no addition under the same reaction. Other products could not be identified by GC analysis, which indicates that the congressional organization supports the applicants.
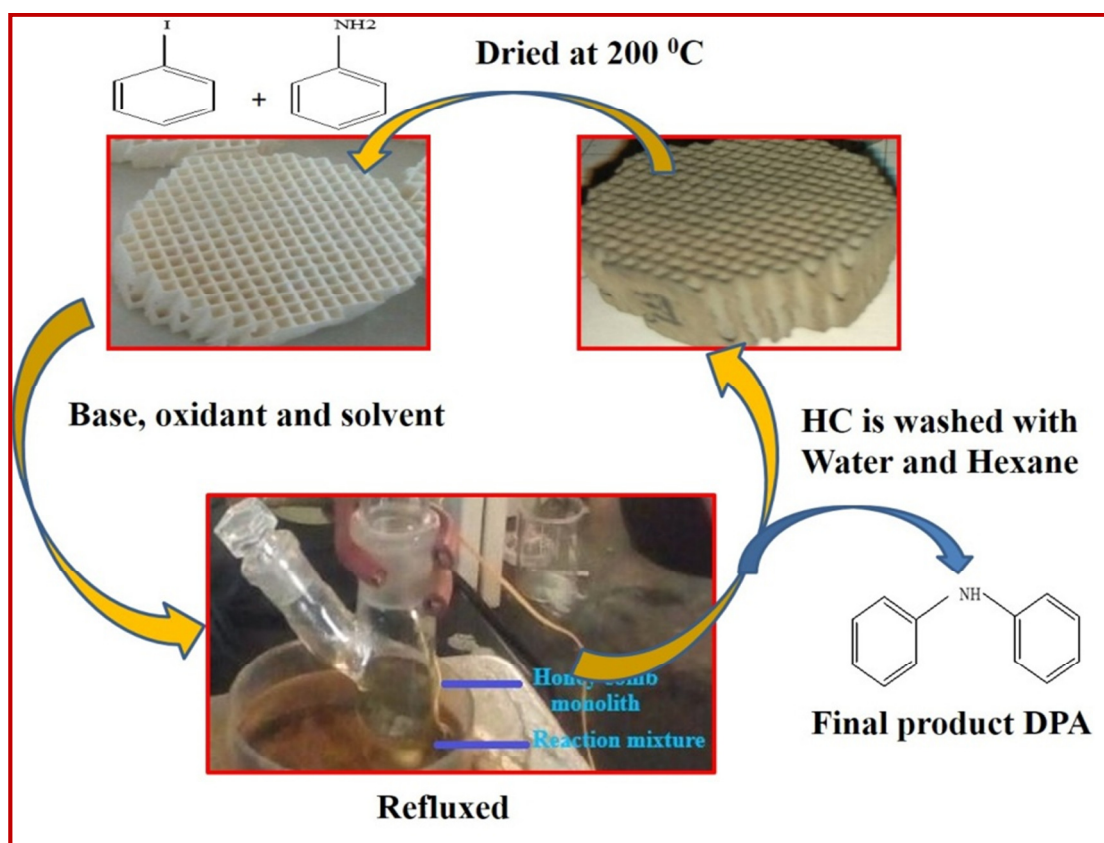
Fig.4.6 : Flowchart of recycling of HC monolith catalyst in

the C-N coupling reaction**.**

4.4 RECYCLING OF THE CATALYST

We have developed a protocol for the supplier. Iodobenzene (2 g) and Aniline

(1.5 eq.) Were considered as starting materials using standard standards.

Reinforcement of the $Ti_{0.97}Pd_{0.03}O_{1.97}$ Monolith Compound: After the reaction was

performed, the electron microscope Monolith was removed and continued to the third

unsaturated phase. (Fig.4.7). $Ti_{0.97}Pd_{0.03}O_{1.97}$ was purified with hexane water, and the

DMF and K_2CO_3 were purified with water. Monolith is frozen at $110\ ^{0}C$ and was used

in new reactions. There is no significant loss and a significant role for the

Iodobenzene reaction and aniline, which summarized in the below table. Even after

the 6th cycles of the C-N coupling reaction over $Ti_{0.97}Pd_{0.03}O_{1.97}$ coated monolith, the

yield obtained 99% in 6h. This indicates that the $Ti_{0.97}Pd_{0.03}O_{1.97}$ catalyst is not deactivating. The regenerative designs of the HC monolith catalyst are shown in Fig.4.6 After each color, the monolith used by the reaction is quenched and then washed with water to remove the stain, and then used to purify the impurity. The washed monolith was heated in a preheated oven at 200 ° C for 2 hours at room temperature. The lump was reheated to give more reaction. We got 100% resuscitation up to 6th, but in the 7th round, we have reduced yields by 85%. Manufacturer's Recycling Chart. Their reaction time in the 6th cycle was 1 to 3 steps, and the reaction time was 4 hours. The TOF concentration after ten cycles of the reaction was 5090 h^{-1}. Also, for the reconstruction and remodeling of an activator, the reaction was selected between aniline and iodobenzene (Table 4). After performing the reaction, the reaction mixture was dissolved to separate the pure catalysts; the ethyl oils were washed and later heated in the air before regeneration. The catalytic tests were repeated for 10 palladium precursors to test the durability and effectiveness of the powder. The reactor was collected from the reaction using a 100% reaction mixture in the first cycle. The yield of the 10-stage system is slower than the first phase and may result in the disruption of the molecules and the loss of the source. In addition to this, after separation, it wastes water with water, which helps with the filters and leads to some problems.
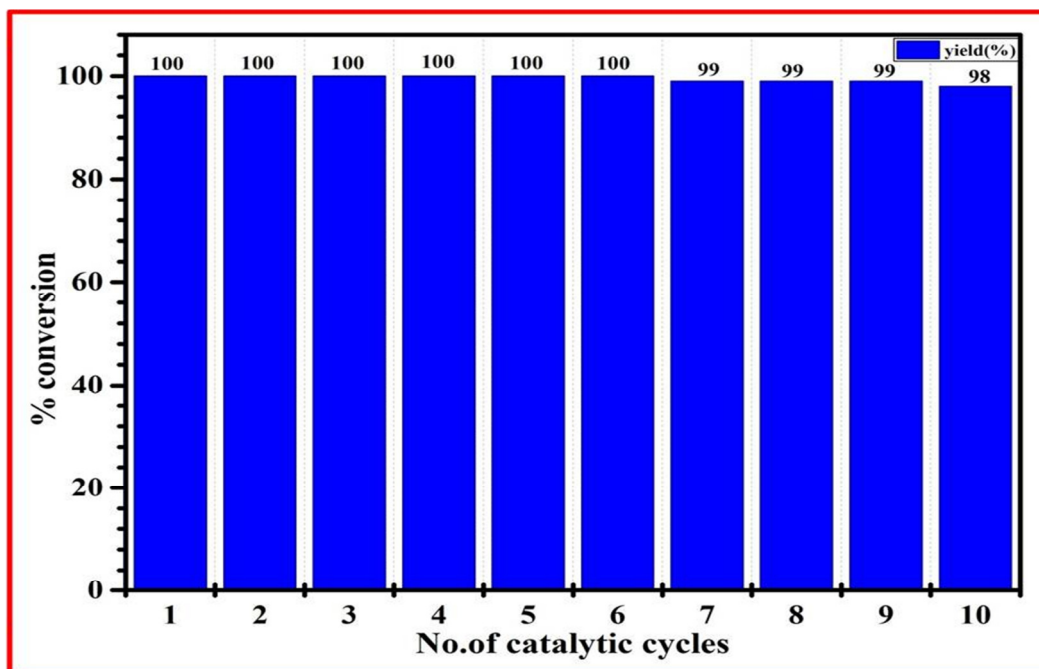
Fig.4.7 : Recycling of the catalyst by employing standard reaction conditions.

Several cycles of the C-N coupling reaction over $Ti_{0.97}Pd_{0.03}O_{1.97}$ coated

monolith (time-4h).

4.5 CHARACTERIZATIONS OF AMINE DERIVATIVES

4.5.1 NMR studies

^{1}H NMR (CDCI$_3$ 200 M Hz) 8 5.68 (bs, IH), 6.92 (t, J= 8Hz, 2H), 7.06 (d, J= SMz, 4H), 7.26 (t, J= SMz, 4H) ^{13}C NMR (C D C I$_3$ 125 M Hz) 6 117.7, 120.8, 129.2, 143.0

IR: 3383 cm ''N-H stretching (aromatic secondary amine) 1319 cm" C-N stretching of secondary amine.

4.5.2 Diphenylamine.55

Purification by flash chromatography (hexanes: ethyl acetate=10:1) gave 200.2 mg of white crystals (0.465 mmol, 93%). ^{1}H NMR: δ 5.70 (s, br, ^{1}H), 6.993-6.951 (m,

2H), 7.092-7.097 (m, 4H), 7.260-7.332 (m, 4H). ^{13}C NMR: δ 115.2, 118.4, 129.3, 146.4.

4.5.3 Triphenylamine.56

Purification by flash chromatography (hexanes: ethyl acetate=10:1) gave 200.1 mg of white crystals (0.465 mmol, 90%). ^{1}H NMR: δ 6.94-6.97 (m, 3H), 7.08-7.087 (m, 6H), 7.30-7.26 (m, 6H). ^{13}C NMR: δ 118.04, 121.2, 129.5, 143.4.

Fig. 4.8 : .a) ^{1}H NMR and b) ^{13}C NMR spectra of Diphenylamine. In CDCl$_3$
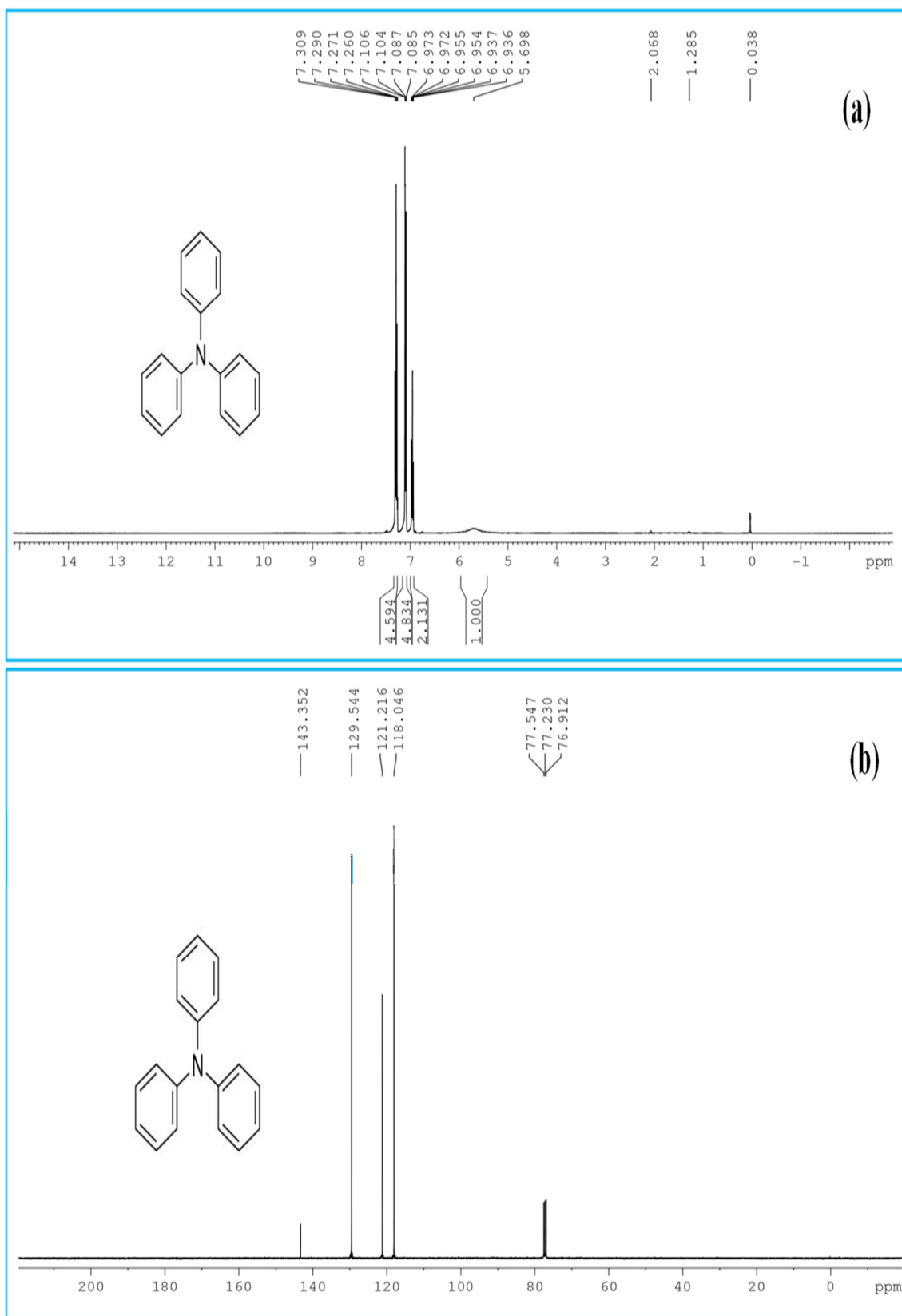
Fig. 4.9 : a) ^{1}H NMR and b) ^{13}C NMR spectra of Triphenylamine.in. In CDCl$_3$.

4.6 CONCLUSIONS

The mixture is tetragonal, and it shows that palladium with TiO_2 does not change the size of the submerged material. Tetragonal has a uniform distribution of spines. X-ray dissociation analysis showed that the average crystallinity of closed palladium doped TiO_2 was 6.24 nm and 7.8 nm. These results reveal the potential of $Ti_{0.97}Pd_{0.03}O_{1.97}$ synthesized as a potential solvent for the active application. Synthesis reactions with different olefins require higher temperatures and longer reaction times. The system has a high cost, ligand elimination and bonding, simple structure, and soft operation. This material provides an environmentally friendly and flexible solution because it produces less waste, is recoverable, and has low efficacy. In short, we have created a new class for C-N reaction products. It is a safe environment with no active ingredients or water filters. These reactions take on many different functions. The reactions were carried out using a monolith cordite coating using a particular method, which is also helpful in restoring the material. The self-assembled system successfully binds the Buchwald-Hartwig imaging alien reaction to zero conditions in the atmosphere in a 0.03 mol% method. Self-assembly retains aromatic amines and aliphatic amines. Catalyst maintains its integrity in its subsequent sequence and is easily accessible and recycled three times without its catalytic activity. We are most aware that this is the first national report of the proposed palladium agreement, containing special Buchwald-Hartwig ammunition, which is unique palladium.

References

[1]. J. G. De Vries, Canadian Journal of Chemistry, vol. (2001), 79, no. 5-6, pp. 1086-1092.

[2]. R. F. Heck, R. F. Heck, and E.-U. Chimiste, (1985, vol. 179, Academic Press, London, UK.

[3]. A. Biffis, M. Zecca, and et al. J. of Mol. Catalysis A: Chemical, (2001) vol. 173, 249-274,

[4]. W. Chen, R. Li, B. et al., European J. of Organic Chemistry, no. 5, pp. 1177-1184, 2006.

[5]. S.T. Gulati, in: A. Cybulski, J.A. Mouliji (Eds), Marcel Dekker, New York, pp. 15-58(1988)

[6]. T.H. Elmer, assigned to corning glass works, (1976) U. S. Patent 3,930,821.

[7]. W. B. Kolb, A. A. Papadimitriou, R. L. Cerro, and et al., Chem. Eng. Prog. (1993), 63-67.

[8]. E. G. Bordeje, F.Kapteijn, J.A. Moulijn, Carbon (2002), 40, 1079.

[9]. E. A. Obuya, W. Harrigan, and et al. J. of Molecular Catalysis A: Chemical, vol. 340, no. 1-2, pp. 89-98, 2011.

[10]. S. J. Tauster, S. C. Fung, R. T. K. Baker, and et al., Science, (1981), vol. 211, article 4487.

[11]. K. Esumi, R. Isono, T. Yoshimura, Langmuir. 2004, 20, 237.

[12]. A.J. Bard, Science 207. 1980, 139.

[13]. Willner, R. Maidan, D. Mandler, H. Durr, G. Dorr, K. Zengerle, J. Am. Chem. Soc., 1987, 109, 6080.

[14]. J. M. Calatayud, P. Pardo, and J. Alarcon, vol. 139, pp. 33–41, 2017.

[15]. S. Ogasawara and S. Kato, Journal of the American Chemical Society, vol. 132, no. 13, pp. 4608-4613, 2010.

[16]. Y. Shao, J. Sui, G. Yin, Y. Gao, Appl. Catal. B-Environ. 2008, 79, 89-99

[17]. H. Dislich, J. Non-Cryst. Solids. 1984, 63, 237-241.

[18]. Bhaskar Devu Mukri, M S. Hegde, J. Chem. Sci. Vol. 129, No. 9, September 2017, pp. 1363–1372

[19]. J.P.D. Lucia, L.E. Lampbell, Advanced Materials in Catalysis, Academic Press (1977)

[20]. I. M. Lachmann, Sprechsaal 119, 1116 (1986)

[21]. I. M. Lachmann, R. N. McNally, Ceram. Eng. Sci. Proc. 2,5 (1981)

[22]. M. Lachmann, R. N. McNally, Ceram. Eng. Progr. 18,29 (1985)

[23]. M. Lachmann, J. L. Willians, Catal. Today 14, 317 (1992)

[24]. A. A. Nijhuis, A. E. W. Beers, T. Vergunst, I. Hoek, F. Kapteijn, J.A. Moulijn, Catal. Rev. Sci. Eng. 43(4), 345 (2001)

[25]. T. Boger, A. K. Heibel, C. M. Sorensen, Ind. Eng. Chem. Res. 43, 4602 (2004)

[26]. P. A. Beauseigneur, I. M. Lachmann, M. D. Patil, S. H. Swaroop, R. R. Wusirika, assigned to corning Inc., U. S. Patent 5,334,570 (1994)

[27]. M. F. M. Zwinkels, S. G. Jaras, P. G. Menon, Stud. Surf. Sci. Catal. 91,85 (1995)

[28]. V. Blachou, D. Goula, C. Phillippopoulos, Ind. Eng. Chem. Res. 31, 364 (1992)

[29]. (a)   A. S. Guram, R. A. Rennels, S. L. Buchwald, Chem., Int. Ed. 34 (1995) 1348–1350;

   (b)   J. Louie, J. F. Hartwig, Tetrahedron Lett. 36 (1995) 3609–3612.

[30]. (a)   M. B. Smith, J. March, USA, (2007);

   (b)   H. Fuwa, T. Kobayashi, T. Tokitoh, Y. Torii, H. Natsugari, 61 (2005) 4297–4312;

   (c)   F. Y. K Wong, S. L. Buchwald, Org. Lett. 5 (2003) 793–796.

[31]. R. N. Salvatore, C. H. Yoon, K. W. Jung, (2001) 7785–7811.

[32]. H. Veisi, N. Morakabati, New J. Chem. 39 (2015) 2901-2907.

[33]. F. Heshmatpour, R. Abazari, RSC Adv. 4 (2014) 55815-55826.

[34]. R. Fareghi-Alamdari, M. G. Haqiqi, N. Zekri, New J. Chem. 40 (2016) 1287- 1296.

[35]. N. Zarnaghash, F. Panahi, A. Khalafi-Nezhad, J. Iran Chem. Soc. 12 (2015) 2057–2064.

[36]. Y. Hiraiz, Y. Uozumi, Chem. Commun. 46 (2010) 1103-1105.

[37]. M. A. Topchiy, P. B. Dzhevakov, M. S. Rubina, O. S. Morozov, A. F. Asachenko, M. S. Nechaev, Eur. J. Org. Chem. 10 (2016) 1908–1914.

[38]. S. Sa, M. B. Gawande, A. Velhinho, J. P. Veiga, N. Bundaleski, J. Trigueiro, A. Tolstogouzov, O. M. N. D. Teodoro, R. Zboril, R. S. Varma, P. S. Branco, Green Chem. 16 (2014) 3494-3500.

[39]. C. Torborg, M. Beller, Adv. Synth. Catal. 351 (2009) 3027–3043.

[40]. J.P. Corbet, G. Mignani. Chem. Rev. 106 (2006) 2651–2710.

[41]. B. Schlummer, U. Scholz, Adv. Synth. Catal. 346 (2004) 1599–1626.

[42]. M. Pagliaro, V. Pandarus, R. Ciriminna, F. Béland, P. Demma Carà, ChemCatChem, 4 (2012) 432–445.

[43]. N. Oger, F.-X. Felpin, ChemCatChem 8 (2016) 1998-2009.

[44]. Lunxiang, J. Liebscher, Chem. Rev. 2007 (107) 133–173.

[45]. X. Huang, K. W. Anderson, D. Zim, L. Jiang, A. Klapars, S. L. Buchwald, J. Am. Chem. Soc. 125 (2003) 6653 -6655.

[46]. E. R. Strieter, D. G. Blackmond, S. L. Buchwald, J. Am. Chem. Soc. 125 (2003) 13978 – 13980.

[47]. B. H. Lipshutz, S. Ghorai, A. R. Abela, R. Moser, T. Nishikata, C. Duplais, A. Krasovskiy, R. D. Gaston, R. C. Gadwood, J. Org. Chem. 76 (2011) 4379–4391.

[48]. A. Baeza, C. Burgos, J. Alvarez-Builla, J. J. Vaquero, Tetrahedron Lett.48 (2007) 25972601.

[49]. D. Bauer, D. A. Whittington, A. Coxon, J. Bready, S. P. Harriman, V. F. Patel, A. Polverino, J.-C. Harmange, Bioorg. Med. Chem. Lett. 18 (2008) 4844-4848.

[50]. a)   R. D. Chambers, Fluorine in organic chemistry. CRC Press: 2004.

b)   P. Kirsch, Modern Fluoroorganic Chemistry: Synthesis, Reactivity, Applications Wiley. VCH: 2004.

c)   K. Müller, C. Faeh, F. Diederich, Fluorine in pharmaceuticals: looking beyond intuition.Science. 317 (2007) 1881-1886. d) M. Schlosser, Angew. Chem.Int. Ed. 37 (1998) 1496-1513.

[51]. M. Kosugi, M. Kameyama, T. Migita, Chem. Lett. (1983) 927-928.

[52]. C. Torborg, M. Beller, Adv. Synth. Catal. 351 (2009) 3027–3043.

[53]. J.-P. Corbet, G. Mignani. Chem. Rev. 106 (2006) 2651–2710.

[54]. B. Schlummer, U. Scholz, Adv. Synth. Catal. 346 (2004) 1599–1626.

[55]. Liu, Y.; Bai, Y.; Zhang, J.; Li, Y.; Jiao, J.; Qi, X. Eur. J. Org. Chem. 2007, 6084-6088.

[56]. Chen, C.; Li, Y.; Yang, L. J. Mol. Catal. A: Chem. 2007, 269, 158-162.

Effective Removal of Congo red Dye from Aqueous Solution Using TiO₂ and Pd Doped TiO₂ Nano Particles as Adsorbents: A Comparative Study
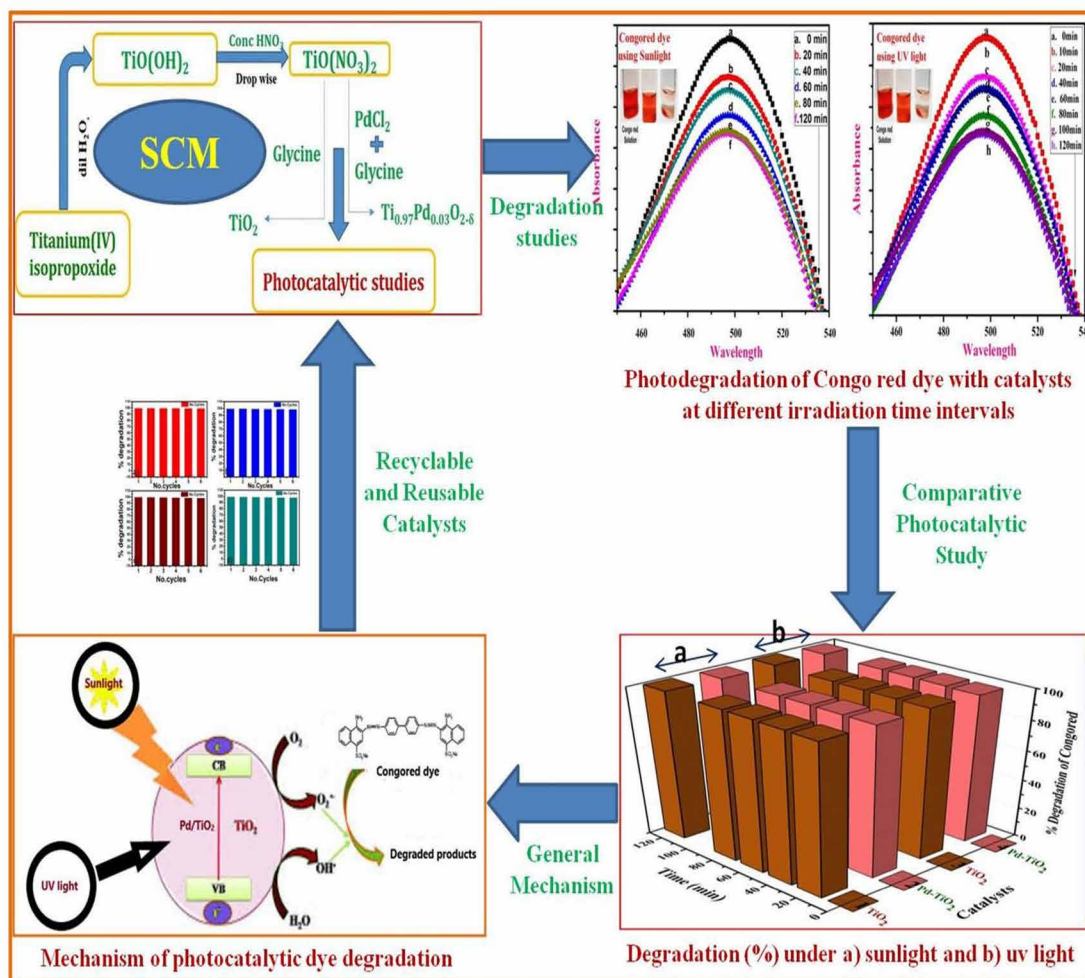
Paper Communicated: "Relative Study of TiO₂ and Pd Doped TiO₂ Nano Catalysts for Water Purification under Solar and Ultraviolet Irradiation", **Energy and Environmental Science,** Royal Society of Chemistry, ISSN-1754-5706 (Under Review).

CHAPTER 5

Effective Removal of Congo red Dye from Aqueous Solution Using TiO_2 and Pd doped TiO_2 Nano Particles as Adsorbents: Comparative Study

The photodegradation of Congo Red (CR.) by using TiO_2 and Pd doped TiO_2 nanoparticles was investigated. The TiO_2 and Pd doped TiO_2 nanoparticles were prepared by solution combustion method using Glycine as fuel, and they are characterized by Scanning Electron Microscopy (SEM), X-Ray Diffraction (XRD), Energy Dispersive X-ray (EDX), Brunauer Emmett-Teller surface area determination and bandgap was determined by using UV-absorption spectroscopy. All experiments were carried out under natural Sunlight and UV light. The percentage of degradation of Congo red dye was examined, using nanoparticles, by varying the dye concentration and catalyst loading. The rate of degradation was highly efficient in 20ppm and 40ppm dye concentration, with constant catalyst concentration 0.1g/1000ml for both nanoparticles. It proves that synthesized TiO_2 and Pd doped TiO_2 nanoparticles are useful in removing the Congo red from the aqueous solution through degradation.

5.1 INTRODUCTION

TiO_2 is the best catalyst due to its high photocatalytic activity, chemical stability, and insolubility in water, low cost, non-toxicity, and availability. But it is impaired by its wide bandgap (3.2 eV), which requires the high energetic and expensive UV light irradiation. Any method which shifts the optical response of Titania from the UV to the visible range will have a profound positive effect on the efficiency of the catalysts [1, 2]. The photoactivity of Titania is altered by doping with transition metals like Pt, Pd, Au, Ag, and Cu [3, 4]. Titanium dioxide has considerable advantages over other similar photocatalysts due to its good characteristics in terms of chemical stability, endurance, thin-film transparency, and lower production costs [5, 6]. The activity of the anatase phase of TiO_2 for the photodegradation of various pollutants is, in general, much higher than that of rutile. It has been shown that the photocatalytic activity of TiO_2 is influenced by the crystal structure, surface area, crystallinity, and porosity [7, 8].

Dyes are widely used in industries such as textiles, rubber, paper, plastic, cosmetics, etc. Dyes can be divided into several categories, based on their chemical nature: anionic or cationic and basic or reactive dyes. Azo dyes are the largest group of the synthetic colorants known and the most popular group released into the environment. Wastewater containing dyes may be toxic, carcinogenic, and mutagenic [9,10]. The photocatalytic degradation of various organic dyes such as Methylene blue (MB), Alizarin S (AS), Methyl red (M.R.), Congo red (C.R.), and Orange G (O.G.) was investigated using nanosized anatase Titania TiO_2 and Pd doped titania ($Ti_{0.97}Pd_{0.03}O_{1.97}$) were prepared by solution combustion method.

We have synthesized nano TiO_2 and Pd doped TiO_2 by solution combustion method, which absorbs the UV and most of the visible light of the solar spectrum. The photocatalytic activity of this catalyst was evaluated by measuring degradation rates of various organic dyes such as Congo red under solar irradiation. The photocatalytic activity of the combustion synthesized Titania, and palladium doped Titania was compared with commercial TiO_2 under similar conditions. The catalyst has been characterized using X-ray diffraction (XRD) technique, gravimetric-differential thermal analysis (TG-DTA), FTIR SEM, and UV-Vis spectrophotometer.

Congo red (C.R.) dye is one of the most important secondary diazo dyes used for dyeing cotton in textile industries and also in wood pulp and paper industries. It has an intense red color, complex chemical structure, and has a maximum absorbance at the wavelength of 498 nm (λ_{max}), but it is a carcinogenic dye. Hence it is most important to study the degradation profile of CR [11, 12]. Titania, a semiconductor, has attracted more research interest due to its large bandgap ~3.0–3.2 eV. the decolorization of CR has been carried out by many types of research over different catalysts such as TiO_2 and Pd doped TiO_2, etc., a higher percentage of decolorization with less catalyst loading (Catalyst weight in mg/Dye concentration in ppm=20mg) at the shorter time was obtained over our catalysts [13,14]. From literature, in 2011, Obuya and coworkers photo-deposited Pd NPs of diameters within 2-5 nm on electrospun TiO_2. In 2014, Nasrollahzadeh and his group dispersed 40 nm Pd NPs on commercial TiO_2 using a simple drop drying process. At low-temperature treating, denote a favorable application and TiO_2-based catalyst [15, 16]. Titanium dioxide (TiO_2), as a photocatalyst is promising due to its merits of strong photo-oxidizing

power, chemical stability, non-toxicity, and low cost. Unmodified TiO_2 suffers from narrow light-response range, difficult catalyst recovery with low efficiency, and fast recombination [17]. However, it exhibits unique structural, thermal, and electronic properties based on the preparation methods where the size, shape, crystal structure, and phases are tuned for specific applications. Improvising the characteristics of TiO_2 by affecting its synthesis route by doping, impregnation, and bandgap engineering have evolved Nanostructured TiO_2 for dye degradation, pesticide redemption, micropollutants mitigation, and for solar cells [18, 19, and 20]. Congo red widely used in textile, printing and dyeing, paper, rubber, and plastic industries and banned in many countries because of health concerns. Synthetic dyes, such as CR, are difficult to biodegrade due to their stable compounds and complex aromatic structures and affect carcinogen and mutagen [21-25]. Another research investigated the degradation of CR in the presence of different catalysts [26-32]. To improve catalytic ability and widen application fields, modification of TiO_2 with noble metals such as Pt, Pd, and Au is often adopted due to their high effectiveness and good stability (Długokęcka et al., 2017). Palladium (Pd) is a known noble metal with new properties; Palladium is one of the most active elements for interacting with the surface of oxides as support. Previous studies have reported that the photocatalytic performance of Pd-doped TiO_2 is affected by crystal size and morphology of Pd. The Pd-doped TiO_2 catalysts with highly dispersed small Pd particles are reported to be more active concerning strong metal-support interactions (Banerjee et al., 2016). To our best knowledge, fewer studies have been reported to evaluate photocatalytic degradation of dye mixtures using Pd-doped TiO_2, including the effect of the chemical structure of dyes. Although some researchers suggested that such catalysts are promising to treat dye-containing solutions (Abdelaal and Mohamed, 2013; Kuvarega et al., 2011; Leelavathi et
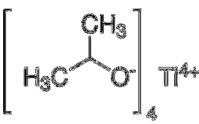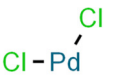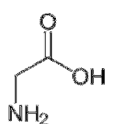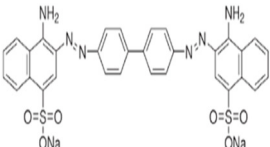
al., 2013), it is not enough to convince because the chemical structure of the pollutants is an important factor affecting the directly photocatalytic performance of the catalysts. The possible photocatalytic reaction can be proposed as follows (Abou-Gamra and Ahmed, 2016; Amreetha et al., 2016; Chen et al., 2008; Hu et al., 2015; Kaur and Singhal, 2014; Trandafilović et al., 2017) Palladium doped Titania is most useful for the high oxygen storage capacity.

In this present study was mainly focused on the investigation of photocatalytic degradation of Congo Red (CR) and examine the effectiveness of synthesized TiO_2 and Pd doped TiO_2. The identification of degradation product of Congo red using solar and UV light irradiation technique. The effect of parameters, such as pH, initial dye concentration, catalyst loading, transition metal doping on TiO_2 by substitution, and impregnation, was examined, taking Congo red as a specific dye for analysis. The photocatalytic degradation obtained with Sunlight has been compared with that obtained by irradiation with mercury vapor lamp using the same TiO_2 and Pd doped TiO_2 catalyst.

5.2 Methods and Materials

5.2.1 Materials:

Table 5.1. Chemicals and specification used.

Name/ Molecular formula	Structure	Specification	Suppliers
Titanium tetra (IV) isopropoxide ($Ti(OC_3H_7)_4$)		Molar mass: 284.22 g/mol Density: 0.96 g/cm3	Sigma-Aldrich
Palladium chloride ($PdCl_2$)		Molar mass: 177.33 g/mol Density: 4 g/cm3	Sigma-Aldrich
Glycine (NH_2CH_2COOH)		Molar mass: 75.07 g/mol Density: 1.61 g/cm3	Merck
Congo red dye ($C_{32}H_{22}N_6Na_2O_6S_2$) ($\lambda max = 497nm$)		Molar mass: 696.7 g/mol Density: 0.995 g/mL	Merck

5.2.2 Methods

The photodegradation of the Congo red dye solution process was operated in the presence of Sunlight and UV light irradiation which is directly under sunlight and under a UV lamp. All parameter was set in the UV-Vis spectrometer to analyze the degradation of Congo red dye solution.

5.2.3 Synthesis of TiO_2 and $Ti_{0.97}Pd_{0.03}O_{1.97}$ powdered catalysts

Synthesis of TiO_2 and $Ti_{0.97}Pd_{0.03}O_{1.97}$ powdered catalysts was prepared in the solution combustion method. The complete explanation was reported in earlier chapter 2.
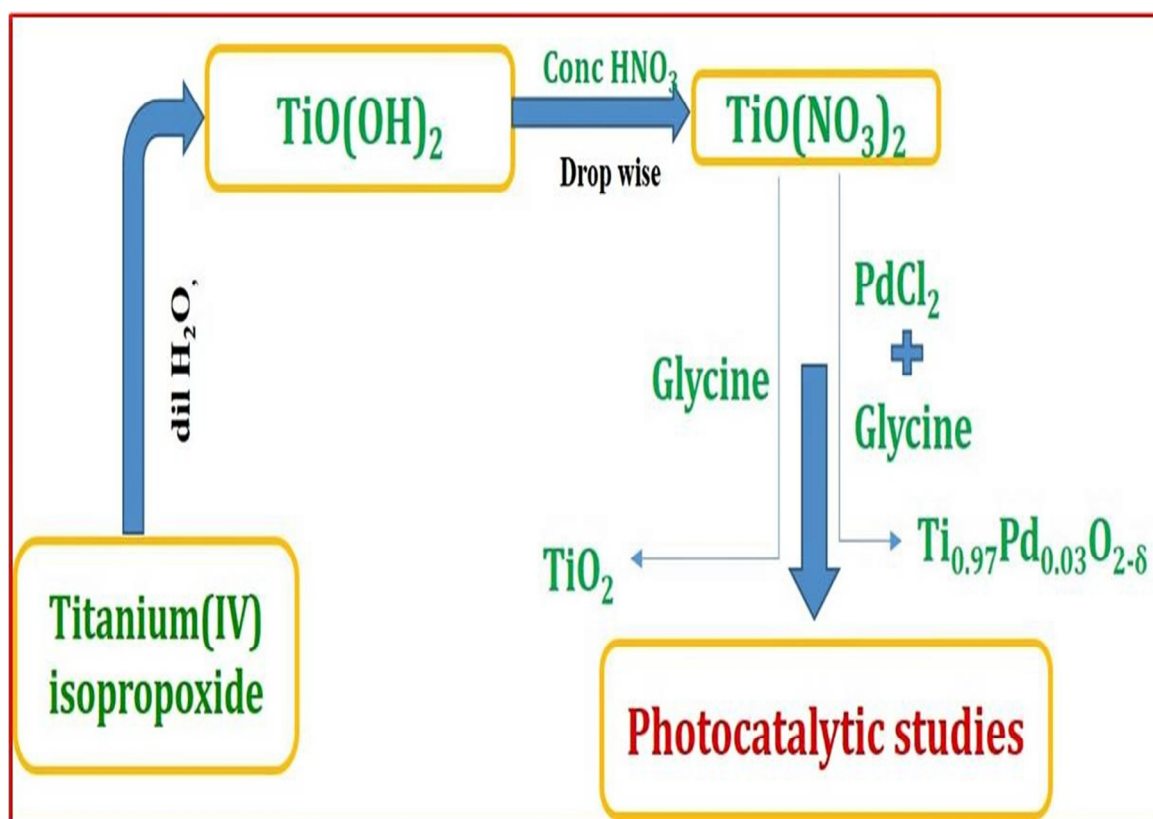
Fig. 5.1 : Flowchart for the synthesis of un-doped TiO_2 and Pd-doped TiO_2 catalysts

5.2.4 Preparation of Stock Solutions

The stock solution was prepared by 100mg of each organic compound CR, dissolved in 1 liter distilled water to get 1000 ppm concentration. From 1000 ppm, different initial concentrations of 10-60 ppm are prepared. The absorbance of each compound is determined by using a UV-Visible spectrophotometer. Absorbance values are recorded at the corresponding maximum wavelength (λ_{max}). The absorbance values for the corresponding wavelength and calibration curve of each compound, i.e., CR at $\lambda=476$ nm. The Photocatalytic Degradation of Congo red dye has no observable degradation of dye over TiO_2, and $Ti_{0.97}Pd_{0.03}O_2$ Catalysts was observed either without irradiation or without a catalyst. The adsorption capacity of the solution combustion-synthesized and undoped

titania (TiO_2) and palladium doped Titania ($Ti_{0.97}Pd_{0.03}O_{1.97}$) for Congo red dye was evaluated in aqueous media. 0.1 g of Congo red dye is dissolved in 1000ml standard flask, and it makes up to the mark by using distilled water, which is a 1000 ppm concentrated solution was made. The 5ml of the above-prepared solution (1000 ppm) was taken into 250 ml standard flask, and it makes up to the mark of the container that is a 20ppm, 40ppm, the concentrated solution was made separately. The prepared 20ppm solution was transferred entirely to the Petri dish along with the magnetic stirrer. The catalysts were added in 60 mg, the reaction was started immediately take 5 ml of solution from the above solution into the test tube it was considered as zero min there is no reaction shown, after 5 min similarly we have to take 5ml from the above solution with continuous stirring then similarly 20, 30, 40, 50, 60, 80, 100 and 120 min we have to take up to the solution turns to colorless (zero absorbance). The 100 ml sample of Congo red dye was mixed with 60mg of the catalyst, the suspension was stirred, and the concentrations of the organics were measured in the dark over a time of period. The adsorption was not apparent within 2 h. Hence, the initial concentration was taken in all cases. The slopes calculated based on three to five points were nearly constant. The initial position, (t) 0, was taken after the addition of the catalyst. The effect of catalyst loading on the photocatalytic degradation of Congo red dye was studied by varying the amount of TiO_2 and $Ti_{0.97}Pd_{0.03}O_2$ catalysts loading was chosen for the degradation of all the organics. The spectra of the CR dye in the visible part have maximum absorbance at 466 and 498nm, respectively. The absorbance intensity decreases for CR dye solutions with increasing the time of UV-irradiation exposure, suggesting dyes degradation. Almost complete decolonization of the dyes was observed after 10 min for the CR dye.

Experiments performed "in the dark," i.e., without irradiation, also shown. The comparison between TiO_2 and palladium doped TiO_2 photocatalysts.

5.2.5 Photodegradation

Photocatalytic experiments were conducted under direct Sunlight and UV light. The CR solution was prepared by dissolving 60mg of azo dye with 1000mL double distilled water using a 1000ml volumetric flask and degradation in the presence of TiO_2 and Pd doped TiO_2 nanoparticles at different catalyst dosages and initial dye concentration. Initially, 1000ml of 20ppm of dye samples were tested with catalyst dosage (60mg), by varying dye concentration (20ppm to 40ppm) and different conditions for Sunlight and UV light. All the experiments were carried out in the presence of direct sunlight and UV light. The whole experimental set-up was placed under Sunlight between 11 a.m. and 2 p.m. and the average intensity of sunlight during this period is 834×100 lux unit using lux meter and UV light was carried out in the dark conditions at room temperature. After the photocatalytic degradation, the extent of degradation was estimated by recording the absorbance of the dye solution using a spectrophotometer. The influence of operational parameters like catalyst amount, the initial level of CR dye, and pH of dye solution on the photocatalytic degradation of C.R. dye was studied to determine the optimum conditions for higher photocatalytic degradation efficiency. UV-visible spectrophotometer was used to analyze the photocatalytic performance of the synthesized nanocomposite. 60 mg of the composite was added to 20 ppm of 1000 mL of the dye solution under continuous stirring. After establishing adsorption-desorption equilibrium for 30 minutes in dark condition, the photocatalytic study was carried out under 400 watts tungsten halide lamp embedded in a wooden breakfront. In pre-determined time intervals, 5 mL of aliquots were drawn, centrifuged, and the translucent dye solutions were analyzed using a UV-

visible spectrophotometer at the respective absorption wavelength (λ max= 497 nm) of the CR dye. The percentage was calculated by equation 1,

Photocatalytic degradation %= $[(C_0-C_t)/C_0] \times 100$…….(1)

Where C_0 is the initial concentration of the dye, and Ct is the concentration of the dye at a time interval, t.

5.3 Results and discussion

5.3.1 Fourier Infrared spectroscopy analysis (FTIR)

FT-IR spectra of un-doped TiO_2 and Pd-doped TiO_2 are shown in Fig. 5.2 a) and b). Both FT-IR spectra from Fig.5.2. Point out four-fold Ti coordination in the vitreous matrix. The broad peaks appearing at 3854-3751 cm^{-1} are assigned to vibrations of -OH groups and the peaks 1767 and 1781 cm^{-1} is the O-H stretching bands. The peaks at ~2341 cm^{-1} were assumed to be due to the species containing CN bonds and the bands at 1185-1163 cm^{-1} could be ascribed to nitrogen oxide species. The broad absorption bands between 400 and 800 cm^{-1} are mainly ascribed to Ti-O and O-Ti-O flexion vibration. When metal ions are doped to the surface of TiO_2, the absorption band transforms and simultaneously new absorption band appears.
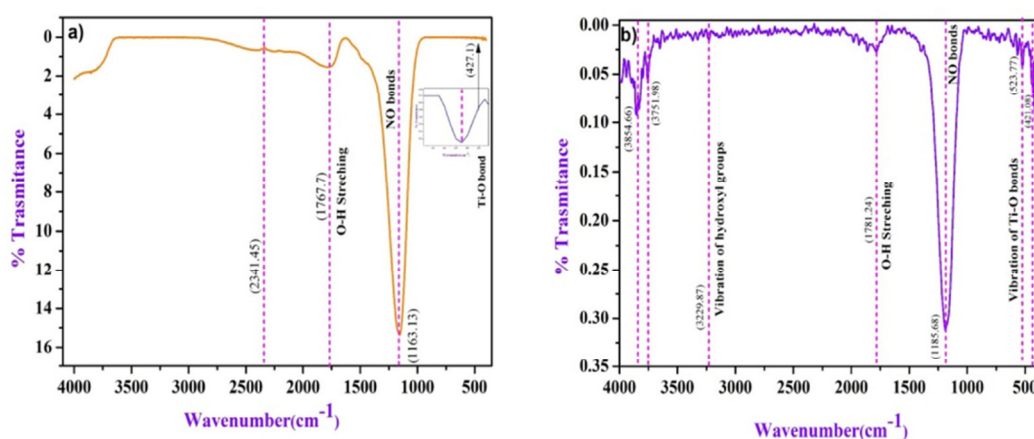
Fig. 5.2 : FTIR spectra of a) TiO_2 and b) Palladium doped TiO_2

5.3.2 Field Emission-Scanning Electron Microscope studies (FESEM)

SEM images of the synthesized TiO_2 and palladium doped TiO_2 are shown in Fig.5.3 the SEM images show bright nanostructures can be seen as grain size of ~ 1µm to 200nm and the tetragonal morphology with uniform particle distribution. In Fig. 5.3. The undoped TiO_2 demonstrating the particles are in little accumulation and tetragonal morphology. The SEM analysis showed that the doped palladium on TiO_2 does not affect the morphology and structure of the TiO_2 nanoparticle. The SEM experiments showed that palladium doped TiO_2 did not affect the morphology and structure of TiO_2 nanoparticle. FE-SEM was employed to study the properties of the synthesized catalyst. The SEM images are also utilized to examine the approximate particle size of the catalyst. Fig. 5.3. Shows typical SEM images of 0.03% Pd doped TiO_2 powder catalyst at a couple of magnification. The above figures reveal that the approximate particle size is between 1µm to 10µm, and however, it is observed that distinct particles can agglomerate more into larger particulates of 100 to 200 nm.
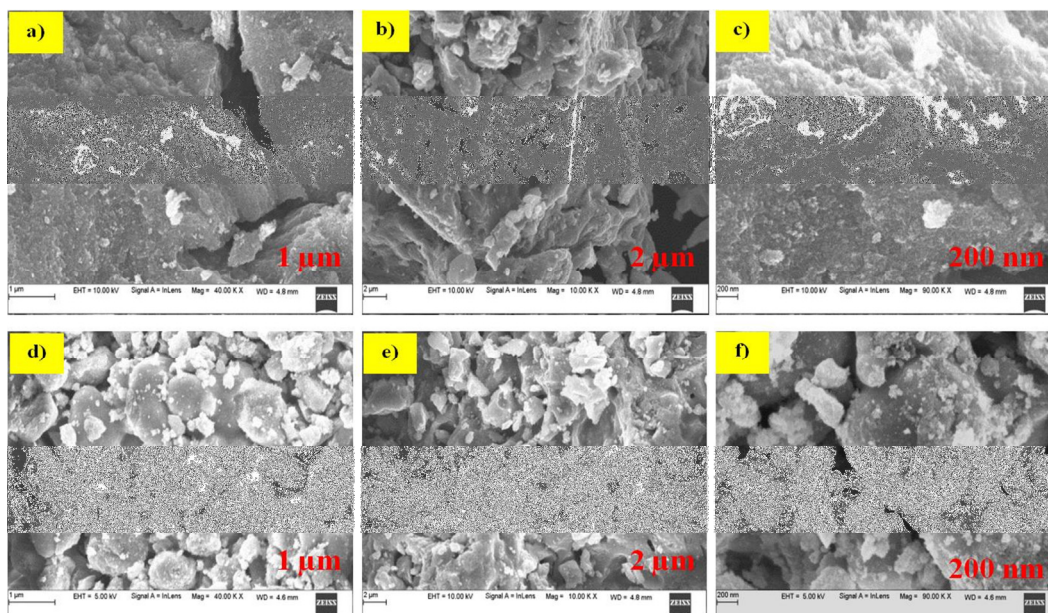
Fig. 5.3 : SEM images of a) 1µm b) 2 µm and c) 200 nm of Undoped TiO_2 and

d) 1µm e) 2 µm and f) 200 nm of Palladium doped TiO_2

5.3.3 Energy-dispersive X-ray spectroscopy analysis (EDAX)

The EDAX spectra of TiO_2 and Pd doped TiO_2, as shown in Fig. 5.4, which endorses the arrangement of the improved samples with the existence of the intensity corresponding to Ti, Pd, carbon, and oxygen. In the EDAX spectrum (Fig. 4) of the produced TiO_2 and Pd doped TiO_2, Ti, Pd, and O were observed. Energy-dispersive X-ray spectroscopy (EDS) of Pd-TiO_2 is shown in fig.4, which confirm the existence of Ti, O, and Pd with weight percent. The EDS spectral analysis made to randomly selected points of SEM images showed for the 0.03% of Pd doped TiO_2 titanium, palladium, oxygen, and carbon as the main elements, whereas the noble metals are not detected. The existence of Ti, Pd, C, and O has been detected. The presence of the carbon peak is because of the use of concentrated nitric acid during the preparation of Pd doped TiO_2 of catalyst. The figure shows the EDAX spectrum of sample Pd doped TiO_2 shows various atomic percentages such as titanium, palladium, oxygen, and carbon shows 18.21%, 0.79%, 54%, and 27% of carbon impurity respectively are shown in Fig. 5.4. The investigation shows that Pd is presented to the extent of 0.79%, which is near to the compositions take in the preparations. The presence of Pd from the EDAX study confirms the substitution of Pd ion in the TiO_2 lattice.
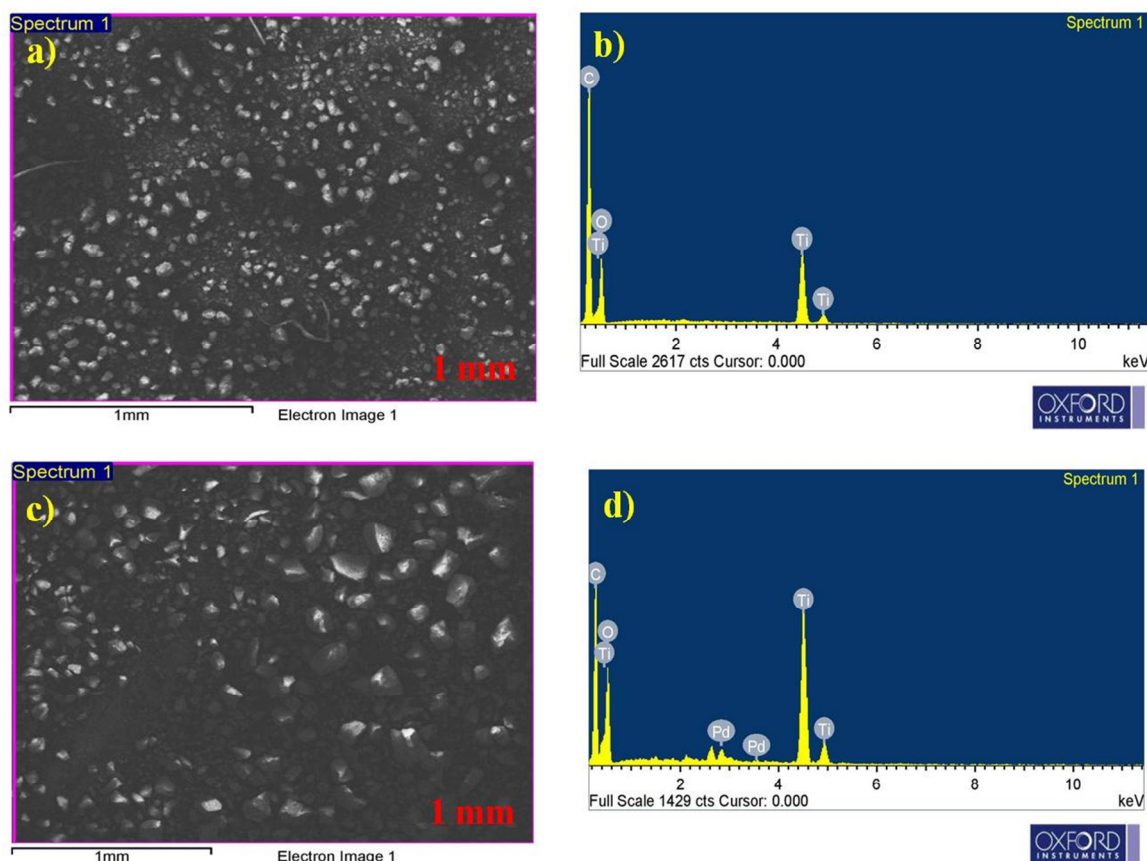
Fig. 5.4 : EDAX images of a) 1mm b) and c) 1 mm d) of Undoped TiO_2 and

0.03% Pd doped TiO_2.

Table - 5.2 : The weight percentage of elements in EDAX spectra

Elements in TiO$_2$	Weight (%)	Atomic (%)	Elements in Pd doped TiO$_2$	Weight (%)	Atomic (%)
O K	8.74	57.42	O K	7.79	54.00
Ti K	6.32	13.88	Pd L	0.76	0.79
C	3.28	28.70	Ti K	7.86	18.21
Totals	18.34	100.00	C	2.92	27.00
			Totals	19.33	100.00

5.3.4 Thermal Analysis

The thermal analysis of TiO_2 and palladium TiO_2 was shown in Fig.5.5 a) and Fig.5.5 b) respectively. In Fig. 5.5 a), the TG curve can be divided into two stages. The first step is from room temperature to 110 $°C$, over which the mass loss of 6% was observed, which caused by dehydration from the catalyst. The second stage is from 110 to 200$°C$, where the mass loss is $\sim$5%. This study indicates that the first species to leave the surface of TiO_2 is water. Thus the weight loss in TGA cannot account for carbon. In Fig. 5.5 b), the TG curve can be divided into three stages. The first decomposition starts at 100 ^0C due to the loss of a water molecule. The second decomposition was occurred at 100-300 ^oC because of degradation processes of the organic matter, more pronounced for Pd-doped TiO_2. The final decomposition occurred at 680 ^0C. This is due to the conversion of reactant to product.
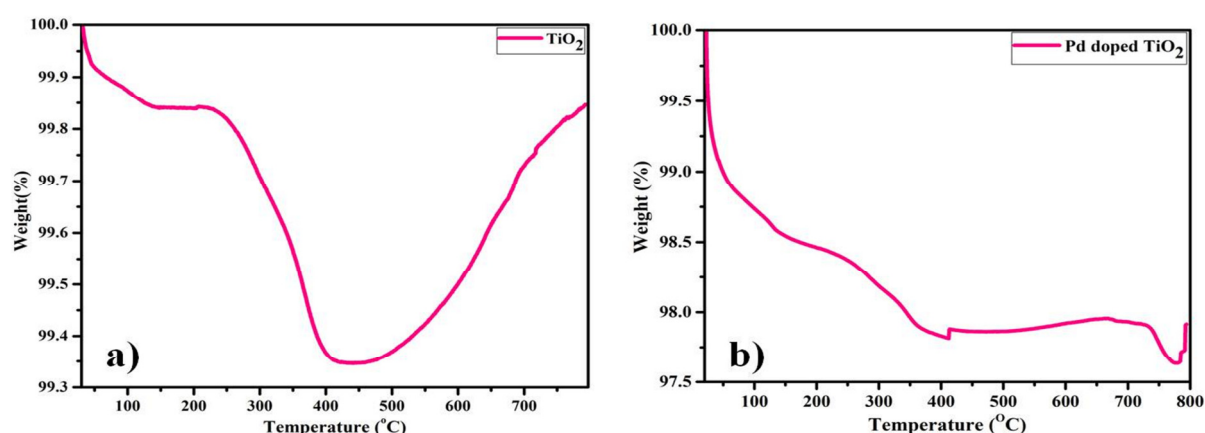
Fig. 5.5 : Thermal behavior of (a) Undoped TiO_2 (a) and (b) 3% Pd-doped TiO_2

5.3.5 UV-VIS ANALYSIS

The optical absorption spectra of combustion synthesized and TiO_2 and Pd doped TiO_2 are shown in Fig. 6. Pd doped TiO_2 shows a single peak at 400nm (which corresponds to band-gap energy of 3.10 eV). In comparison, the combustion synthesized TiO_2 shows two optical absorption thresholds at 659 and 418nm that correspond to the

band-gap energy of 2.18 and 2.65eV, respectively. Combustion synthesized TiO_2 absorbs appreciably at wavelengths lesser than 600nm. The solar wavelength spectrum (Fig.5.6 a)) shows the maximum irradiance at the wavelength region of 450–480nm. Since combustion synthesis TiO_2 band-gap corresponds to this part, it can absorb relatively higher photon flux compared to Pd doped TiO_2. The irradiances corresponding to the wavelengths of 400, 467, and 570nm are 1.556, 1.962, and 1.799Wm^{-2} nm^{-1}, respectively. The absorbed photon flux ratio for combustion synthesized TiO_2 is 1.62 and 2.35 times higher than Pd doped TiO_2 for the absorption thresholds of 467 and 570nm, respectively. Combustion synthesized TiO_2 indeed showed high photocatalytic activity under solar radiation. The phase transition to the rutile phase also does not occur. The decrease in the band-gap can be due to carbide ion substitution for oxide ion in the TiO_2, similar to the observation by Khan et al. [33]. The UV absorption spectrum of combustion synthesized TiO_2 is close to that of carbon substituted TiO_2 reported by Khan et al. [33]. All these features seem to add up to give higher photocatalytic activity under solar exposure. The UV-visible spectra of the undoped TiO_2 and Pd doped TiO_2 are shown in fig. the absorption spectra of Pd doped TiO_2 consists of a single broad, intense peak at 365.85 to 404.93 nm can be attributed to the charge-transfer from the valence band to the conduction band. The Undoped TiO_2 showed absorbance in the shorter wavelength region at 380 nm. The bandgap of pure TiO_2 is 3.39 eV, and Pd doped TiO_2 shows a slightly decreased bandgap at 3.39 eV to 3.06 eV with doping of different composition of Pd metal doping.
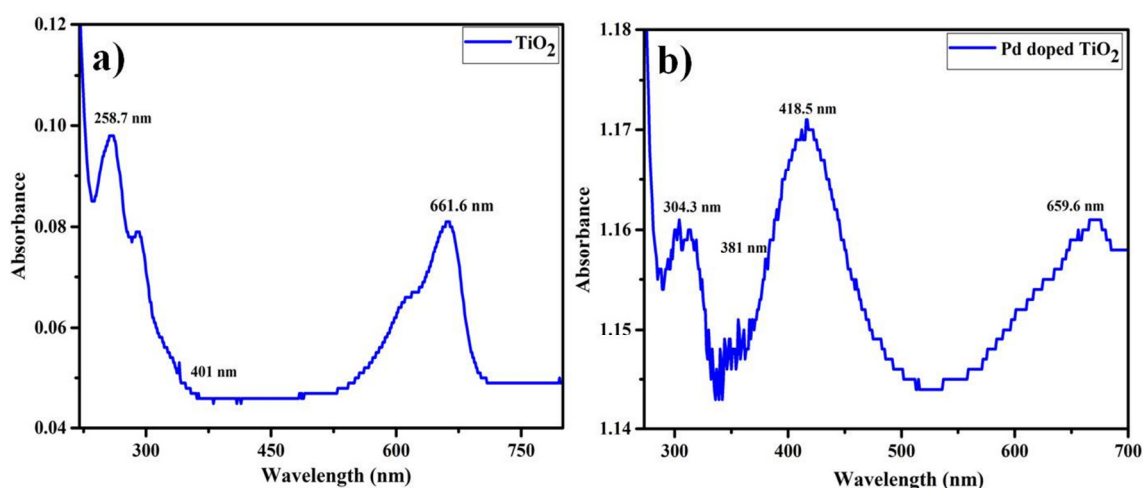
Fig. 5.6 : UV-Vis absorption spectra of a) TiO_2 and b) Pd doped TiO_2.

5.3.6 Photocatalytic Activity

Congo red (CR) was selected as a probe molecule to assess the photocatalytic activity of the sample under the visible light because of its excellent adhesion properties and little cost. In the absence of TiO_2 and Pd doped TiO_2 photocatalyst, the direct photolysis of Congo red did not show any reduction in the concentration, indicating that Congo red is photostable [34]. Fig. 5.7 shows the absorption spectra of Congo red during photocatalytic degradation in the presence of TiO_2 and Pd doped TiO_2 nanorods. Dye degradation is completed in two stages, one is absorption and the next one is the degradation of dye. The typical absorption peak at 497 nm for Congo red slowly decreased with an increase in irradiation time, and at last, the absorption peak disappears, and the color of the Congo red solution turns red to colorless. The % degradation of Congo red was monitored by the UV-visible spectrophotometer, and it shows 99% degradation. The peak at 497 nm (π-π*) and peak at 343 nm (n-π*) electron transition in Congo red is related to an azo group [35]. The pseudo-first-order reaction can be explained by the kinetics model by plotting -ln (C/C_0) against time t (see Fig. 5.7). C_0 is the initial concentration of dye, and C is the concentration of Congo red dye at different

time intervals. For comparison, a blank Congo red solution was carried out by following the similar experimental conditions and procedure without introducing photocatalyst [36]. The prepared sample (TiO_2 and Pd doped TiO_2) were compared with various photocatalyst having nanorods morphology for the degradation of Congo red reported earlier. From the comparison, we conclude that the prepared sample showed better photocatalytic performance in 120 min having 1 M Congo red concentration at natural pH (Fig.5.7). The photodegradation of Congo red follows the first-order reaction kinetics that obeys the equation $\ln(C_0/C) = kt$, where k is the rate constant, t is the irradiation time; C_0 and C are the initial and concentration at time t. The first-order rate constant value is higher for both TiO_2 and Pd-doped TiO_2 catalysts.

5.3.7 UV light determined photocatalysis
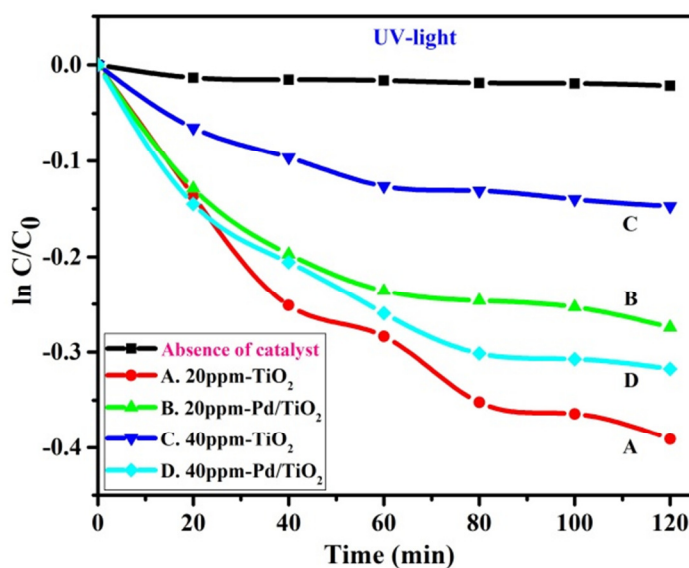
Fig. 5.7 : Degradation profile for the Congo red dye under UV irradiation.

The photocatalytic activity of both the TiO_2 and Pd doped TiO_2 Catalyst has been investigated under UV irradiation. Congo red has been selected as a model dye for the evaluation of the photocatalytic activity. Congo red is a structurally stable anionic dye, which is represented in the inset of Fig. 7. The absorption spectrum of an aqueous

solution of Congo red is illustrated in Fig. 7. The absorption band at 343 nm is associated with the π–π^* transition of the aromatic ring and the band at 496 nm can be assigned to the n–π^* transition of the lone pair present in the N atom of the chromophoric –N=N– azo moiety [37]. The degradation of the dye by photocatalysis can be followed by monitoring the decrease in the intensity of the absorption band at 497 nm, indicating cleavage of the –N=N– bond. Initially, a new experiment was conducted where the dye and the catalyst suspension were stirred magnetically in the dark before irradiation. Congo red degradation was negligible in the absence of light. The experiment was also conducted in the presence of light but without the catalyst to ensure that there is no photolysis of the dye in the absence of a catalyst. Fig. 5.7 displays the degradation profile of Congo red in the presence of TiO_2 and Pd doped TiO_2 Catalysts under UV irradiation. For comparison, the degradation of Congo red by anatase TiO_2 nanoparticles with Pd doped TiO_2 under UV irradiation in the same experimental conditions is also shown in fig.7. It is evident from the degradation profile that TiO_2 exhibits a slightly higher photocatalytic activity than Pd doped TiO_2.

5.3.8 Visible light determined photocatalysis.
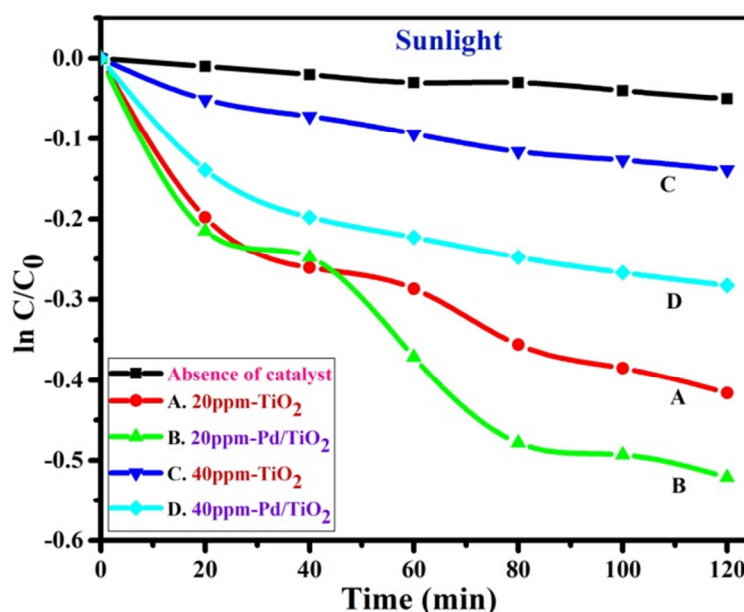
Fig. 5.8 Degradation profile for the Congo red dye under sunlight irradiation.

In Fig. 5.8 represents the degradation of the dye under sunlight using nano TiO_2 and Pd doped TiO_2. Unsurprisingly, the photocatalytic activity of anatase is vastly diminished in the presence of the sun. The broad band gap of anatase TiO_2 results in the inability of the catalyst to absorb energy in the visible region. From Fig.8, it can be discerned that the photocatalytic activity of nano TiO_2 is more than Pd doped TiO_2. It is well recognized that as the redshift in the absorption edge extends towards the visible region, the utilization of photons in the visible region increases. This indicates that the smaller the bandgap, the higher the photocatalytic activity in the visible area. Accordingly, Pd doped TiO_2, with the lowest bandgap as calculated from the DRS data, should have shown higher photocatalytic activity than nano Pd doped TiO_2 under sunlight irradiation. On the contrary, it is observed that although the absorption edge of nano Pd doped TiO_2 being smaller in the visible region, it degrades the dye faster than its bulk counterpart. Therefore, it is likely that the higher activity of nano TiO_2 is due to the particle size effect. It is believed that as the particle size becomes smaller, in addition to the increase in the surface area, the distance to reach the reaction site will be shortened for the excitons on the surface of the catalyst [38]. Therefore, the electron-hole recombination rate decreases, thereby enhancing the photocatalytic activity [38]. Furthermore, the recyclability of the bulk and nanocatalyst after three photoreactions in the presence of solar radiation follows the same trend as the photocatalytic activity already discussed in the previous section. From the above discussion, it can be established that TiO_2 shows slightly high photocatalytic activity in the UV as well as the visible region. Furthermore, in comparison with UV irradiation, the rate of Congo red degradation under solar irradiation is higher. Hence, the degradation and removal rate of Congo red is more feasible under sunlight rather than in UV light for the TiO_2 catalyst.

5.3.9 Photocatalytic Studies- Sunlight
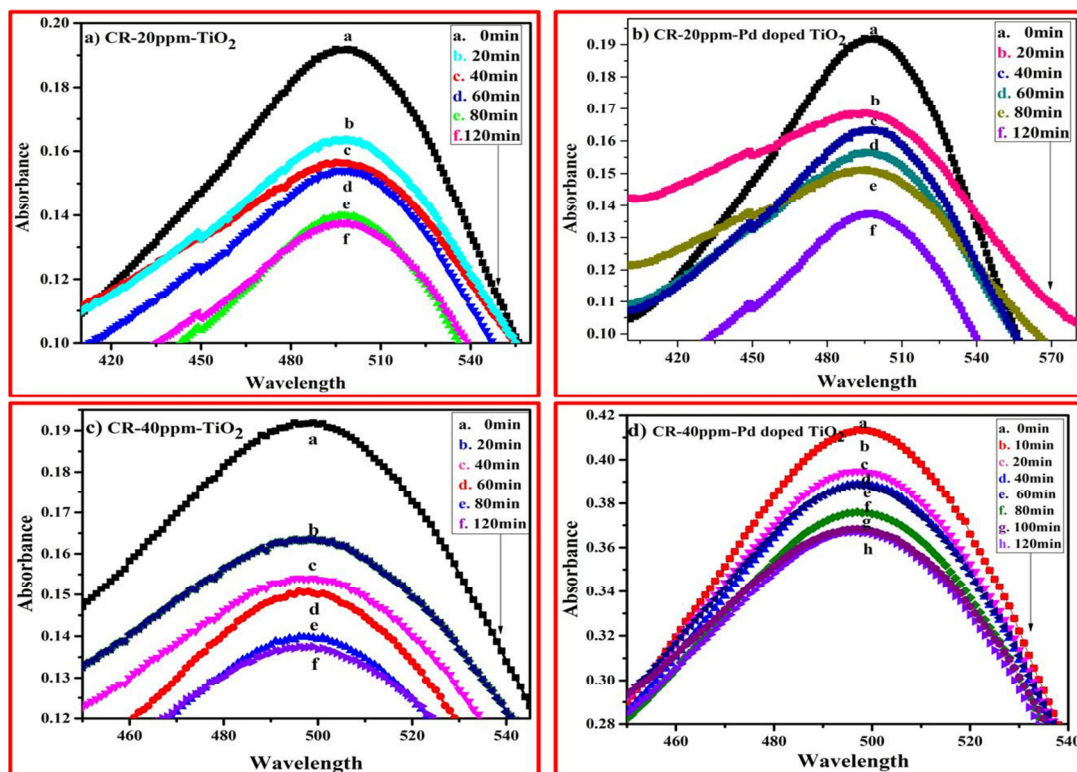
Fig.5.9 : Successive UV-Vis spectra of CR degradation at different time intervals

The degradation efficiency of Congo red is found to decrease with an increase in the initial dye concentration. The influence of initial dye level, photocatalytic degradation of Congo red, was studied in the concentration range of 10ppm to 40ppm. Fig.5.9. showed that the photocatalytic activity of the best TiO_2 and Pd doped TiO_2 photocatalysts on CR under solar light illumination. The maximum UV-Vis absorptions for CR are at the wavelength of 498 nm. The maximum absorption occurred almost at the same wavelength throughout the photodegradation period. The absorption band in the range for CR was in the range of 400-600 nm (Fig.5.9). The absorbance of the spectra rapidly decreased with increasing irradiation time, and the peak of spectra almost disappeared after a few hours (120min) solar irradiation as TiO_2 promotes catalytic photodegradation of dyes.

Table- 5.3 : 20 ppm Congo red dye + 60 mg TiO$_2$ catalyst + Sunlight

Sl	Time(t) min	Conc.(C) ppm	C/C0	ln C/C0	log C/C0	% of degradation
1	0	40	1	0	0	0
2	20	38.35	0.95	-0.051	-0.0222	98.96
3	40	37.57	0.93	-0.072	-0.0315	99.01
4	60	36.41	0.91	-0.094	-0.0409	99.03
5	80	35.73	0.89	-0.116	-0.0506	99.06
6	100	35.35	0.88	-0.127	-0.0555	99.07

Table-5.4 : 20 ppm Congo red dye + 60 mg Pd doped TiO$_2$ catalyst + Sunlight

Sl	Time (t) min	Conc.(C) ppm	C/C0	ln C/C0	log C/C0	% of degradation
1	0	20	1	0	0	0
2	20	16.4	0.82	-0.198	-0.0861	99.04
3	40	15.4	0.77	-0.261	-0.1135	99.18
4	60	15.0	0.75	-0.287	-0.1249	99.21
5	80	14.0	0.70	-0.356	-0.1549	99.24
6	100	13.6	0.68	-0.385	-0.1674	99.28

Table – 5.5 40 ppm Congo red dye + 60 mg TiO_2 catalyst + Sunlight

Sl	Time(t) min	Conc.(C) ppm	C/C0	ln C/C0	log C/C0	% degradation
1	0	20	1	0	0	0
2	20	16.13	0.806	-0.215	-0.0936	99.04
3	40	15.63	0.780	-0.248	-0.1079	99.15
4	60	13.82	0.690	-0.371	-0.1611	99.18
5	80	12.42	0.620	-0.478	-0.2076	99.21

Table: 5.6 40 ppm Congo red dye + 60 mg Pd doped TiO_2 catalyst + Sunlight

Sl	Time(t) min	Conc.(C) ppm	C/C0	ln C/C0	log C/C0	% degradation
1	0	40	1	0	0	0
2	20	35	0.87	-0.139	-0.0604	99.52
3	40	32.91	0.82	-0.198	-0.0861	99.58
4	60	32.08	0.80	-0.223	-0.0969	99.60
5	80	31.25	0.78	-0.248	-0.1079	99.61

Rate parameters of a) TiO_2 b) Pd doped TiO_2 under

Sunlight by using Congo red dye

5.3.10 Photocatalytic Studies- UV-light
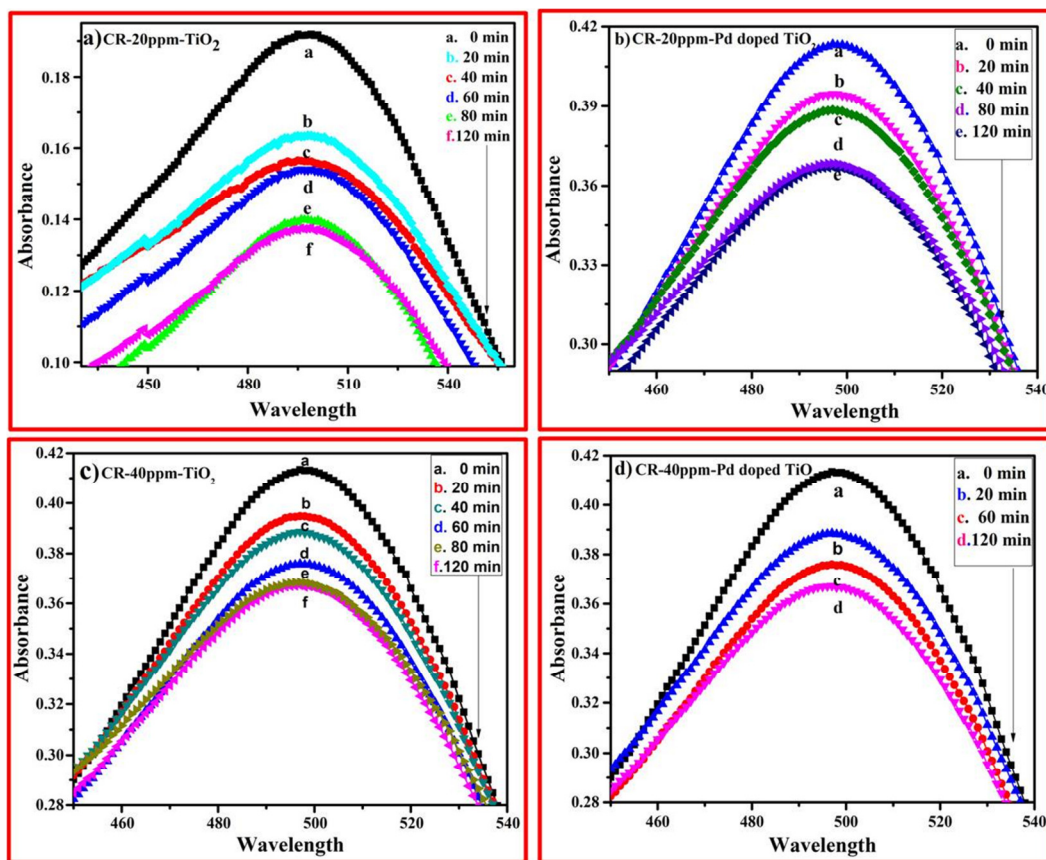
Fig.5.10 : Successive UV-Vis spectra of CR degradation at different time intervals

The photocatalytic activity of TiO_2 and Pd doped TiO_2 a catalyst was studied by the degradation of CR under UV light irradiation concerning time. The aqueous solution of CR initially shows an absorption maximum at 498 nm. Fig. 5.10 show a tremendous decrease in absorption maxima resulting in 90.55 % of degradation in just 120 mines. For comparison sake, we have also performed a similar experiment using synthesized Pd doped TiO_2 and degradation reached only 90.23 % in 120 min. Further, The orange color of the initial solution changes to almost colorless at 120min in the presence of TiO_2 and Pd doped TiO_2 catalysts under UV light irradiation concerning time indicates destruction of dyes. The degradation of Congo red is further established by UV Vis absorption of the dye recorded at different intervals of degradation, as represented in Fig. 10. The results of

the absorption spectra are concurrent with the above FTIR analysis. Aqueous solutions of Congo red exhibit well-defined maxima at 497 nm, which is associated with the n–p* transitions of the non bonded electron present in the N atom of the azo group. It is evident from the spectra that there is a gradual reduction of the –N=N– peak with time, which indicates cleavage of the azo group leading to the degradation of the dye. In general, photodegradation of the dye over a semiconductor is driven either by photosensitization of the dye or by photocatalytic oxidation. [39] In the photosensitization process, the dye is stimulated by absorbing visible light photons and the subsequent transfer of electrons to the conduction band of the catalyst, which reacts with the oxygen present in the media to produce a superoxide oxidant. In the case of photocatalytic degradation, electron-hole pairs generated over the semiconductor react either with oxygen or with hydroxyl ions to produce superoxide and hydroxyl radicals as oxidants. As the bandgap widens due to the reduction in the particle size, the charge carrier transport in photocatalysis also differs. The electrons in the conduction minima and the holes present in the valence maxima have relatively higher oxidation and reduction potentials, respectively [39]. As a consequence of the higher redox potential, smaller particles can degrade the dye faster than bigger particles in the bulk. The influence of the particle size is also reflected in the higher amount of absorption of photons, thus facilitating the faster removal of the dye over the surface of the catalyst [40]. Since the surface energy is higher in nano TiO_2, photocatalytic oxidation of the organic moiety present on the catalyst is expected to be higher than in the Pd doped TiO_2. The presence of these defects in the semiconductor hinders the migration of electron-hole pairs to the surface and also promotes the recombination rate. Therefore, the probability of the diffusion of photo-generated excitants to reach the reaction site decreases, causing diminished photocatalytic activity.

Table – 5.7 : 20 ppm Congo red dye + 60 mg TiO_2 catalyst + UV -light

Sl	Time (t) min	Conc.(C) ppm	C/C0	ln C/C0	log C/C0	% of degradation
1	0	40	1	0	0	0
2	20	34.63	0.865	-0.1450	-0.0629	99.51
3	40	32.57	0.814	-0.2057	-0.0893	99.58
4	60	32.60	0.815	-0.2045	-0.0888	99.60
5	80	31.13	0.778	-0.2510	-0.1090	99.62

Table: 5.8 : 20 ppm Congo red dye + 60 mg Pd doped TiO_2 catalyst + UV-light

Sl	Time(t) Min	Conc.(C) ppm	C/C0	ln C/C0	log C/C0	% degradation
1	0	20	1	0	0	0
2	20	17.59	0.879	-0.1289	-0.0560	99.04
3	40	16.43	0.821	-0.1972	-0.0856	99.16
4	60	15.81	0.790	-0.2357	-0.1023	99.21

Table: 5.9. 40 ppm Congo red dye + 60 mg TiO_2 catalyst + UV-light

Sl	Time(t) min	Conc.(C) ppm	C/C0	ln C/C0	log C/C0	% degradation
1	0	40	1	0	0	0
2	20	37.49	0.937	-0.0650	-0.0282	98.96
3	40	36.33	0.908	-0.0965	-0.0419	99.02
4	60	35.27	0.881	-0.1266	-0.0550	99.05
5	80	35.08	0.877	-0.1312	-0.0570	99.08

Table: 5.10. 40 ppm Congo red dye + 60 mg Pd doped TiO_2 catalyst + UV-light

Sl	Time (t) min	Conc.(C) ppm	C/C0	ln C/C0	log C/C0	% degradation
1	0	20	1	0	0	0
2	20	19.29	0.964	-0.0366	-0.0159	99.00
3	40	15.57	0.778	-0.2510	-0.1090	99.22
4	60	15.07	0.753	-0.2836	-0.1232	99.25
5	80	14.07	0.703	-0.3523	-0.1530	99.30

Rate parameters of a) TiO_2 b) Pd doped

TiO_2 under Sunlight by using Congo red dye

5.3.11 Comparison of degradation percentages of CR Dye
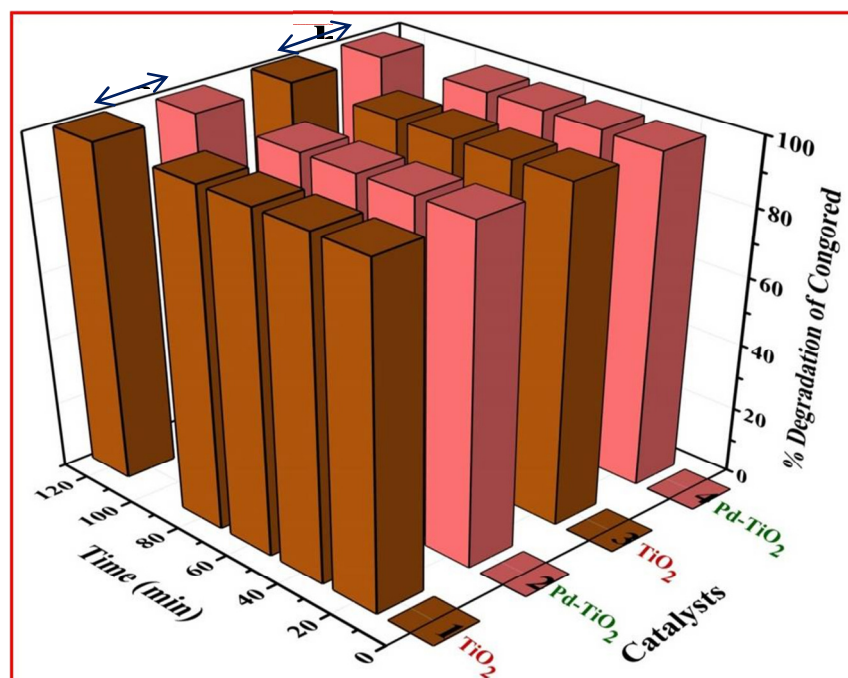
Fig.5.11 : Effect of irradiation time on photodegradation; (a) Degradation percentage under sunlight radiation, (b) Degradation percentage under UV-radiation.

It is found that nano TiO_2 degrades 99.58% of the CR dye, Pd doped TiO_2 99.26%, whereas anatase TiO_2 removes 99% of the color (Fig.5.11). Though anatase has a bandgap of 3.2 eV and thus is expected to degrade the dye faster, it is remarkable that the rate of degradation is higher with the TiO_2 catalyst. It can be inferred from this experiment that anatase TiO_2 is more efficient than Pd doped TiO_2 for the photocatalytic degradation of Congo red. This could imply that TiO_2 prohibits effective electron-hole pair recombination due to its layered structure, thereby enhancing its photocatalytic activity. The higher activity exhibited by nano TiO_2 under UV irradiation can be attributed to its higher bandgap of 3.2 eV compared to Pd doped TiO_2. Hence, efficient utilization of photons under UV irradiation is more probable for nano TiO_2 than the Pd doped material to facilitate the photodegradation of the dye.

Table – 5.11 : Comparison of photocatalysts performance

Sl No	Light Source	Catalysts	Amount of catalyst dosage	The concentration of dye solution	Degradation time (min)	% of degradation
1	Sunlight	TiO_2	60 mg	20 ppm 40 ppm	120 min	99.38 99.09
2	UV light	$Ti_{0.97}Pd_{0.03}O_2$	60 mg	20 ppm 40 ppm	120 min	99.40 99.21

For comparison, the photodegradation of CR by TiO_2 and Pd doped TiO_2 catalysts that without any catalyst were also carried out. The photodegradation of CR in different catalyst aqueous dispersions is shown in fig. 5.10 The result indicates that CR solution is stable under visible and UV-visible light irradiation in the absence of any catalyst. When

TiO_2 and Pd doped TiO_2, a sample has been added to the CR solution; the photocatalytic degradation rate is reached to about 90% within 120 min irradiation. The percentage degradation with the presence of the catalyst using an artificial UV lamp is nearly similar to the sunlight radiation. Artificial UV lamp radiation will give more percentage of degradation. The presence of TiO_2 as catalyst degrades the CR dye more than the absence of catalyst when treated under Sunlight and UV light. The percentage degradation of Congo red dye, the higher percentage of degradation are under artificial UV radiation compared to the direct sunlight radiation. This is because the artificial UV irradiation is more reproducible than sunlight, and this can bring higher efficiency in the degradation of dye. In reported that the energy of UV irradiation is mainly comparing to the bandgap energy of TiO_2. In sunlight, only 5% of total radiation possesses the optimum strength for the bandgap excitation of the electron. The experiment proved that the uses of titanium dioxide as a catalyst in photodegradation of Congo red dye enhanced the degradation process. Both treatments of dye between direct sunlight radiation and artificial UV lamp radiation show higher degradation percentages with slightly different in the presence of a catalyst. Treatment of Congo red dye with artificial UV lamp show 90.55% degradation after 120 minutes reaction time and 90.29% degradation when treated under sunlight. With the absence of catalysts, there is a vast difference in the percentage of degradation of Congo red dye after treated with both radiations. In the first part of photocatalytic studies, all critical experimental parameters, such as pH, dye concentrations, and catalyst amount, were optimized. The detailed experimental procedure conducted for optimization studies has been studied. The photocatalytic performance of TiO_2 and Pd doped TiO_2 under visible light was evaluated by monitoring photodegradation of CR dye at room temperature ($25 \pm 2°$ C). The spectral absorption
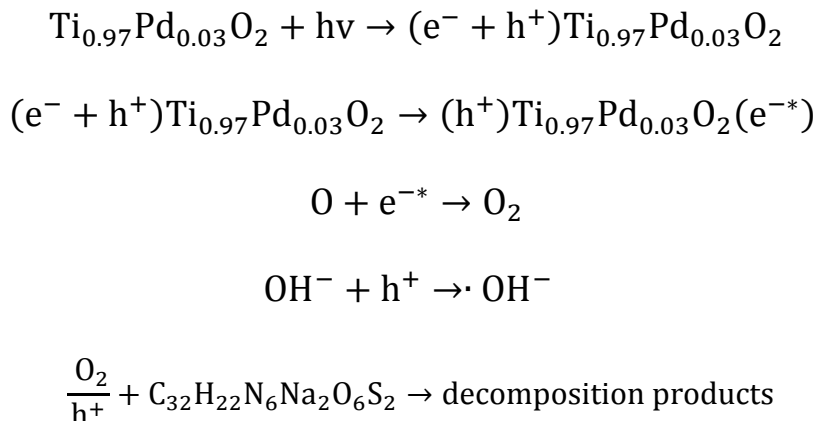
changes obtained for CR azo dye aqueous solutions (with an initial concentration of 20 and 40 ppm each) at various time intervals in the presence of TiO_2 and Pd doped TiO_2 under visible light irradiation are shown in Fig. 9. In the case of CR dye, the sharp absorption peak at 498 nm and a weak absorption peak at 350 nm is attributed to the azo bonds and naphthalene ring structures, respectively [41]. As shown in Fig. 5.9 and 5.10 , in the presence of sulfated TiO_2 and Pd doped TiO_2 the intensities of both these peaks gradually decrease to time after visible light irradiation. This indicated the rupture of azo links and naphthalene rings during the degradation process [42]. Fig. 5.9 and 5.10 show photodegradation rates of CR under different reaction conditions. It was well established that degradation is not possible in the absence of light as well as in the absence of a catalyst. However, complete degradation (~ 99 %) of CR was obtained only within 120 min. Under visible light irradiation with TiO_2 and Pd doped TiO_2 catalysts.

The resulting UV spectra reveal a decrease in maximum absorbance peak corresponds to each dye concerning time. The maximum absorbance peak of CR at 500 nm decreases rapidly, and decomposition reached to 99.37% after 120 mins (Fig.10).

5.3.12 Mechanism for Photocatalytic Activity of Pd doped TiO_2

CR dye was used as a perfect pollutant to assess the photocatalytic activity of TiO_2 and Pd doped TiO_2 nanocomposite under UV light irradiation. 60 mg of TiO_2 and Pd doped TiO_2 nanocomposites were added to the 250 ml CR dye solution (20 ppm). The combined suspensions were first magnetically stirred for 30 min to attain the adsorption-desorption equilibrium. Below the ambient conditions, the combined suspensions had been open to visible light irradiation created by using a 400W metal Philips lamp (wavelength: 254 nm). At certain periods, 5 ml of mixed suspensions were removed. The

filtrates had been analyzed by recording the UV-vis spectrophotometer (UV-2600, Shimadzu).
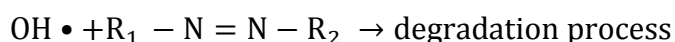
$$Ti_{0.97}Pd_{0.03}O_2 + hv \rightarrow (e^- + h^+)Ti_{0.97}Pd_{0.03}O_2$$

$$(e^- + h^+)Ti_{0.97}Pd_{0.03}O_2 \rightarrow (h^+)Ti_{0.97}Pd_{0.03}O_2(e^{-*})$$

$$O + e^{-*} \rightarrow O_2$$

$$OH^- + h^+ \rightarrow \cdot OH^-$$

$$\frac{O_2}{h^+} + C_{32}H_{22}N_6Na_2O_6S_2 \rightarrow \text{decomposition products}$$

The mechanism for the photodegradation of dyes using Pd-doped TiO_2 catalysts. Under UV irradiation, electrons are excited and transferred from the valence band (VB) to the conduction band (CB). In the meantime, the holes are created in the valence band. However, these charged carriers are easy to recombine; therefore, only a fraction of photogenerated electron-hole pairs take part in the photocatalytic reaction, leading to a decrease of photocatalytic activity of TiO_2. After doping with Pd^{2+}, the photo reduced electrons are trapped to the energetically favorable Pd^{2+} ion, resulting in the enhanced electron-hole separation of Pd-doped TiO_2. Particles can reduce the surface adsorbed O_2 into anionic superoxide radical ($\cdot O^{2-}$), which may oxidize organic pollutants into small molecules as well as parts of $\cdot O^{2-}$ can react with H^+ to generate H_2O_2, which is further excited by electrons and changed into $\cdot OH$ radicals. On the other hand, the holes can oxidize the surface adsorbed water or hydroxyl molecules by interfacial charge transfer to form OH radicals, which are highly reactive species (Amreetha et al., 2016; Hu et al., 2015). The holes can attack dye molecules by themselves to convert to by-products. The

active species, holes, OH radical, and $\cdot O^{2-}$ can effectively degrade dyes into more small intermediates and the final products (CO_2 and H_2O).

5.3.13   Mechanism for Photocatalytic Activity of TiO_2

The degradation of dye occurs due to the effect of the catalyst, which is titanium dioxide. The wavelength and intensity of the UV light irradiation source affect the degradation of dye in aqueous solution using titanium dioxide catalyst powder in the photocatalytic process [43]. According to [44], when the catalyst is irradiated by a photon that has the same energy or higher energy than catalyst bandgap, the surface of the catalyst will produce electron-hole pairs. These electron holes will react with electron donors in aqueous solution forming powerful oxidizing free radicals such as hydroxyl radicals. The hydroxyl radical (OH•) will oxidize the organics on the surface. Also, during the production of hydroxyl radicals, the surface of the catalyst produces the superoxide anion radical (O^{2-}•). This reaction will happen when the electron at the surface of the catalyst are trapped and removed by reaction with the absorbed oxygen in aqueous media. The reactions of the catalyst are as follows.

$$TiO_2 + h\nu \rightarrow h^+VB + e^-CB$$

$$h^+VB + H_2O \rightarrow OH^- + H^+$$

$$h^+VB + OH^- \rightarrow OH\bullet$$

$$e^-CB + O_2 \rightarrow O^{2-}\bullet$$

$$OH\bullet + R_1 - N = N - R_2 \rightarrow degradation\ process$$
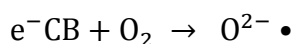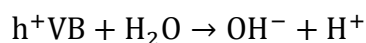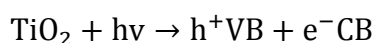
The potential radicals have degraded the dyes into the generation of various reaction intermediates, followed by the formed intermediates that were completely mineralized into carbon dioxide, water, ammonium, and the nitrate ion, as shown in Eq. 9.

$$CR\ dye +\bullet OH + O_2^- \rightarrow \text{intermediate products} \rightarrow CO_2 + H_2O$$

Relating to the equation, the energy from light radiation is essential in the degradation process of the dye. The power is needed to produce the hydroxyl radical and superoxide anion radical. It will degrade all contaminants, including organic substances into the non-harm compounds such as H_2O and CO_2 [45].

5.3.14   Recyclability

The recyclability of both the bulk and nanocatalyst samples (Fig.5.12) has been investigated. The catalysts after the reaction were centrifuged, thoroughly washed with water to remove adhered dye moieties, and then dried to run the photoreactions. It is found that there is some reduction of the activity in both nano TiO_2 and Pd doped TiO_2 after the subsequent photocatalytic reaction. However, it is interesting to note that compared to the bulk material, the photocatalytic activity of nano TiO_2 decreases significantly after the reuse of the catalyst. This could be due to the increased surface area of nano TiO_2 and Pd doped TiO_2, resulting in the increased absorption of the dye on the catalyst. Hence, after the photoreaction, firmly adhered dye hampers further photocatalytic activity. Also, it is noteworthy that the structure of the enzyme is retained even after several photoreactions. The degradation experiment was repeated by using the usual procedures mentioned above, and such six repeat cycles were conducted. For every repeat cycle, the TiO_2 and Pd doped TiO_2 photocatalysts showed degradation efficiency

of more than 90 %. Thus, it can be concluded that catalyst retains excellent stability, reusability, and recyclability during the degradation process.
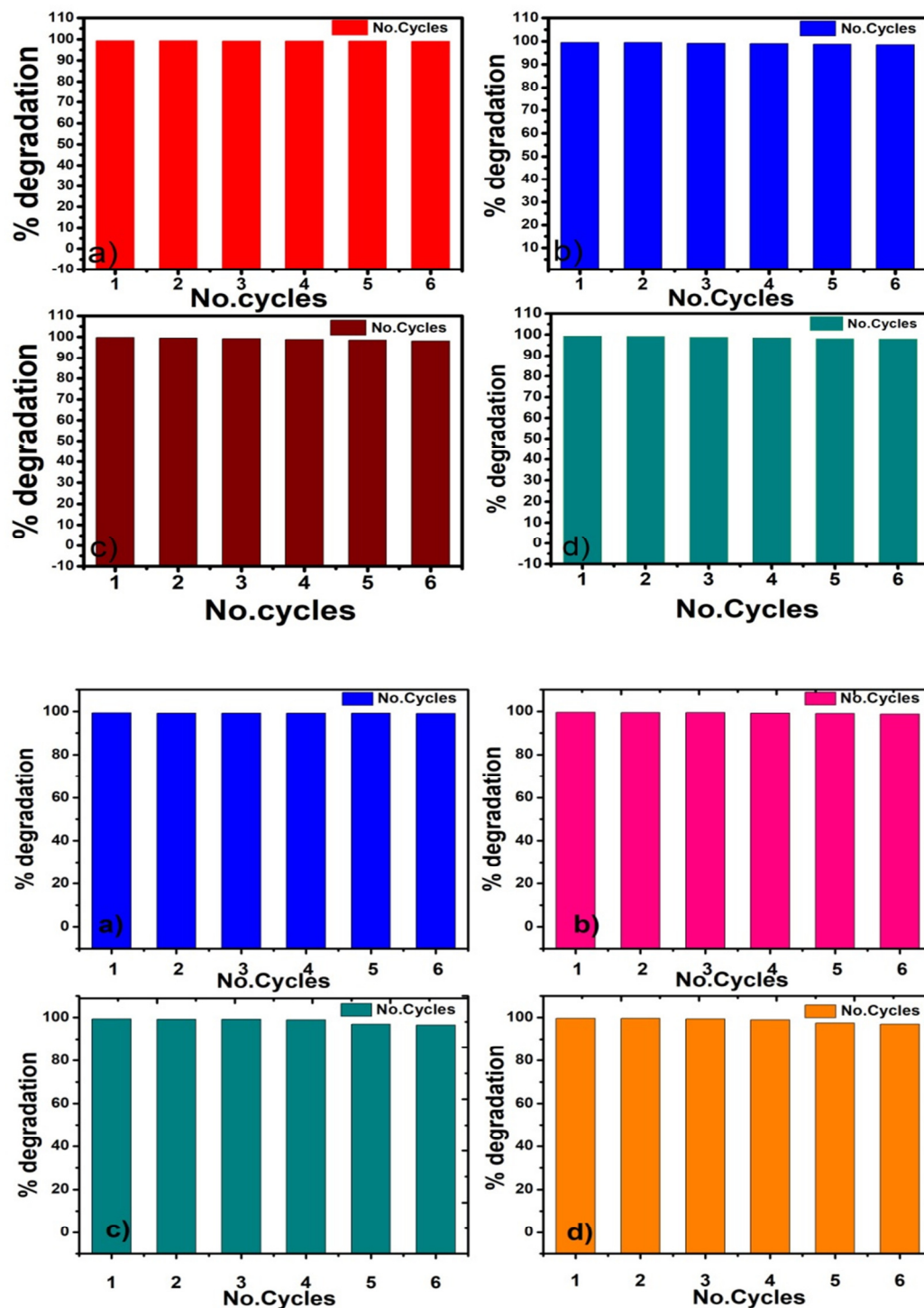

Fig.5.12 : Reusability and recyclability of TiO_2 and Pd doped TiO_2 for CR

5.4 Conclusion

The higher solar and UV light photocatalytic activity of combustion synthesized TiO_2 and Pd doped TiO_2 catalysts can be attributed to the nano-size, crystal structure (anatase), crystallinity, large amount surface hydroxyl groups and decreased band-gap energy of the catalyst which enhances the solar energy absorption. Photocatalysis is a very effective method for the degradation of industrial or textile dyes. In this study, TiO_2 and Pd doped TiO_2 nanoparticles were synthesized and characterized by XRD, SEM, and EDX. It was observed that the synthesized, effective in degrading selected azo dye (CR) entirely in a short interval of time (120 minutes). From this experiment, we can conclude that the TiO_2 and Pd doped TiO_2 nanocatalysts degrade the CR dye over a short interval of time with the help of sunlight and UV light. Even though the result was achieved more than 99%, we still believe that if this experiment was done over a more extended period that the concentration of the dyes would have been zero. The photocatalytic activity of these synthesized compounds and TiO_2 have been tested for the degradation of Congo red dye under solar light irradiation. Among the catalysts tested, TiO_2 NPS was found to be the most active. The optimum condition for 99 % degradation of Congo red dye was found to be 100 mL of 1×10^{-4} M of dye solution along with 0.1 g of TiO_2 and Pd doped TiO_2 NPs under solar and UV light irradiation for 120 min. The active catalyst TiO_2 and Pd doped TiO_2 NPs were found to be efficiently recyclable several times.

Reference

[1] R. Vaithiyanathan, T. Sivakumar, Water Sci. Technol. 63 (3) (2011) 377.

[2] A. Valentine Rupa, R. Vaithiyanathan, T. Sivakumar, Water Sci. Technol. 64 (5) (2011) 1040.

[3] H. Gerischer, A. Heller, J. Phys. Chem. 95 (1991) 5161.

[4] B. Ohtani, K. Iwai, S. Nishimoto, S. Sato, J. Phys. Chem. B. 101 (1997) 33499. R. Vaithiyanathan, T. Sivakumar, Water Sci. Technol. 63 (3) (2011) 377.

[5] M.R. Hoffman, S.T. Martin, W. Choi, D.W. Bahnemann, Chem. Rev. 95 (1995) 69.

[6] M.A. Fox, M.T. Dulay, Chem. Rev. 93 (1993) 341.

[7] H. Harada, T. Ueda, Chem. Phys. Lett. 106, (1984) 229.

[8] R.I. Bickley, T.G. Carreno, J.S. Lees, L. Palmisano, R.J.D. Tilley, J. Solid State Chem. 92, (1991) 178.

[9] Alves De Lima RO, Bazo AP, Salvadori DMF, Rech CM, de Palma Oliveira D, de Aragaˇo Umbuzeiro G (2007) Mutat Res Gen Toxicol Environ 626:53

[10] Brown MA, Devito SC (1993) Crit Rev Environ Sci Technol 23:249.

[11] Rajeev K. Wahi, William W. Yu, Yunping Liu, Michelle L. Mejia, Joshua C. Falkner, Whitney Nolte, Vicki L. Colvin, J. Mol. Catal. A: Chem. 242 (2005) 48.

[12] Agus Purwanto, Hendri Widiyandari, Takashi Ogi, Kikuo Okuyama, Catal. Com- mun. 12, (2011) 525.

[13] Khaled Melghit, S. Odheiba, Al-Shukeili, Issa Al-Amri, Ceram. Int. 35, (2009) 433.

[14] Mohamed Ksibi, Sylvie Rossignol, Jean-Michel Tatibouet, Christos Trapalis, Mater. Lett. 62 (2008) 4204.

[15] Y. Shao, J. Sui, G. Yin, Y. Gao, Appl. Catal. B-Environ. 2008, 79, 89-99

[16] H. Dislich, J. Non-Cryst. Solids. 1984, 63, 237-241.

[17] X.Bian, J.Chen, R.Ji, Degradation of 2,4-Dichlorophenoxyacetic Acid (2,4-D) by Novel Photocatalytic Material of Tourmaline-Coated TiO2 Nanoparticles, Kinetic Study and Model, Mater. 6 (2013) 1530-1542.

[18] J. Tifeng, H. Guo, Q. Zhang, Q. Peng, Y. Tang, X.Yan, B. Li, Reduced Graphene Oxide-Based Silver Nanoparticle-Containing Composite Hydrogel as Highly Efficient Dye Catalysts for Wastewater Treatment. Sci. Rep., 5 (2015) 11873.

[19] D. Mao, X. Shimin, W. Tianhui, Z. Deqiang, Z. Qian, F. Zihong, Z. Yao J. Fangying, H. Qiang, X. Xuan, Preparation of a Microspherical Silver-Reduced Graphene OxideBismuth Vanadate Composite and Evaluation of Its Photocatalytic Activity. Mater. 9 (160) (2016) 1-14.

[20] Z. Lu, Z. Yu, J. Dong, M. Song, Y. Liu, X. Liu, D. Fan, Z. Ma, Y. Yan and P. Huo, Construction of stable core-shell imprinted Ag-(poly-o-phenylenediamine)/CoFe2O4 photocatalyst endowed with the specific recognition capability for selective photodegradation of ciprofloxacin, RSC Adv., 7 (2017) 48894-48903.

[21] Afkhami, and R. Moosavi, Adsorptive removal of Congo red, a carcinogenic textile dye, from aqueous solutions by maghemite nanoparticles, 174, 2010, 398–403.

[22] C. Cripps, J.A. Bumpus, S.D. Aust, Biodegradation of azo and heterocyclic dyes by Phanerochaete chrysosporium, Applied Environmental Microbiology, 56(4), 1990, 1114-1118.

[23] S. Dafare, P. S. Deshpande, and R. S. Bhavsar, Photocatalytic degradation of congo red dye on combustion synthesized Fe2O3, Indian Journal of Chemical Technology, 20, 2013, 406–410.

[24] S. Rouf, M. Nagapadma, and R.R. Rao, Removal of Harmful Textile Dye Congo red from Aqueous Solution Using Chitosan and Chitosan Beads Modified with CTAB, Int. Journal of Engineering Research and Applications, 5(3), 2015, 75–82.

[25] H. Zhu, J. Yao, R. Jiang, Y. Fu, Y. Wu, and G. Zeng, Enhanced decolorization of azo dye solution by cadmium sul fi de / multi-walled carbon nanotubes/polymer composite in combination with hydrogen peroxide under simulated solar light irradiation, Ceramics International, 40, 2014, 3769–3777. doi.org/10.1016/j.ceramint.2013.09.043

[26] L. G. Devi, B. N. Murthy, and S. G. Kumar, Photocatalytic activity of TiO2 doped with Zn2+ and V5+ transition metal ions : Influence of crystallite size and dopant electronic configuration on photocatalytic activity, Materials Science and Engineering B, 166, 2010, 1–6. doi.org/10.1016/j.mseb.2009.09.008.

[27] H. Guo, Y. Ke, D. Wang, K. Lin, R. Shen, J. Chen, and W. Weng, Efficient adsorption and photocatalytic degradation of Congo red onto hydrothermally synthesized NiS nanoparticles, Journal of Nanoparticles Research, 15, 2013, 1475. doi.org/10.1007/s11051-013-1475-y.

[28] W. Konicki, D. Sibera, E. Mijowska, Z. Lendzion-bielun, and U. Narkiewicz, Equilibrium and kinetic studies on acid dye Acid Red 88 adsorption by magnetic ZnFe2O4 spinel ferrite nanoparticles, Journal of Colloid and Interface Science, 398, 2013, 152–160. doi.org/10.1016/j.jcis.2013.02.021.

[29] H. Lachheb, E. Puzenat, A. Houas, M. Ksibi, E. Elaloui, C. Guillard, and J. Herrmann, Photocatalytic degradation of various types of dyes (Alizarin S, Crocein Orange G, Methyl Red, Congo Red, Methylene Blue) in water by UV-irradiated titania, Applied Catalysis B: Environmental, 39, 2002, 75–90.

[30] R.K. Wahi, W.W. Yu, Y. Liu, M.L. Mejia, J.C. Falkner, W. Nolte, and V.L. Colvin, Photodegradation of Congo Red catalyzed by nanosized TiO2, Journal of Molecular Catalysis A: Chemical, 242, 2005, 48–56. doi.org/10.1016/j.molcata.2005.07.034.

[31] Y. Yao, S. Miao, S. Liu, L.P. Ma, H. Sun, and S. Wang, Synthesis, characterization, and adsorption properties of magnetic Fe3O4@ graphene nanocomposite. Chemical Engineering Journal, 184, 2012, 326–332. doi.org/ 10.1016/ j.cej.2011.12.017.

[32] H. Zhu, R. Jiang, L. Xiao, Y. Chang, Y. Guan, X. Li, and G. Zeng, Photocatalytic decolorization and degradation of Congo Red on innovative crosslinked chitosan / nano-CdS composite catalyst under visible light irradiation, Journal of Hazardous Materials, 169, 2009, 933–940. doi.org/10.1016/ j.jhazmat.2009.04.037.

[33] S.U.M. Khan, M. Al-Shahry, W.B. Ingler Jr., Science 297 (2002) 2243.

[34] S. I. Mogal, V. G. Gandhi, M. Mishra, S. Tripathi, T. Shripathi, P. A. Joshi, D. O. Shah, Ind. Eng. Chem. Res. 2014, 53, 5749–5758.

[35] H. Kolya, P. Maiti, A. Pandey, T. Tripathy, J. Anal. Sci. Technol. 2015, 6, 1– 7.

[36] Q. Feng, S. Li, W. Ma H. J. Fan, X. Wan, Y. Lei, Z. Chen, J. Yang, B. Qin, J. Alloys Compd. 2018, 737, 197–206.

[37] L. Wang, J. Li, Z. Wang, L. Zhao, and Q. Jiang, Dalton Trans., 2013, 42, 2572.

[38] A. Kudo and Y. Misaki, Chem. Soc. Rev., 2009, 38, 253–278.

[39] H. Zhang, G. Chen, and D. W. Bahnemann, J. Mater. Chem., 2009, 19, 5089–5121.

[40] J. Sundaramurthy, P. Suresh Kumar, M. Kalaivani, V. Thavasi, S. G. Mhaisalkara, and S. Ramakrishna, RSC Adv., 2012,2, 8201–8208.

[41] S.M. Patil, A.G. Dhodamani, S.A. Vanalakar, S.P. Deshmukh, S.D. Delekar, Multiapplicative tetragonal TiO2/SnO2 nanocomposites for photocatalysis and gas sensing, J. Phys. Chem. Solids, 115 (2018) 127-136.

[42] J. Wang, R. Li, Z. Zhang, W. Sun, R. Xu, Y. Xie, Z. Xing, X. Zhang, Efficient photocatalytic degradation of organic dyes over titanium dioxide coating upconversion luminescence agent under visible and sunlight irradiation, Appl. Catal. A, 334 (2008) 227-233.

[43] Konstantinou I K, Albanis T A. TiO$_2$-assisted photocatalytic degradation of azo dyes in aqueous solution: Kinetic and mechanistic investigations: A review. Applied Catalysis B: Environmental, 2004, 49(1):1-4

[44] Barka N, Qourzal S, Assabbane A, Nounah A, Ait-Ichou Y. Photocatalytic degradation of an azo reactive dye, Reactive Yellow 84, in water using an industrial titanium dioxide-coated media. Arabian Journal of Chemistry, 2010, 3(4):279-283

[45] Alahiane S, Qourzal S, El Ouardi M, Abaamrane A, Assabbane A. Factors influencing the photocatalytic degradation of reactive yellow 145 by TiO2-coated non-woven fibers. American Journal of Analytical Chemistry, 2014, 5(08):445-454

SUMMARY & CONCLUSIONS

CONCLUSION

$Ti_{0.97}Pd_{0.03}O_{1.97}$ is an excellent catalyst for the reductions of the aromatic nitro compound to amine, avoiding the formation of toxic hydroxylamine by-product. 100% selectivity of the amine has shown by the $Ti_{0.97}Pd_{0.03}O_{1.97}$ catalyst with high rates of a catalytic reaction. Pd^{+2} doped TiO_2 is shown in high catalytic activity on the solvent and solvent-free reductions of the aromatic nitro compound in 1.2 -1.3 bar pressure of H_2. At the end of the thesis, the conclusion of the consequential outcomes has been done along with the future perspectives of the thesis work.

The research work has presented some new findings as follows:

➢ The average crystalline size of palladium doped TiO_2 is 6.24 nm and 7.8 nm, according to the study, analyzing The X-ray.

➢ The composition part is in the tetragonal system and shows that palladium does not change the dopamine and TiO_2 atoms.

➢ The SEM Analysis analysis found that palladium dopamine donot affects the shape and texture of the TiO_2 nano.

➢ Degenerate and degrading skills on TiO_2 and Palladium Doped TiO_2 counter-count.

➢ Photo-response activity of enzyme with 0.06 g/L density can be upgraded to 80 min 99%.

➢ SCM has been proved to be an excellent way to dope 1 to 3 at % of Pd ions for Ti in TiO_2. It is a batch process. 1 to 2 g of oxides could be routinely prepared

by this way. Titanium isopropoxide was chosen as the source of Ti. $PdCl_2$ was readily available. Several organic fuels have been tried here, and Glycine was found to be satisfactory. TiO_2 and Pd doped TiO_2 are responsible for the performance of these character-supporting features azo color (CR and MR) in just 120 minutes.

➢ The visible light. This simple, cost-effective, and reuse photocatalyst is therefore applied on a large scale to remove hazardous organic motis present in the water body.

As per the aim and objectives of the research work, they successfully synthesized oxides and doped metal oxides with Glycine as an ointment. Inorganic catalysts and oxides are utilized in combination with oxides such as TiO_2; CeO_2 Pd doped TiO_2, and CeO_2. Physical and mechanical properties such as tetragonal alloys and show that doped palladium and TiO_2 do not alter the molecular structure. Tetragonal nerve fibers have a uniform distribution of spines on the surface that reflects the smallest part of the body and the overall shape of the skin. X-ray diffraction analysis revealed that the average crystallinity of closed Palladium doped TiO_2 was 6.24 nm and 7.8 nm. The muscle is small, and the tendon is short. These results show the potential of the synthesized $Ti_{0.97}Pd_{0.03}O_{1.97}$ as a potential solvent for the active application. Reactions of the synthesis of brides with different olefins require higher temperatures and longer reaction times as well $Ti_{0.97}Pd_{0.03}O_{1.97}$ was vital applications for oxygen storage capacity and H2 reduction catalyst in coupling reactions. From the PXRD discovered, the standard crystalline size of CeO_2 and $Ce_{0.98}Pd_{0.02}O_2$ catalysts were obtained at 5.9 nm and 3.1nm. The synthesized nanoparticles having polygonal shape structure; this structure showed that the

$Ce_{0.98}Pd_{0.02}O_2$ catalyst doesn't change morphology. The FTIR structure exhibited the presence of Ce-O stretching bonds of CeO_2. The CeO_2 nanoparticles showed powerful UV-visible absorption at 329 nm with bandgap was resolution relating 3.26 eV, the polygonal shape morphology with uniform distribution of particles. This reveals the $Ce_{0.98}Pd_{0.02}O_2$ was a critical application for element oxygen storage capability, element uptake measurements, CO reaction studies, and reduction catalyst in coupling reactions. The decolorization and degradation efficiency depends upon the calculations of TiO_2 and palladium doped TiO_2 catalyst. The catalytic photocatalyst of the catalyst can be reduced to a concentration of 0.06 g / L for 99% at 80 min. This image was created to quench the emission of fine particles such as Congo red using TiO_2 oil. The reliability of the high-temperature TiO_2 heat exchanger has been based on nano-size, crystalline (anatase) crystals, large hydroxyl groups, and the reduction in the size of the vacuum cavity. For solar energy. These way sides have the advantage of high-throughput, ligand elimination and bonding, simple techniques, and simple operation. This material provides an environmentally friendly and durable solution because it produces less waste, can be recovered and has fewer efficacies.

Appendix - I

List of Scientific contributions in Journals during Ph.D.

List of scientific contributions in journals during Ph.D.

1. **G.O. Obaiah** [a], K.H. Shivaprasad, K. Srikanth Bhat, M.S. Hegde, M. Mylarappa, **"Development and Catalytic Application of Palladium Doped Titania ($Ti_{0.98}Pd_{0.02}O_2$) Through Low Temperature Solution Combustion Method"** **ADVANCED SCIENCE LETTER,** 24 (8), 2018, 6004-6007.

    DOI: https://doi.org/10.1166/asl.2018.12235.

2. **G.O. Obaiah** [a], K.H. Shivaprasad, K. Shrikanth Bhat, M. Mylarappa, **"A Potential Use γ-Al_2O_3 Coated Cordierite Honeycomb Reinforced $Ti_{0.97}Pd_{0.03}O_{2-\delta}$ Catalyst for Selective High Rates in Coupling reactions"** **ELSVIER: Materials Today: Proceedings** 5 (2018) 22466–22472. Volume 5, Issue 10, Part 3, 2018, Pages 22466-22472

    DOI: https://www.sciencedirect.com/science/article/pii/S2214785318317504.

3. **G.O. Obaiah** [a], K.H. Shivaprasad, M. Mylarappa, **"Novel Combustion Synthesis and Characterization of Undoped CeO_2 and Pd Doped CeO_2 Nanoparticles Using Solution Combustion Method"** **SPRINGER: SN-Applied Science** (**Under Review**), Manuscript Id No. D-19-03389-2019.

4. **G.O. Obaiah** [a], K.H. Shivaprasad, M. Mylarappa, **"Synthesis and Structural Characterization of Undoped CeO_2 and Pd doped CeO_2 for Photo Catalytic Studies under Sunlight and UV-Light Irradiation"** **ELSVIER: International Journal of Advanced Science and Technology** Vol. 29, No. 3s, (2020), pp. 1436-1453.

    DOI: http://sersc.org/journals/index.php/IJAST/article/view/6106.

5. **G.O. Obaiah** [a], K.H. Shivaprasad, M. Mylarappa,

   "Palladium Doped TiO$_2$ Nano Catalyst Coated On Cordierite Monolith for High Rate in C-N Coupling Reaction and Their Recyclable Properties" ACS Publications: **General Chemistry, Chemical Reviews Accepted-ISSN:** 0009-2665E-ISSN: 1520-6890

6. **G.O. Obaiah** [a], K.H. Shivaprasad, M. Mylarappa,

   "Novel Synthesis of Palladium Doped TiO$_2$ Nano Catalyst for Selective Reduction of Aromatic Nitro Compounds to Amines" ACS Publications: **General Chemistry, Chemical Society Reviews**

   ISSN: 0306-0012E-ISSN: 1460-4744

7. **G.O. Obaiah** [a], K.H. Shivaprasad, M. Mylarappa,

   "Synthesis, characterization and Augmented photo catalytic activity of TiO$_2$ and palladium doped TiO$_2$ nano particles Under Sunlight and UV-Light irradiation".

   Journal: nature chemistry

Appendix - A

Conference contributions

Participation in Conferences

National Conferences

1. Participated in KSTA National Conference on **"Impact of Science and Technology on Society and Economy"**. Jointly organized by Karnataka Science and Technology Academy **(KSTA), DST, GoK and VSK University, Ballari** organized during March 8-9, 2017. **[Presented a paper entitled: "*A Potential Use γ-Al$_2$O$_3$ Coated Cordierite Honeycomb Reinforced Ti$_{0.97}$Pd$_{0.03}$O$_{2-\delta}$ Catalyst for Selective High Rates in H$_2$+O$_2$ recombination"].*

2. Participated in **KSTA** Department of Science and Technology, Government of Karnataka, Bangalore and Veerashaiva College, Ballari, Jointly Organize Karnataka Science and Technology Academy Conference on **"Science and Society"** on 16th and 17th January 2015, at **Veerashaiva College, Ballari.**

International Conferences

3. Participated in 1st International Conference on Nanoscience and Nanotechnology (**ICNAN 16**), organized by the centre for Nanotechnology (CNR), at **VIT University, Vellore, Tamilnadu,** India during 19th to 21st October 2016. **[Presented a paper entitled: "Development and Catalytic Application of Palladium Doped Titania (Ti$_{0.98}$Pd$_{0.02}$O$_2$) Through Low Temperature Solution Combustion Method"].**

4. Participated in International Conference on Advances in Science and Engineering (**ICASE-2017**) at **East West Institute of Technology, Bangalore, India Regents International College, Bangkok, Thailand** during 19th, 20 and 22nd January 2017. **[Presented a paper entitled: "A Potential Use γ-Al$_2$O$_3$ Coated Cordierite Honeycomb Reinforced Ti$_{0.97}$Pd$_{0.03}$O$_{2-\delta}$ Catalyst for Selective High Rates in coupling reactions"].**

5. Participated in 5th International Conference on Nanoscience and Nanotechnology (**ICONN-2019**) **SRM INSTITUTE OF SCIENCE AND TECHNOLOGY Kattankulthur Tamilnadu,** Organized by department of physics and nanotechnology, SRM IST-India during 28-30 January 2019.

[Presented a paper entitled: "Synthesis, characterization and Augmented photo catalytic activity of TiO_2 and palladium doped TiO_2 nano particles Under Sunlight and UV-Light irradiation"].

6. Participated in 4th International Conference On Science, Agriculture and Technology for Society (**ICSTS-2019**), Organized by **VMS Research Foundation Nagpur, East West Institute of Technology, Bangalore,** and Karnataka during 13-15th May 2019. **[Presented a paper entitled:** "Novel Combustion Synthesis and Characterization of Undoped CeO_2 and Pd Doped CeO_2 Nanoparticles using Solution Combustion Method"].

Appendix - B

Plagiarism Certificate

URKUND

Urkund Analysis Result

Analysed Document: Obalah, Department of Chemistry, VSKUB.pdf (D65607932)
Submitted: 3/17/2020 10:28:00 AM
Submitted By: kumbargoudar@gmail.com
Significance: 2 %

Sources included in the report:

https://hal.archives-ouvertes.fr/hal-00565443/document
https://www.researchgate.net/
publication/334418116_Surface_Temperature_and_Optical_Properties_Pd-
TiO2_Doped_PVA_Nanocomposite
https://www.researchgate.net/publication/271759143_Preparation_of_Pd-doped_nano-
TiO_2_in_microemulsion_and_their_application_in_photodegradation_of_CI_Acid_Yellow_23
https://www.sciencedirect.com/science/article/pii/S2214785318317504.
https://www.researchgate.net/
publication/322538672_Ag_doped_TIO2_nanoparticles_prepared_by_hydrothermal_method_an
d_coating_of_the_nanoparticles_on_the_ceramic_pellets_for_photocatalytic_study_Surface_prop
erties_and_photoactivity
https://www.science.gov/topicpages/p/photocatalytic+dye+degradation
https://www.researchgate.net/
publication/223693878_Solar_photocatalytic_degradation_of_dyes_High_activity_of_combustion
_synthesized_nano_TiO2
https://www.science.gov/topicpages/n/n-doped+tio2+photocatalysts
https://www.science.gov/topicpages/n/n-doped+tio2+photocatalysts.html
https://www.researchgate.net/publication/264987251_Zirconium_and_silver_co-
doped_TiO2_nanoparticles_as_visible_light_catalyst_for_reduction_of_4-
nitrophenol_degradation_of_methyl_orange_and_methylene_blue
https://www.researchgate.net/
publication/229135801_Comparison_of_Zinc_Oxide_Nanoparticles_and_its_Nano-
Crystalline_Particles_on_the_Photocatalytic_Degradation_of_Methylene_Blue
https://sciencedocbox.com/86419400-Chemistry/Photocatalytic-materials.html

Instances where selected sources appear:

28

13/3/2020
LIBRARIAN
Vijayanagara Sri Krishnadevaraya University
Vinayak Nagar, Hospet Road, Cantonment,
BELLARY - 583104. (Karnataka)

Development and Catalytic Application of Palladium Doped Titania (Ti$_{0.98}$Pd$_{0.02}$O$_2$) Through Low Temperature Solution Combustion Method

Authors: Obaiah, G. O[1]; Shivaprasad, K. H[1]; Bhat, K. Srikanth[1]; Hegde, M. S[1]; Mylarappa, M[2]

Get Access   Share   Export

A Potential Use γ-Al$_2$O$_3$ Coated Cordierite Honeycomb Reinforced Ti$_{0.97}$Pd$_{0.03}$O$_{2-\delta}$ Catalyst for Selective High Rates in coupling reactions

G.O. Obaiah [a, b], K.H. Shivaprasad [a] ✉, M. Mylarappa [c, d], K. Srikanth bhat [b]

⊞ Show more

Get rights and content

Abstract

The current work was mair
honeycomb reinforced Ti$_{0.9}$
The Titanium isopropoxid
synthesis of Ti$_{0.97}$Pd$_{0.03}$O$_{2-\delta}$
TiO(NO$_3$)$_2$ solution, 0.3 mm

Don't miss out on relevant research

Register for weekly article and book recommendations based on what you read

Register for free

The obtained sample of the monolith before and after coating and catalytic activity were studied by using PXRD, IR, and Mass spectroscopy. TEM and SEM. The surface image of the catalyst coated monolith was characterized by FEI Quanta scanning electron microscope. In the coupling reactions have been investigated in view of their potential use in the industrial passive autocatalytic recombines (PAR). The recombination reaction of hydrogen and oxygen has been monitored using Ti$_{0.97}$Pd$_{0.03}$O$_{2-\delta}$ catalyst

Previous   Next

Keywords

International Journal of Advanced Science and Technology

SYNTHESIS AND STRUCTURAL CHARACTERIZATION OF UNDOPED CEO2 AND PD DOPED CEO2 FOR PHOTO CATALYTIC STUDIES UNDER SUNLIGHT AND UV-LIGHT IRRADIATION.

G.O. Obaiah, K.H. Shivaprasad, M. Mylarappa

Abstract

The main objective of the analysis is concentrated on the preparation and fabrication of doped and undoped CeO_2 nanoparticles by solution combustion technique to taken glycine as fuel. The correct size and morphology of the doped metal compounds were studied Scanning microscope (SEM). The composition of ceria (CeO_2) and palladium substituted Ceria ($Ce_{0.98}Pd_{0.02}O_2$) was confirmed from the powder X-ray Diffractometer (PXRD). The functional groups were analyzed by Fourier transfer infrared spectroscopic analysis, XRD, RR, UV–Vis, and XPS. Photocatalytic properties of CeO_2 and palladium doped CeO_2 ($Ce_{0.98}Pd_{0.02}O_2$) nanoparticles (NPs) were studied using the radiation conjugation of red (CR) under UV light and sunlight exposure. Based on the XRD analysis, CeO_2 and Pd doped CeO_2 NPs were formed as crystal structures. CeO_2 and Pd doped CeO_2 showed excellent Photocatalytic activity by degrading more than 92% of the CR color in the intervals of 120 min under UV light and sunlight.

 PDF

Published
2020-03-11